Experimental and Numerical Study of Air Curtains in Refrigerated Display Cabinets

James Lam

Submitted in total fulfillment of the requirements of the degree of Masters by Research
June 2013

School of Mechanical and Manufacturing Engineering
Faculty of Engineering

The University of New South Wales

PLEASE TYPE

1.1.1 THE UNIVERSITY OF NEW SOUTH WALES

1.1.2 Thesis/Dissertation Sheet

Surname or Family name: Lam

First name: James **Other name/s:**

Abbreviation for degree as given in the University calendar: ME

School: Mechanical and Manufacturing Engineering **Faculty:** Engineering

Title: Experimental and Numerical study of Air curtain in refrigerated Display cabinets

Abstract 350 words maximum: (PLEASE TYPE)

The analysis of air curtains in refrigerated display cabinets (RDC), in slanted and straight shelf configurations, has been carried out using experimental and numerical methods. Flow visualization was utilized to qualitatively analyze the air curtain and its behavior and Laser Doppler Velocimetry was used to gather quantitative information on the velocity profiles of the air curtain at different heights. Temperature probes were used to gain the experimental temperature values around the cabinet to use for boundary conditions in a CFD model. 3D and 2D models were developed to numerically analyze slanted and straight configurations of the RDC in both transient and steady state simulations. It was shown that 2D simulations can be utilized for the numerical modeling of RDC as they are superior in computational time comparing with 3D simulations and produce results with sufficient accuracy. Slanted and straight shelf configurations have been shown to affect the air curtain via a number of significant mechanisms that effect entrainment and efficiency of the RDC.

The University recognises that there may be exceptional circumstances requiring restrictions on copying or conditions on use. Requests for restriction for a period of up to 2 years must be made in writing. Requests for a longer period of restriction may be considered in exceptional circumstances and require the approval of the Dean of Graduate Research.

FOR OFFICE USE ONLY

Date of completion of requirements for Award:

THIS SHEET IS TO BE GLUED TO THE INSIDE FRONT COVER OF THE THESIS

ABSTRACT

The analysis of air curtains in refrigerated display cabinets (RDC) in slanted and straight shelf configurations was carried out using experimental and numerical methods. Flow visualization was used to qualitatively analyze the air curtain and its behavior. Laser Doppler Velocimetry was used to gather velocity profiles of the air curtain at different heights. Temperature probes were used to get the experimental temperature value around the cabinet to use for boundary conditions. A 3D and 2D mesh were developed to numerically analyze the RDC in slanted and straight configurations. Transient and steady state simulations were carried out. The 2D simulations was discovered to be superior in computational time and accuracy to numerical simulations. Furthermore, the transient simulations provide superior accuracy and lower residual errors. Slanted and straight shelf configurations affect the air curtain in numerous significant criteria that effect entrainment and efficiency of the RDC.

ACKNOWLEDGMENTS

I would like to extend my deepest thanks to my Lord Jesus Christ for making these past years at UNSW an incredible learning experience

I thank my supervisors Tracie Barber and Victoria Timchenko and the late Eddie Leonardi for their guidance and experience in my research.

I like to thank my Dad for the support and guidance over the years and my mom as well.

I thanks NCVers past and present, Dana, Niloufer, Plat, Hoon, Mark, Juen Nin, Megan, Paige, Sarah, Kyloon Jon Jon, Gio, Cyril, Enoch, Denise, Terressa, and many, many, *many* others.

TABLE OF CONTENTS

LIST OF FIGURES

NOMENCLATURE AND ABBREVIATIONS

ACW	=Air Curtain Width
l	=Non Dimensional Air Curtain Width
LDV	=Laser Doppler Velocimetry
NDACW	=Non Dimensional Air Curtain Width
PIV	=Particle Image Velocimetry
RDC	=Refrigerated display cabinet
Re	=Reynolds number
Ri	=Richardson number
SST	= Shear Stress Transport
T_a	=Temperature at ambient
T_s	=Temperature at supply grill
T_r	=Temperature at return grill
X	=Thermal entrainment factor
X_{vmax}	=X position of the traverse system where local maximum velocity was located

CHAPTER 1 – LITERATURE REVIEW

1.1 Introduction

Fig. 1 - Refrigerated Display Cabinet

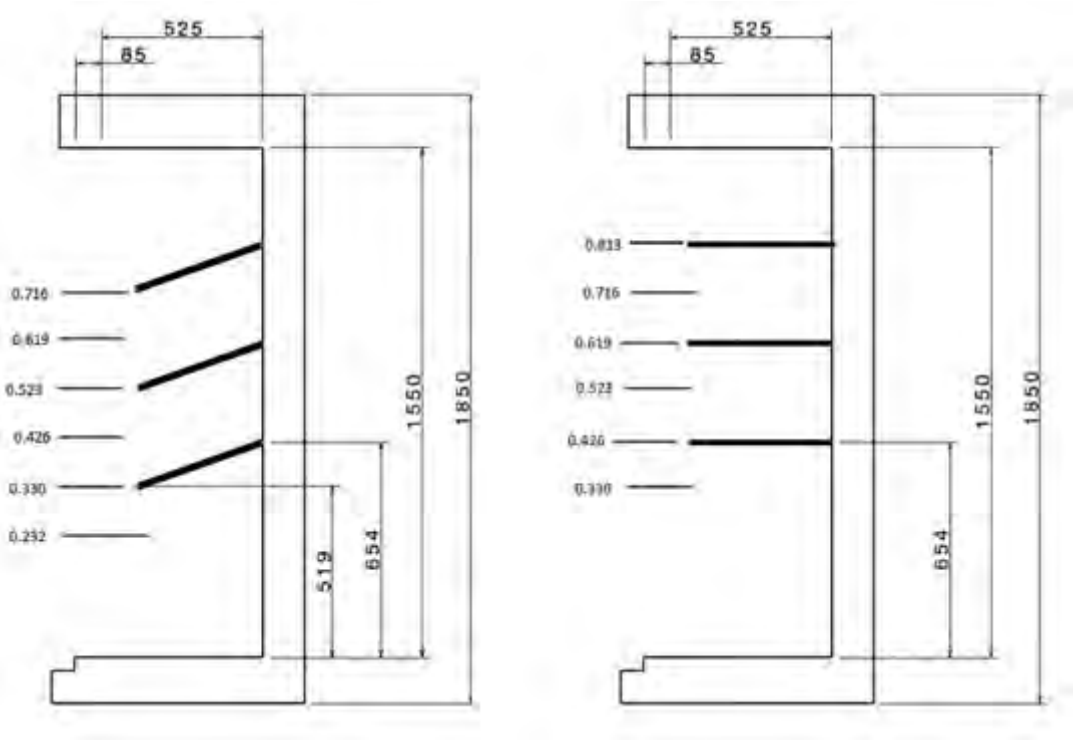

Fig. 2 Profile view of RDC with slanted and straight shelves

Refrigerated display cabinets (RDCs) are widely used by most supermarket and convenience stores around the world. They vary in size and storage capacity depending on what need each supermarket or grocery has to fulfill. The two main types are horizontal display cabinet and vertical. The main difference between the two is the height difference. The horizontal RDC are usually about one meter in height while vertical RDCs are typically 1.5 to 2 meters in height. This thesis will exclusively focus on vertical RDC and it should be noted that when referring to RDCs, it will always be referring to the vertical type. A typical vertical display cabinet can be seen in Fig. 1 and Fig. 2.

When products arrive in the store, they are usually placed in refrigerated cabinets for ease of purchase. Open RDCs, in particular, are popular because of this aspect. This ease of access has been shown to improve sales and attract customers and

that has been the justification for their use despite the increased energy use [1-4]. Open RDCs, aside from normal cabinets, have no door to interfere with the customer. Instead, a jet of air, or air curtain, is used to separate the cool refrigerated air from the warm store air. The main issue with RDCs is the inefficiencies tied with the air curtain. Some estimates say that 70% of the heating load of an RDC comes from the air curtain interacting with the ambient store environment [5]. Since 50 to 60% of a supermarket's energy consumption is given to run RDCs [6, 7], it is of great interest to all parties involved to improve the efficiency of RDCs. The costs associated with improving RDCs even by a small amount can be lucrative [8].

RDCs are designed for an air curtain to come down from the top of the cabinet and be drawn into the return grill and through the evaporator coils where it is cooled. Some air is then pushed through the holes in the back panel into the product area while the majority of the fluid is discharged through the vertical grill again to begin the cycle.

Research in relation to RDCs and air curtains is mainly split into two distinct fields, experimental and numerical. Experimental work has been performed on a wide range of cabinets using an assortment of different instruments. Most of these articles focus on validating the results for numerical work. The numerical work is more varied and covers validation, from parametric studies for optimization purposes, to new models being developed for more accurate comparison to experiments.

The purpose of this research is to investigate the nature of the air curtains on a transient and steady state level and to analyze the resource effectiveness of 2D versus 3D analysis of the air curtain. Also part of this research is to see the effects that straight and slanted shelves will cause to the efficiency of the air curtain

1.2 Factors affecting entrainment

Several key studies have been undertaken to understand the nature of air curtains. Ke Zhi Yu et al [9] focused on the parametric evaluation of the thermal entrainment factor of air curtains, and they concluded that the major factors in thermal entrainment consisted of several geometric and initial conditions of the air curtain. The thermal entrainment factor is calculated as follows for a single band RDC.

$$\boldsymbol{X} = \frac{\boldsymbol{T_r - T_s}}{\boldsymbol{T_a - T_s}} \qquad \text{eq (1)}$$

Where X is the thermal entrainment factor, Tr is the return grill air temperature, Ts is the supply temperature (or discharge grill temperature as references in this thesis) and Ta is the ambient temperature. The important factors highlighted in the paper were air curtain velocity, air curtain temperature, air curtain width, air curtain height, back panel flow and back panel temperature. These parameters were discovered to be the most influential in air curtain performance through the use of CFD. The results were compared to experimental results and the maximum deviation of values came at -9.4% while the average deviation across all values was only 0.1%. This evaluation using CFD is reliable enough to use and it should be a focus on changing these parameters to improve air curtain performance. It should be noted that with the thermal entrainment factor, the variable remains constant except due to significant geometrical changes to the cabinet or changes to the cooling system, affecting discharge and return grill temperature. Subtle changes, such as increasing the angle or slope of the shelves, would not be detected by this equation.

Chen et al [10] also published purely experimental research in 2005 that involved the temperature readings of a cabinet. Temperature sensors were placed on the

midplane of a RDC and the temperature was measured over time. It was noted that a correlation existed between the thermal entrainment of a RDC and the Reynolds number (Re) and Richardson number (Ri). In general, the higher the Re or Ri, the higher the thermal entrainment factor. It should also be noted that only three values were tested and the increase in thermal entrainment factor was small.

Zhikun Cao [11] stated that there were four main issues affecting the cooling loss of an RDC system based on his mathematical two fluid cooling loss model (CLTF). His results were also compared with temperature readings in front of shelves. First the lower the air supply temperature (in relation to the ambient air), the more the cooling loss would be; second, if the discharge grill velocity were to exceed 0.9 ms^{-1} that would lead to an increase in cooling loss; thirdly, the baffle position (height of the discharge grill in relation to cabinet) has an effect on the cooling loss; and finally, the ambient temperature and humidity have a large effect on the performance of an RDC. It should be noted that the system used to come to these conclusions was based on a RDC of specific parameters and as the parameters of the RDC changed, the less effective the CLTF would be. In addition to this, the model was mathematically and temperature based and could not make comments on how the suggested recommendations would affect the flow of the air curtain, only that certain changes in the discharge grill air had a positive or negative effect on the temperature and, therefore, the cooling loss. Validation of the model to experimental temperature results showed good agreement but the model was not able to simulate the temperatures on the lowest (fourth) shelf accurately. This is indicative of the problems with predicting the behavior of an air curtain in the lower regions of the cabinet. The breakdown of models on the lowest level

of the cabinet is a common problem in numerical modeling; all studies in general have a great difficulty getting experimental values to agree with numerical models, even with non-commercial in house code [12, 13].

Fields [7] mentioned the effects of Ri on RDCs. The authors stated that the higher Ri was, the more entrainment there was because of the buoyant acceleration encouraging instabilities. Entrainment was due primarily to eddy engulfment in isothermal curtains and low Ri so that the air curtain tended to neck inwards, toward the back panel. In fact, the higher the Ri, the more this effect became obvious.

Field also used Particle Image Velocimetry (PIV) to gather velocity data on a RDC with a wall instead of shelves. The entrainment was mainly due to high inlet turbulence and shear layer instabilities in the air curtain [5]. Air entrainment and eddy engulfment were also stated as the main reasons for the thermal instabilities of the air curtain [14].

(Re) is also an important value in another study of air curtains; several researchers have taken the time to assess its effects on the performance of RDCs [15-17]. Navaz et al [7] believed that the main causes of entrainment were the Re, the velocity profile and back panel flow; a low Re was better but it could not be reduced indiscriminately of other factors because if the Re was too low there would be no sealing effect of the air curtain. A separate study by Field also concluded that a low Re was better because the lower the Re the less energy loss there was to the system.

Amin et al [18, 19] produced a set of parameters that affect entrainment outside of the refrigeration effect on a RDC. The discharge grill temperature (at constant

ambient temperature) and buoyancy are not key factors in vertical RDCs. This was validated in subsequent work which also describes the momentum and the heat convection as the key factors to entrainment in specific cases where the momentum is sufficient. If the momentum drops below a critical value, however, the temperature difference and buoyancy take a predominant role over the convection and momentum [18]. According to Amin et al [19], Re of the discharge grill was also a key factor as well as the geometry of the cabinet. Since the Re of the cabinet studied is fixed due to geometrical constraints, this study will focus on the velocity fields in this specific geometric design. Since the Re states the momentum of the inlet, the effect that the shelf angle can be studied to see the effect on the maximum velocity due to the change in the shelf angle.

Further studies have shown that the Ri was one of quantity that was important and the subject of much commentary [2, 7, 20, 21]. Ri is defined as the ratio of potential energy to kinetic energy. Yun Guang Chen et al [2, 22] noted though CFD simulation that a Ri of 0.2 promoted good insulation in a wall cavity approximating an RDC without shelves. When the Ri value rises to 0.32, insulation was no longer achieved. It is important to note that the cabinet had a 2:1 height to depth ratio and the Ri would change based on these two values. The critical Ri number for a cabinet of this height to width ratio was 0.14; any deviation from this number would result in more entrainment. Mhiri [20]. found the critical Ri to be 0.1 with a slightly different cabinet design.

A study by Chen [21] noted that the lower the height to depth ratio was, the higher the Ri needed to be. This was a numerical study performed on a wall cavity calculation domain with three straight shelves. This meant that the initial momentum to

retain sealing was decreased, therefore, increasing the efficiency of the RDC. They also stated that the effect of shelves was significant in that if there is not enough initial momentum, the air curtain would move towards the back of the RDC due to the negative buoyant nature of the air curtain. Shelves alleviate this need for an optimum momentum to seal a non-shelves cabinet by providing a support structure for the air curtain to "bounce" off on. This causes the cabinet to be thermally sealed with a much lower air curtain momentum than with non-shelved RDCs. This would incur a decrease in energy consumption as there fan required to sustain the air curtain would not have to be as powerful. This work also presented dimensionless variables to assist the design of the cabinet. For the placement of shelves, it was mentioned that the horizontal distance from the discharge grill to the edge shelf over the width of the discharge grill should range from 0-0.5. These series of papers note the importance of shelves to sealing of the cabinet and allowing for less energy to be spent for the maintaining of the temperature and the air curtain and achieving the correct Ri number for the appropriate dimensions of the cabinet.

It was noted that for Ri increasing from 0 to 0.47 there was a greater tendency for the air from the discharge grill to get thinner immediately. The higher Ri was, the more prominent the negative buoyancy effect was. The spreading of the air curtain also had ties with Ri. As a high Ri leads the curtain to spread out more slowly, lower Ri leads the curtain to spread out more quickly. There was one exception to this rule in the Ri studied in this work but it was attributed to high turbulence levels of that particular curtain. This implies that high inlet turbulence also leads to a quicker spreading of the air curtain. This was attributed to the negative buoyant effect of the air curtain. The

negative buoyancy effects are no longer significant after the air curtain has travelled four discharge grill widths from the discharge grill. The air curtain behaves in an isothermal manner after this point and spreads as such. The range of non dimensional length studied did not see the peak velocity of the air curtain decrease significantly. The universal observation on all air curtain behavior was made: that after the region of buoyant acceleration, air curtains spread linearly along the length of the curtain [7]. The effect of the wall on the flow, however, is not negligible and neither is the effect of the shelves [21].

A robust study has been carried out on how having specific Ri numbers affect the sealing of an RDC. This was to assist those with limited knowledge of flow sciences to effectively improve an RDC without robust computational equipment. Hammond et al determined that while a low velocity is generally better for turbulence, the lower it becomes, the less likely the cabinet is to seal due to the lack of kinetic energy. The lack of sealing due to lower Re is can be seen by the air curtain deflecting inwards [23]. It should be noted that robust direct relationships have not been established to link subtle geometric changes to the cabinet to Ri. Such subtle changes, such as changing the angle of the shelves, can have an effect on the kinetic energy of the system, therefore, changing the Ri of the system indirectly. In addition the weakness in non dimensional relationships such as Ri is that the entire system is summarized by a single quantity. For simplifications sake, this is an adequate reason but to state that a system will be stable within geometrical standards can also oversimplify a problem.

In one experimental paper Evans et al [24] used packs made out of cellulose with the same thermal conductivity as raw meat to test the efficiency of RDCs. These

M-Packs were greatly affected by the geometry. Evans et al stated that even cabinets of similar designs could have very different temperature performance as seen by their M-pack experimental data. This study implies that everything from discharge and return grill placement, back panel hole placement, height width and shelf placement and angles are can be a significant contributing factor even in similarly designed cabinets.

An experimental study of eddy structures in air curtain systems by Loubiere concluded that the Re was responsible for the formation of vortices [16]. Field et al studies the nature of air curtains by replacing the product shelves with a wall. This allowed them to focus on the nature of air curtain behavior on a more fundamental level. In earlier work the inlet turbulence was kept high and it was concluded that turbulence is one of the causes of entrainment. Using a structure to limit the inlet turbulence, such as a honey comb, would limit the entrainment of the RDC [5]. The vortices engulf warm air and bring this warm air into the return grill, therefore increasing the heat load on the RDC [5, 7].

The flow from the back panel has been cited as a contributing factor in thermal sealing of the RDC [9, 17, 25]. Though it has been mentioned as important, no thorough investigation has been undertaken involving the effect of back panel flow. Navaz stated the importance of the back panel but opened the question as to what flow from the back panel was optimal for the support of the air curtain. The estimated entrainment rate calculated by the PIV system was also similar to the CFD simulations though not completely accurate [17]. Gray concluded that 70% of the air flow through an RDC should be delivered through the air curtain and 30% of the air should be delivered through the back panel [25]. Different patterns and configurations were not investigated

but it was mentioned that the back panel must be designed in a manner that allows the back panel flow to support the air curtain despite the presence of shelves or products.

The current state of numerical models in resolving these flow behaviors can be summarized as such: there are no transient models of open RDC to date and a grand majority are run as a 2D simulation. A deeper review of experimental and numerical techniques will be covered in chapters 2 and 3 respectively.

The velocity profiles of air curtains have not been widely investigated. The shelf angle and the effect on the air curtain, though related to the geometry, have not been carried out extensively. The kinetic energy of the air curtain can be observed using the velocity profile at different shelves. The change in the shelf angle can also be used to see the difference in the maximum velocity and lead to better efficiency and sealing. In addition to this, no paper to this date has analyzed an air curtain of an open RDC as a transient system. This study delivers results that analyze an open RDC using 2D and 3D computational analysis as well as discussing the impact of the angle of shelves on the flow field of the air curtain. This study uses experimental data to validate the results as well as experimental analysis and flow data to show the impact shelf angle has on the flow field.

CHAPTER 2 - EXPERIMENTAL METHODOLOGY

2.1 Introduction

The experimental work performed for this study was for two reasons. The first is to provide validation data to compare to the simulation results. The second was to analyze the effect of how the slanted and straight nature of the shelves affects the air curtain. This chapter details the laser system used to acquire the velocity data and the experimental setup and procedure, following a review of possible experimental techniques.

2.2 Experimental Techniques used for RDC Analysis

2.2.1 PIV

Particle Image Velocimetry (PIV) is a popular experimental technique to use with air curtains. There are several papers that use this technique to validate their numerical simulations [7, 17, 26]. Navaz et al used PIV to validate the CFD simulations. The CFD situations were very comparable to the PIV experimental data and proved to be a valuable tool for verification purposes. The estimated entrainment rate calculated by the PIV system was also similar to the CFD simulations though not completely accurate [17]. Further work by Navaz found that the PIV system was useful. An in-house code called ROYA was used for the CFD simulations and a general correlation between the experimental and numerical findings was established [26]. It is to be noted that the ROYA code has not seen widespread use.

Fields et al [15] used a PIV system to observe the eddy engulfment by replacing the shelves with a wall. This was to provide a more basic understanding of the nature of

air curtains without the interference of shelves. This study helped to qualitatively show the eddy engulfment in action via the PIV system.

2.2.2 LDV

Laser Doppler Velocimetry is another popular experimental technique. It can be used for a variety of fluids such as water and air and can be used to analyze complicated flow patterns and behaviors [27-31]. LDV experiments as far as ORCS are concerned are fairly few [17, 26]. In these papers, the LDV system was used to validate CFD results and proved adequate in doing so.

LDV was used to investigate the flow behavior at the discharge grill at two separate points along the length of the cabinet. This was used to see whether the cabinet can be assumed to be two dimensional in flow behavior. This was concluded to be the case [17].

LDV, in comparison to PIV, has only been conducted on a very limited scale due to the limited volume of measurement and time needed to measure a large volume such as an air curtain. Despite this, the fact remains that data gathered from LDV systems are quite reliable. LDV data were compared to PIV in the discharge and return grill section and the data were almost identical [17].

2.2.3 Infrared Thermography

Infrared Thermography is used in several papers regarding open RDCs [26, 32]. This experimental method involves gathering temperature data rather than velocity data like PIV and LDV systems. This is a strong technique if real time data is needed as the camera can record over a period of time [32] .

The main disadvantage with this technique is the need for a sheet to be placed within the flow in question. Thermal cameras are not able to record the temperature changes of ambient air; it must focus on a surface, in most cases a sheet, to display the temperature differences. Though somewhat reliable the data are not 100% accurate as the thermal sheet cannot be at the exact temperature of the flow [32]. For this reason, thermography should be limited to qualitative analysis only, not quantitative.

The main use of thermography, and all the experimental techniques mentioned above, was to validate numerical analysis. The real life data is crucial in the validating of CFD simulations.

2.2.4 Tracer Gas technique

The tracer gas technique is a unique way of analyzing the entrainment rate of RDCs. The method involves the introduction of a tracer gas into the RDC system. The volume introduced is carefully controlled and the RDC allowed to run until the tracer gas is detected and reduced to zero. Using mass flow rate equations the quantity of tracer gas taken out of the system over time is calculated. This allowed for the calculation of the entrainment rate. This is a relatively new technique and, therefore, has not seen widespread use [8].

2.2.5 Temperature probes

Chen et al [10] published an experimental paper in 2005 that involved the temperature readings of a cabinet. Temperature sensors were placed on the midplane of an RDC and the temperature measured over time. It was noted that a correlation existed between the thermal entrainment of an RDC and the Re (Re) and Richardson number (Ri), where Re is the ratio of inertia forces to viscous forces and Ri is the ratio of potential to kinetic energy. In general, the higher the Re or Ri, the higher the thermal entrainment factor. It should be noted that only three values were tested and the increase in thermal entrainment factor was small. The perforation of the back panel was also briefly examined. In the author's paper, the cabinet was run with three different perforations patterns on the back panel sections. These perforations were not show in any figures but stated in numerical form as perforations density. The effects noted were that the more densely perforated the back panel, the lower the temperature overall. It can only be assumed that the perforations were uniform in characteristics as no schematic was given of the back panel. Subsequent air velocities were not given with more perforations of the back panel. This brief investigation gives reason to further investigate the possibilities of using the back panel to not only cool the RDC as a whole but further investigate the interactions between back panel flow and air curtain [10].

2.2.6 Experimental Technique Overview

There is not a large amount of velocity profile data regarding RDC despite the important role it plays in the validation of simulations. Only Field [5, 15] uses experiments to examine flow behavior of air curtains without the aid of numerical techniques. Other published work use experimental data for validation purposes only. Using simulations can be useful and less time consuming; however, the experimental

area should be explored more in varied situations to make sure the true nature of air curtains is understood.

A combination of certain techniques has been used to study phenomena related to RDC but on a less theoretical approach. One such example (Ndoye et al [33]) where temperature probes and a traverse system were used to measure temperature along the width of two cabinets facing one another. The results were a detailed temperature analysis of the "cold aisle effect" produced by the spilling of the air curtain into the aisle. They also used flow visualization to see the flow patterns associated with the "cold aisle effect". Given the available technique it was considered that LDV would give the insight required for this problem.

2.3 Experimental Systems

2.3.1 Laser Doppler Velocimetry

LDV laser systems allow for non intrusive acquisition of velocity data from a flow field. The general theory used behind these systems will be discussed below while the following sections will detail the experimental setup.

LDV systems use monochromatic crossing lasers to measure the velocity of a flow field. The crossing lasers produce a fringe interference which is detected by a probe within the system. This fringe changes when a particle (typically seeded within the flow) passes through the measurement volume of the crossing lasers. Through the Doppler effect, the velocity can be measured in this manner.

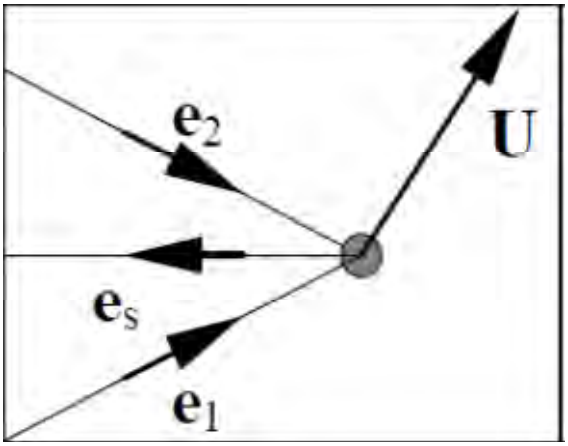

Fig. 3 - Diagram of Two Light Sources with Backscatter (BSA Flow Software Reference Guide)

The above diagram shows an example of two light sources reflecting off a light. Particle where e_1 and e_2 indicate vectors of incoming light e_s indicates the vector of backscattering

$$f_{s,1} = f_1\left[1 + \tfrac{\mathbf{U}}{c} \cdot (e_s - e_1)\right]$$
$$f_{s,2} = f_2\left[1 + \tfrac{\mathbf{U}}{c} \cdot (e_s - e_2)\right] \qquad \text{eq. (2)}$$

Where f_s denotes the frequency of the light the receiver perceives, f indicates the frequency of the light being emitted, **U** indicates the velocity vector being measured and c is the speed of light. The measurements are made more feasible by splitting a single laser into two and having the two parts cross. So this means $f_1 = f_2$. This allows for what's called a beat frequency to be calculated. So,

$$f_D = f_{s,2} - f_{s,1}$$
$$= f_2\left[1 + \tfrac{\mathbf{U}}{c} \cdot (e_s - e_2)\right] - f_1\left[1 + \tfrac{\mathbf{U}}{c} \cdot (e_s - e_1)\right]$$

Since $f_2 = f_1$,

$$
\begin{aligned}
f_D &= f_I\left[\tfrac{\mathbf{U}}{c}\cdot(e_1 - e_2)\right] \\
&= \frac{f_I}{c}\left[\left|e_1 - e_2\right|\cdot\left|\mathbf{U}\right|\cdot\cos(\varphi)\right] \\
&= \frac{1}{\lambda}\cdot 2\sin\left(\frac{\theta}{2}\right)\cdot u_x \\
&= \frac{2\sin\left(\frac{\theta}{2}\right)}{\lambda}u_x
\end{aligned}
\qquad \text{eq. (3)}
$$

Where f_D is the beat frequency, θ is the angle between the incoming lasers and φ is the angle between the vector **U** and the direction of the measured flow field.

2.4 Experimental Setup – LDV

Fig. 4 Refrigerated Display Cabinets with Laser Doppler Velocimetry Probe

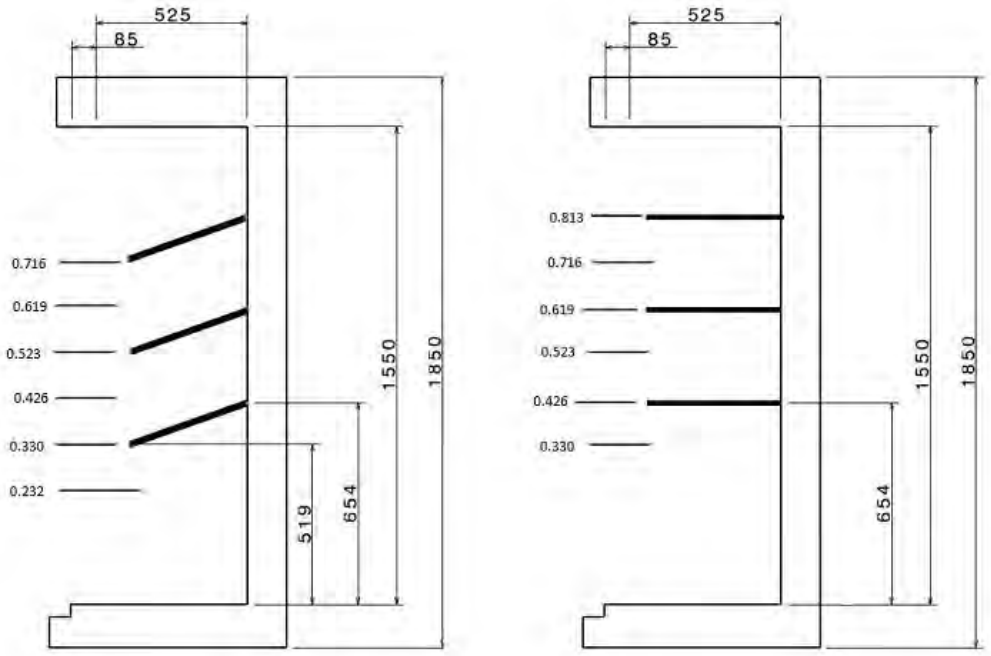

Fig. 5 - Cabinet configuration and heights of LDV measurements of the flow field in mm

The RDC shown in Fig. 5 is 1224 mm wide, 1570 mm tall from discharge to return grill and 610 mm deep from the edge of discharge to the back panel. The horizontal lines represent the locations where the measurements were taken and the numbers are the non dimensional height. The model number was an Austral XM20S1M5G-4W used with refrigerant R404A. The refrigerator rating is 2567W based on 75% runtime after defrost AS1731.12 for climate class 3. A fog machine, model M-6000, was used to seed the flow and determine the draught in the room with and without the ventilation system over several days. There was no appreciable effect on the fog. Temperature readings of the room were taken at different times of the day for several days and it remained consistent at around 24 degrees Celsius.

The one-dimensional LDV system model (see Fig. 4) is a Measurement Science Enterprise Inc mini-LDV-G5-240 diode laser. The LDV laser system has a fringe

spacing of 9.01 nm at a wavelength of 658 nm with max power set at 60 mW. The measured probe volume is 240mm away the probe with the dimensions of 150 X 300 μm by 4 mm.

The probe was mounted on a three dimensional DANTEC traverse displacement system capable of moving in three perpendicular directions parallel to the cabinets' height, width and length in increments of 0.01mm. The traverse system has a movement range of 0.5 meters in a defined X, Y, and Z direction. This displacement system was not able to cover the entire range of the cabinet, so custom brackets and mounts were manufactured in order to achieve the desired range required to cover the entire height of the cabinet.

The burst signal processing program used to collect velocity data is provided with the LDV system. The program then uses the frequency detected by the LDV of the seeded flow to determine velocity using the Doppler effect (discussed above). The back of the cabinet was painted matt black in order to prevent the laser from scattering or reflecting from the back of the cabinet to the laser sensor, which can cause inaccuracies in the data. Each data point was taken in a 60 second intervals.

The procedure and equipment to measure the back panel flow is identical to measuring the discharge grill flow except the laser is mounted on a bracket that turns it 90 degrees. This is so the laser is perpendicular to the flow in question. The measurements were taken in levels just as in measuring the discharge flow. These levels are slightly different and correspond directly to the 32 holes in the back panel. The measurement volume is sufficiently small enough to get flow just in front of the hole. The size of the probe prevents the measurement volume to approach closer than 3 cm to

the back panel holes. As such, it is not the actual back panel flow data but it is close enough to approximate and use for CFD analysis.

2.5 Experimental Procedure – LDV

2.5.1 Discharge grill to return grill flow

The RDC was turned on and let to run for about ten minutes to allow the air curtain temperature to stabilize. Once this was done, the traversing system was moved every sixty seconds to give sufficient time for the laser to gather the velocity data.

The cabinet is seeded with the M-6000 model fog machine through the return grill so that the fog runs through the cooling coils before being discharged. The fog machine was used in controlled bursts to seed the flow.

Measurements were taken at six discrete heights on the cabinet. At each height, the laser was moved along the width of the air curtain to take three measurements every five millimeters until the velocity of the profile reached 20% of the maximum velocity. The number of points taken across the width varied with respect to the height of the cabinet as the more confined the flow was, the fewer points that needed to be taken to reach the limits of the air curtain. Three measurements were taken at each point in this manner in order to account for the inconsistent flow behavior on the lower levels of the cabinet. These measurements were repeated several times for repeatability and the results were averaged for each discrete point measured. The largest standard deviation of all data lines gathered at a distinct height was 0.045 and the lowest was 0.019.

2.5.2 Back panel flow

The measurements were taken in levels just as in measuring the discharge flow. These levels are slightly different and correspond directly to the 32 holes in the back panel. The measurement volume is sufficiently small enough to get flow just in front of the hole. The size of the probe prevents the measurement volume to approach closer than 3 cm to the back panel holes. As such, it is not the actual back panel flow data but it is close enough to approximate and use for CFD analysis.

2.6 Experimental Setup – Laser sheet

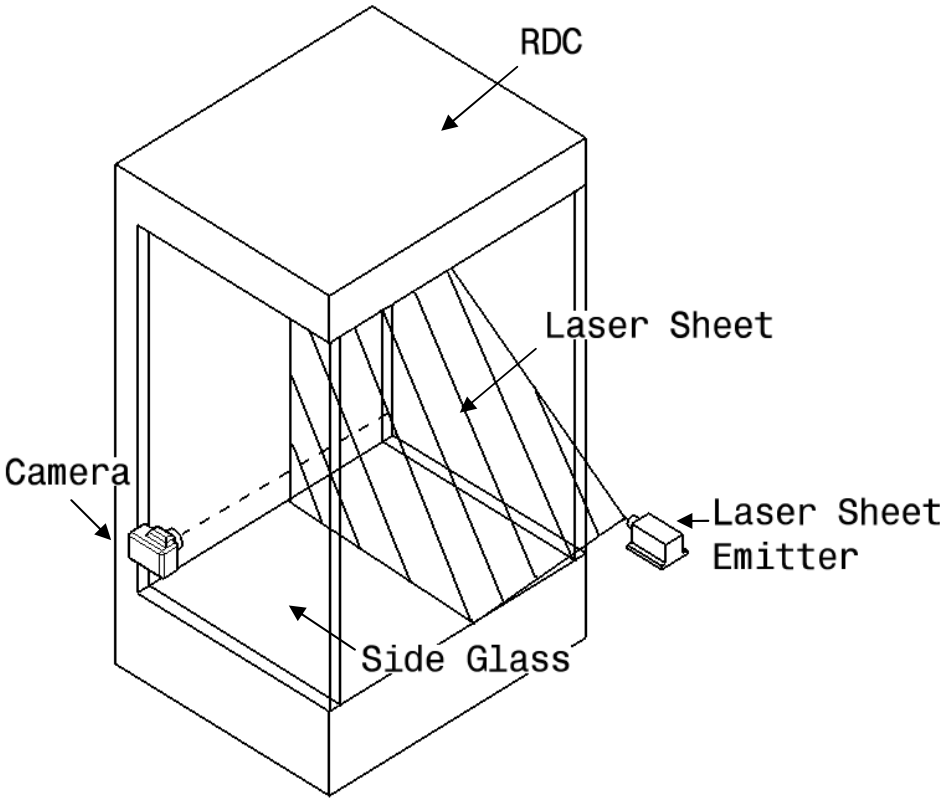

Fig. 6 - Isometric view of Cabinet with Laser Sheet

Flow visualization was performed on the cabinet to determine the location of the air curtain. The laser sheet had a power rating of 500mv and the laser frequency was

532nm. The sheet was placed in the midplane of the cabinet with a camera perpendicular to the sheet. The flow was then seeded from the return grill and photos were taken with a Nikon E90 camera. The result was the midplane being illuminated by the laser sheet, giving an overview of how the flow behaved.

The laser sheet was mounted on a movable pedestal and fixed with clamps and bolts. It was then positioned at the optimal distance so that the laser was illuminating the entire height of the cabinet in the midplane of the RDC. The camera was placed perpendicular to the laser sheet behind the glass side of the RDC. The camera was set to the highest light sensitivity of 1200 in the ISO option for brightness and a 0.2-0.4 second shutter time for clarity and definition of the flow regime.

2.7 Experimental Procedure – Laser sheet

All the lights were extinguished in the outside environment so as to allow for the illumination of the flow to be clearer. The cabinet was warmed up for ten minutes so the air curtain could stabilize. A fog machine was used to seed the flow at the return grill of the RDC and was blown until the laser sheet illuminated the flow. Photos were then taken using a Nikon E90 camera until insufficient number of fog particles illuminated the flow. The fog machine was used to reseed the flow. Several hundred photos were taken to ensure that the air curtain behavior would be captured. The same procedure was completed on the RDC with the shelves removed.

2.8 Experimental setup - Thermocouples

The RDC is set up in a room with a stable temperature atmosphere and the refrigerator was left to run for several defrost cycles while the data logger records the temperature every five seconds. This allows for a full range of temperature to be gathered and the temperature at the coldest possible of the RDC to be attained. The 34 channels are connected to two 32 channel slots in the data collection device, seventeen in each.

The refrigerator was hooked up to a series of thermocouples to measure the temperature, they were 24G Teflon coated thermocouples hooked up to a NI data collector and the collector connected to a PC. A labview program was used to gather the data. There were 34 channels of data being measured one for the return grill, one for the discharge grill and remaining for the 32 back panel holes on the midplane of the RDC. A heat bath was used for the calibration of the thermocouples. The heat bath was set at several temperatures and the electrical output of the thermocouples measured. The temperatures were then compared to the thermocouple output and calibrated appropriately.

The thermocouples are set into place without blocking any of the back panel holes. The thermocouple wires were run along the inside of the cabinet to ensure that the airflow is not disturbed by the presence of the cables. Each thermocouple head is soldered together to provide more accurate data in each area, especially the small area associated with the back panel holes.

CHAPTER 3 - NUMERICAL METHODOLOGY

3.1 Introduction

In this Section the numerical model is discussed, assumptions and boundary conditions are listed and justified. A discussion of the numerical models used in this study as well as rationale on the use of the current model and systems are then presented. Please refer to Fig. 5 and section 2.4 for physical characteristics of the RDC.

3.2 Numerical Simulations and Models used for RDC Analysis

Computational Fluid Dynamics (CFD) is complex fluid based problems and can be studied by solving the governing equations of fluid flow, the Navier Stokes equations. It is a far more inexpensive way of studying different configurations of fluid flow without having to build an expensive experimental rig [34]. Before 2000, most CFD codes were developed in house and used to model very specific problems. The more popular use of CFD in recent years has caused a surge of commercial codes to be written for the ease of the user. As of 2006, there were 15 commercial codes available [34]. A wide number of sources agree that CFD is a very useful tool in optimization and analysis of RDCs, air curtains in general and heat transfer regarding food processes [34-40]. As with any CFD it is imperative that the results of the simulation are compared with real experimental data [7, 17, 26]. It is interesting to note that all published RDC simulations have been carried out in steady state analysis. Smale et al [34] published a review of the numerical models for refrigerated food applications. A main point to this publication was the accuracy of the widely popular k-ε model. It was stated that k-e model and its many variants have difficulty comparing to experimental results [34]. This seems to be only true in certain applications where complex fluid flows exist because numerous papers have stated that the results are in good enough agreement with

experimental data for engineering applications [9, 21, 41]. RDCs, however, do experience very complex fluid flow patterns simply by the interaction of the air curtain with the ambient air.

More accurate models have been developed and tested in recent years. These new models, called the Two Fluid (TF) model and Modified Two Fluid (MTF) model, were developed by Ke-Zhi Yu et al. The models were compared to k-ε, Reynolds Stress, LES, Low Reynolds Stress and Free Jet. TF and MTF were found to be more accurate than all the other models tested, especially in predicting the spilling for the air curtain. It should be noted that the experimental temperature data gathered at the lower end of the cabinet did not match well with TF and MTF. This was the same of all other models as well. The use of these new models has not been seen outside of their own developed papers [12, 13]. It should be further noted that the results of these papers did not show good agreement at the lower regions of the cabinet. It can be concluded that the low areas of the cabinet show a complex flow regime difficult to resolve numerically.

A more recent work using the MTF was published with another algorithm called the adaptive support vector machine. With this, the energy consumption and the defrosting water quality were seen to reduce significantly using the predicted parameters by these two models [42].

Only one CFD study available used a full 3D simulation [34]. This 3D CFD study was conducted by D'agaro et al [43] The main finding was that 3D effects were not negligible in cabinets under 2 meters long. In fact, according to the simulation and actual experimental data, cabinets of this nature have a 20% reduced efficiency. Ambient room velocity also proved to be an important aspect in RDC performance. The

experimental results and the results of the full 3D simulation were not comparable. This is caused by the complexity of the model and the uncertain nature of the boundary conditions.

Foster et al [44] performed a full 3D simulation of an air curtain to restrict cold room infiltration. For this particular application of air curtain technology, the flow cannot be considered to be 2D in nature. The importance of validating the data with experimental LDA experiments was also mentioned even though it was not performed.

No investigation to date has analyzed the air curtain in a transient state. As all publications thus far have been published at a steady state analysis, treating the system as quasi steady and analyzing the system in a transient model needs to be performed in order to investigate if the transient analysis could improve the numerical results. This chapter investigates both 2D and 3D numerical models of an RDC. These findings would allow for not only more accurate results but also assist in the performance requirements needed to run a full 3D case.

3.3 Governing equations for the Flow Field

The numerical model was carried out using the commercial Computational Fluid Dynamic (CFD) package ANSYS 12.0. In its most basic from, CFD solves flow field problems by discretizing the governing equations using finite volume method, and solving the flow field in each discrete gridpoint of computational domain. The governing equations for the flow field can be written as following:

Conservation of mass

$$\frac{\partial \rho}{\partial t} + \frac{\partial (\rho u)}{\partial x} + \frac{\partial (\rho v)}{\partial y} + \frac{\partial (\rho w)}{\partial z} = 0 \qquad \text{eq. (4)}$$

Conservation of momentum

In x direction:

$$\frac{\partial (\rho u)}{\partial t} + \frac{\partial (\rho u^2)}{\partial x} + \frac{\partial (\rho uv)}{\partial y} + \frac{\partial (\rho uw)}{\partial z} = -\frac{\partial \rho}{\partial x} + \frac{1}{\mathrm{Re}}\left[\frac{\partial \tau_{xx}}{\partial x} + \frac{\partial \tau_{xy}}{\partial y} + \frac{\partial \tau_{xz}}{\partial z}\right] \qquad \text{eq. (5)}$$

In y direction:

$$\frac{\partial (\rho v)}{\partial t} + \frac{\partial (\rho uv\ )}{\partial x} + \frac{\partial (\rho v^2)}{\partial y} + \frac{\partial (\rho vw)}{\partial z} = -\frac{\partial \rho}{\partial y} + \frac{1}{\mathrm{Re}}\left[\frac{\partial \tau_{xy}}{\partial x} + \frac{\partial \tau_{yy}}{\partial y} + \frac{\partial \tau_{yz}}{\partial z}\right] \qquad \text{eq. (6)}$$

In z direction:

$$\frac{\partial (\rho w)}{\partial t} + \frac{\partial (\rho uw)}{\partial x} + \frac{\partial (\rho vw)}{\partial y} + \frac{\partial (\rho w^2)}{\partial z} = -\frac{\partial \rho}{\partial z} + \frac{1}{\mathrm{Re}}\left[\frac{\partial \tau_{xz}}{\partial x} + \frac{\partial \tau_{yz}}{\partial y} + \frac{\partial \tau_{zz}}{\partial z}\right] \qquad \text{eq. (7)}$$

Conservation of energy

$$\frac{\partial (\rho E_T)}{\partial t} + \frac{\partial (uE_T)}{\partial x} + \frac{\partial (\rho vE_T)}{\partial y} \frac{\partial (\rho wE_T)}{\partial z} = -\frac{\partial (up)}{\partial x} - \frac{\partial (vp)}{\partial x} - \frac{\partial (wp)}{\partial x} - \frac{1}{\mathrm{RePr}}\left[\frac{\partial q_x}{\partial x} + \frac{\partial q_y}{\partial y} + \frac{\partial q_z}{\partial z}\right]$$
$$+ \frac{1}{\mathrm{Re}}\left[\frac{\partial}{\partial x}\left(u\tau_{xx} + v\tau_{xy} + w\tau_{xz}\right) + \frac{\partial}{\partial y}\left(u\tau_{xy} + v\tau_{yy} + w\tau_{yz}\right) + \frac{\partial}{\partial z}\left(u\tau_{xz} + v\tau_{yz} + w\tau_{zz}\right)\right] \qquad \text{eq. (8)}$$

Two sets of the computational models were constructed and used for simulations of the flow; one was a three dimensional model which was used for steady state calculations and another one was a two dimensional model which was used for transient calculations. These models are described below.

3.4 Three Dimensional Models

3.4.1 Straight Shelf Mesh

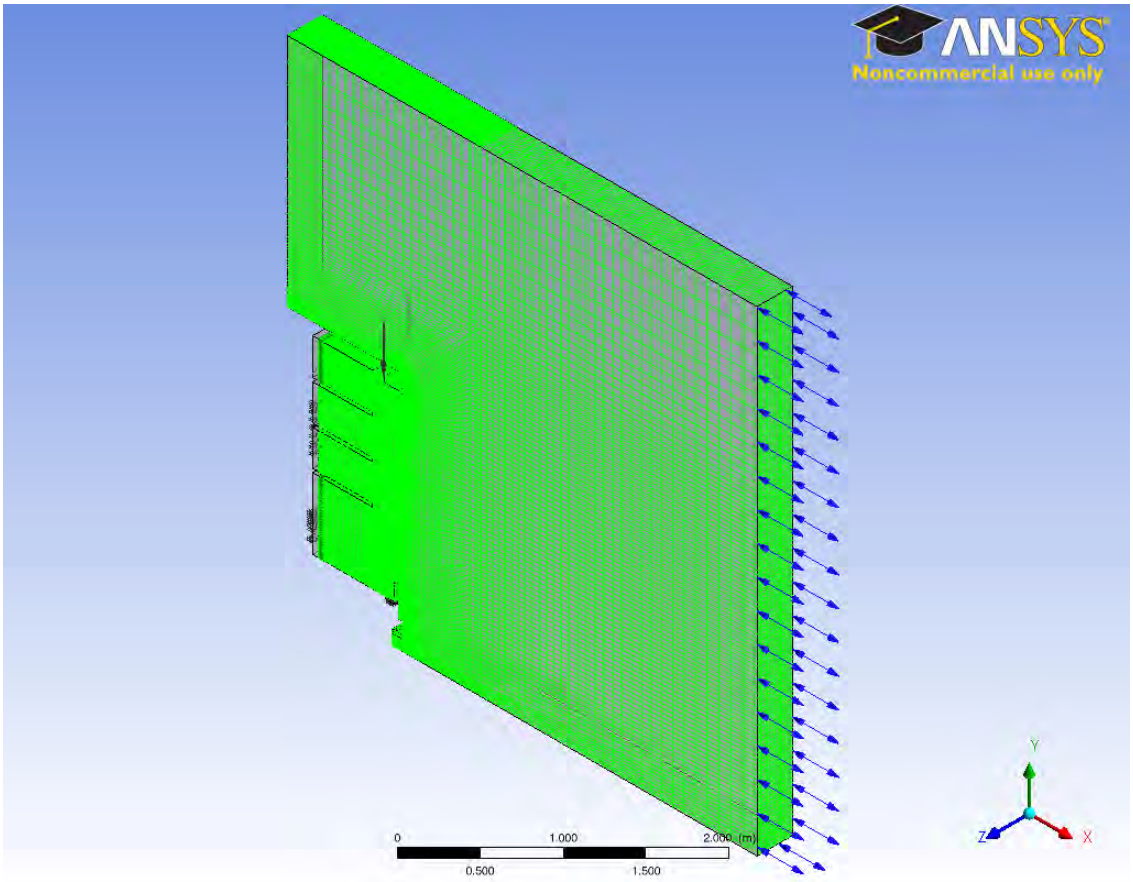

Fig. 7 Three Dimensional Straight Shelf Model of an Open Refrigerated Display Cabinet

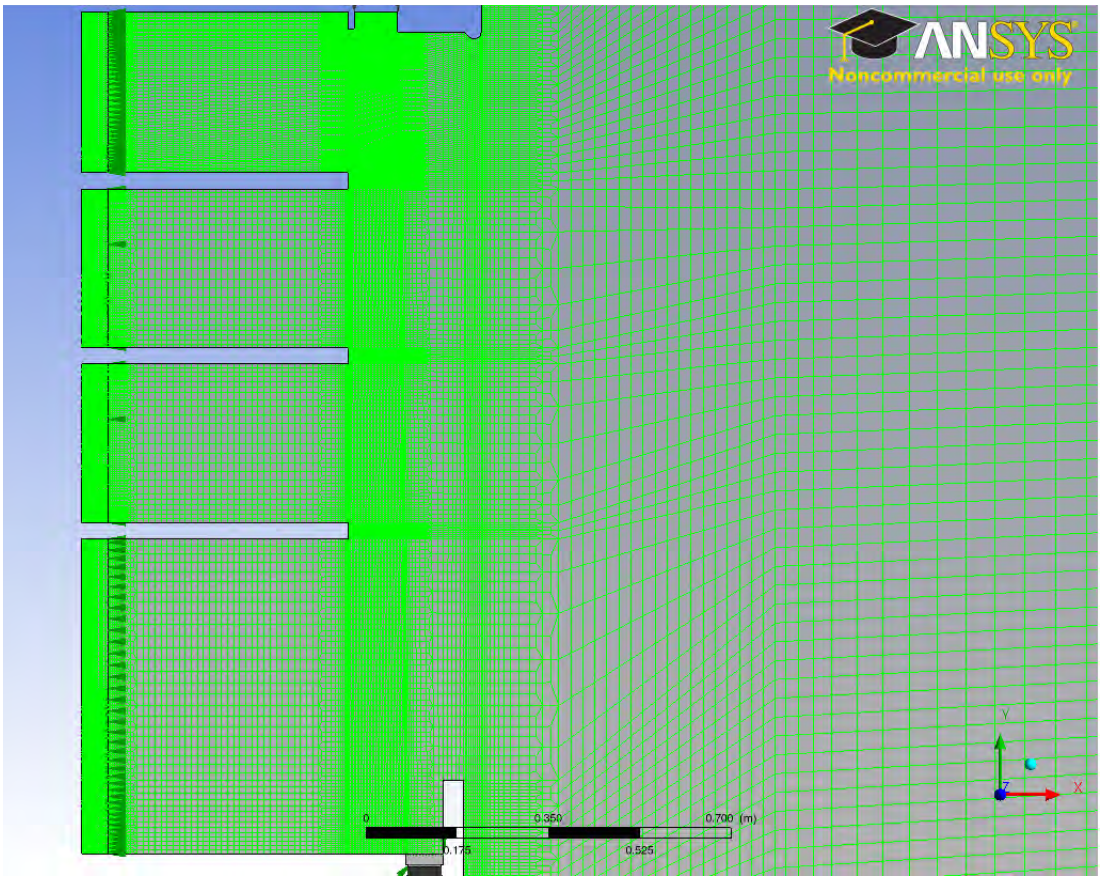

Fig. 8 – Enlarged View of 3D Straight Shelf Mesh

The three dimensional model has been constructed with the total mesh count of 7.95 million elements. The turbulence model was set as Shear Stress Transport (SST) in the ANSYS CFX for steady state and transient state. SST proved to be the most stable across all runs in transient and steady state. Other models such as k ε models were either not stable or did not reach a desirable level of convergence. The transient time step was set at 0.05s real time with maximum 20 iterations per time step.

The three dimensional model dimensions were based on the geometrical parameters of real open refrigeration cabinet (CAD file given by our industrial partner AUSTRAL). The mesh for the flow domain consists mostly of a structured grid except the back panel sections, the discharge and return grill. Due to the limitations of current

computing power and the need to create a fine mesh for the back panel holes, the mesh had to be non conformal. There were five sections that had non conformal boundaries with the main body, the four back panels and the return grill. The top back panel mesh count was 386,900 elements, the second from the top back panel was 967,600 elements, the third from the top back panel mesh was 1,114,800 elements, the bottom back panel was 1,553,600 elements and the return grill had 235,604 elements.

The simulation was run on a cluster off site and used 16 cpus with 30gb of RAM. For a steady state simulation about 300 iterations were attained for 14 hours of real time running on the cluster. A fully rendered cabinet would take much more processing power than the numbers quoted above with a much higher demand for cpu and RAM. Due to computational limitations, a transient version of the 3D simulation was not run.

3.4.2 Straight Shelf Boundary Conditions for Three Dimensional Model

The boundary conditions for the three dimensional simulation, except the side boundaries, are all based on the experimental data gathered with either the LDV or thermocouples. The side boundary conditions proved difficult to replicate since it was a mid section slice and not a full rendering of the cabinet. Thus, a different set of experimental data was gathered with walls erected in the physical cabinet in order to better replicate the real life situation in the numerical model. The side boundaries in the three dimensional simulation were set as the walls. The boundary condition farthest from the cabinet was set as an open boundary. The summary of all other parameters used at the boundaries of computational domain is presented in the table 1 below.

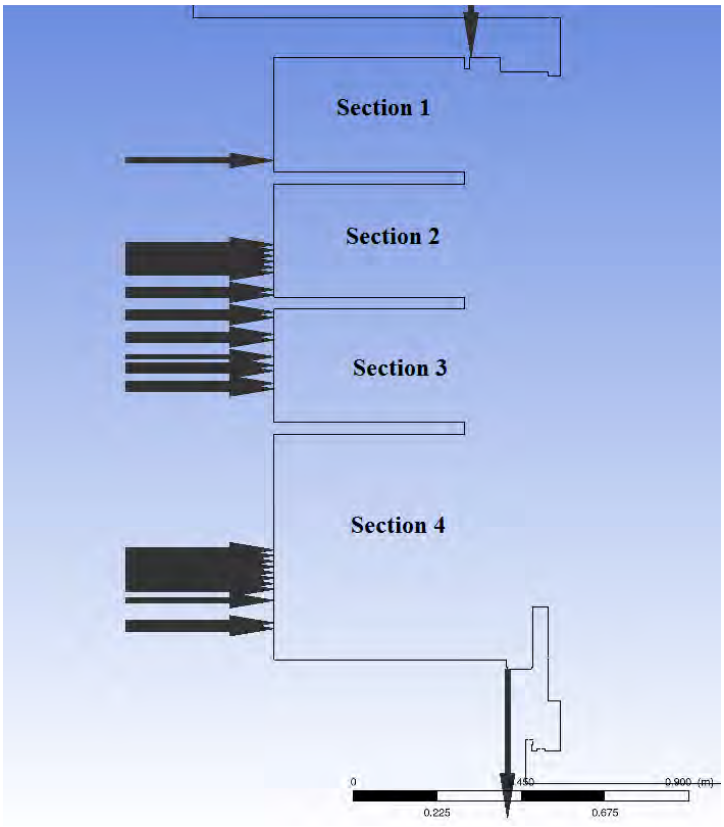

Fig. 9 - Back Panel Inlet and Sections Diagram

Each section in Table 1 is detailed in Fig. 9 above. The rows in the table are referring to the inlets indicated by the black arrows pointing to the back of the cabinet. Each row was assigned a specific velocity and temperature value as dictated by experimental results.

Table 1 – Boundary Conditions for Inlets and Return Grill

Boundary	Velocity Applied (ms^{-1})	Temperature Applied (C)
Discharge Grill	1.0 peak velocity, parabolic profile	-5
Section 1 Row 1 Back Panel	0.52	2.34
Section 1 Row 2 Back Panel	0.1	1.5
Section 2 Row 1 Back Panel	0.28	2.75
Section 2 Row 2 Back Panel	0.38	1.8
Section 2 Row 3 Back Panel	0.46	1.78
Section 2 Row 4 Back Panel	0.43	1.5
Section 2 Row 5 Back Panel	0.3	2.17
Section 2 Row 6 Back Panel	0.19	1.5
Section 2 Row 7 Back Panel	0.21	1.13
Section 2 Row 8 Back Panel	0.27	1.24
Section 3 Row 1 Back Panel	0.25	1.4
Section 3 Row 2 Back Panel	0.15	0.82
Section 3 Row 3 Back Panel	0.15	1.4
Section 3 Row 4 Back Panel	0.43	1.94
Section 3 Row 5 Back Panel	0.34	1.4
Section 3 Row 6 Back Panel	0.27	1.73
Section 3 Row 7 Back Panel	0.38	1.4
Section 3 Row 8 Back Panel	0.47	0.96
Section 3 Row 9 Back Panel	0.13	2.95
Section 4 Row 1 Back Panel	0.16	1.5

Section 4 Row 2 Back Panel	0.2	4.03
Section 4 Row 3 Back Panel	0.17	3.51
Section 4 Row 4 Back Panel	0.11	2.02
Section 4 Row 5 Back Panel	0.2	2.1
Section 4 Row 6 Back Panel	0.22	3.57
Section 4 Row 7 Back Panel	0.12	3.12
Section 4 Row 8 Back Panel	0.12	3.5
Section 4 Row 9 Back Panel	0.21	3.23
Section 4 Row 10 Back Panel	0.23	3.48
Section 4 Row 11Back Panel	0.23	3.17
Discharge Grill	1.1 peak velocity, linear profile as dictated by Experimental data	N/A

3.4.3 Slanted Shelf 3D Mesh

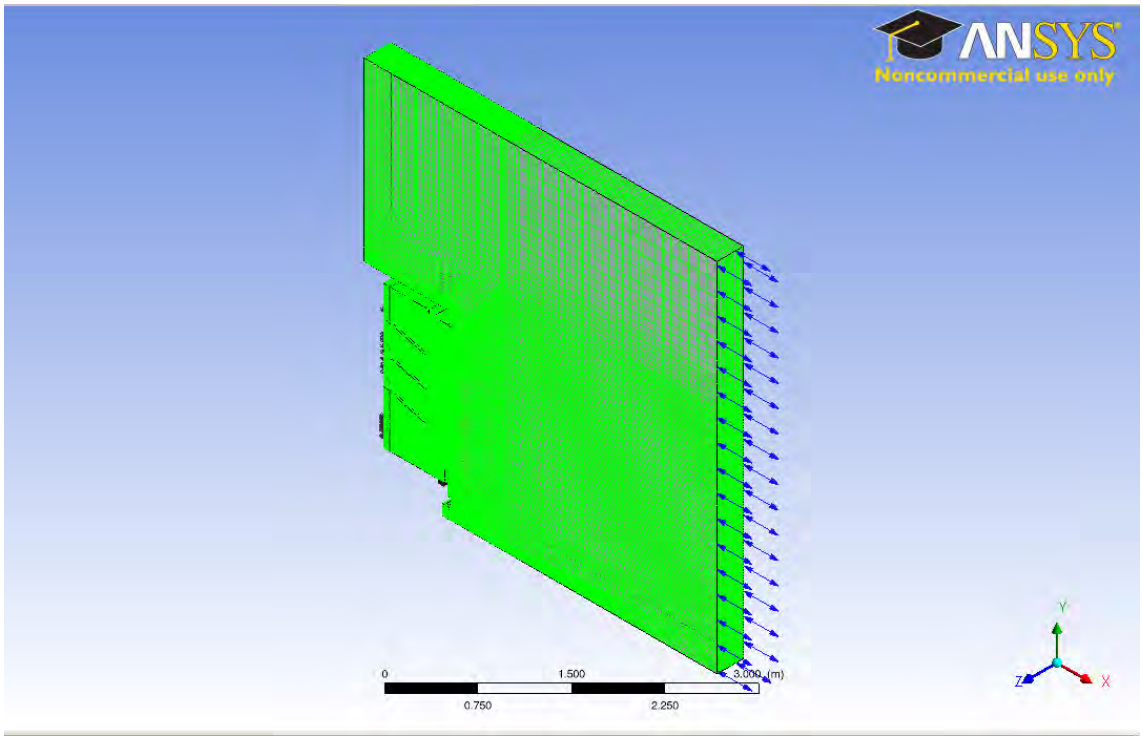

Fig. 10 - Isometric view of 3D Slanted Shelf Mesh

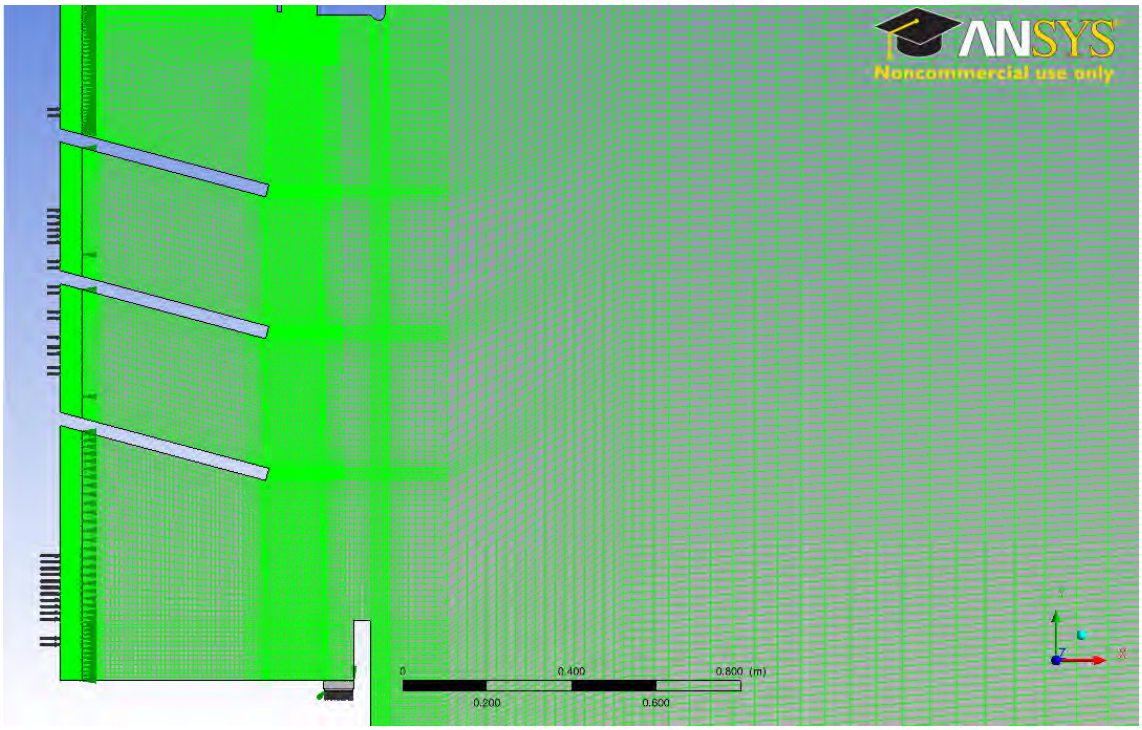

Fig. 11 - Enlarged View of 3D Slanted Shelf Mesh

The slanted shelf 3D mesh has 8.3 million elements in total and uses the same turbulence model as its straight shelf counterpart (SST). The back panel mesh is the same as for the 3D straight shelf mesh and the same computer system was used for this mesh. For more information see section 3.4.1.

3.4.4 Slanted Shelf Boundary Conditions for Three Dimensional Model

The boundary conditions for the slanted 3D mesh configuration are the same for the straight shelf configuration (see Table 1)

3.5 Two Dimensional Models

3.5.1 Straight Shelf Mesh

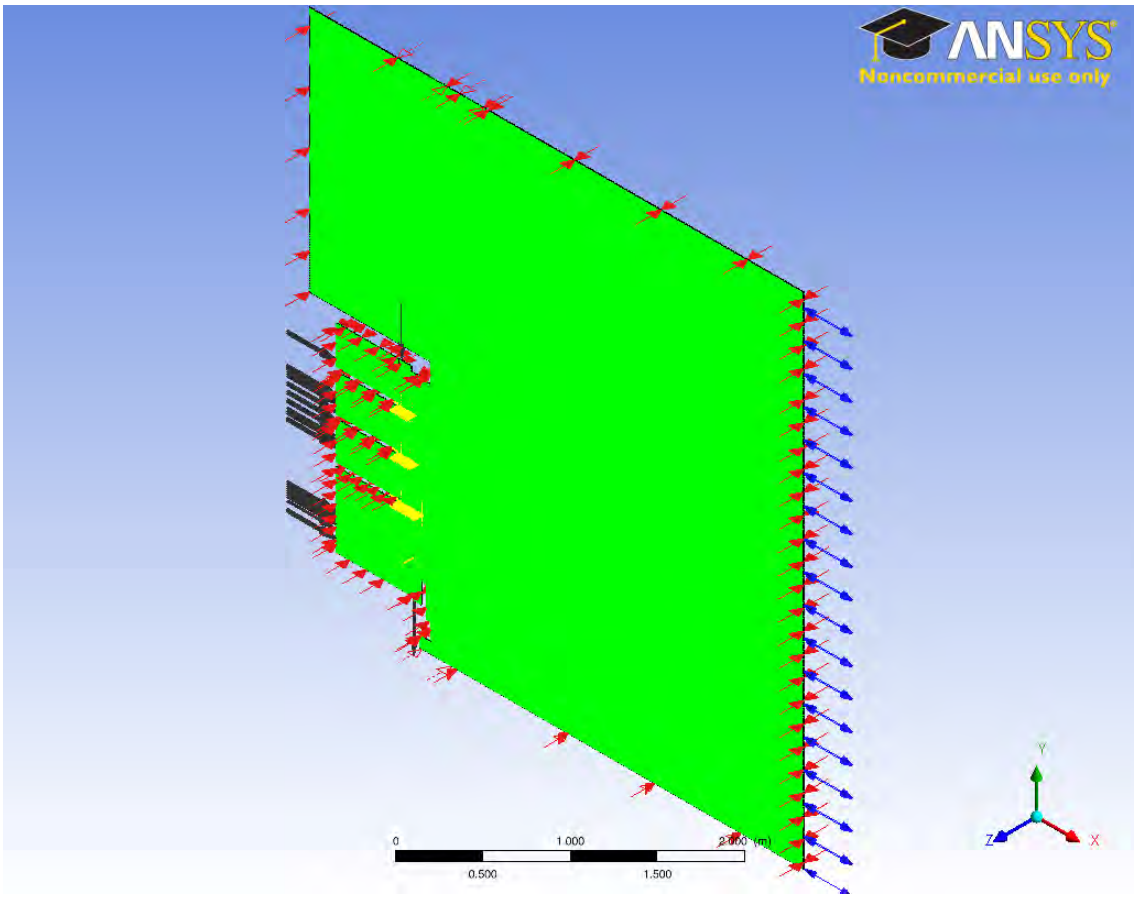

Fig. 12 – Two Dimensional Model of Straight Shelf Open Refrigerated Display Cabinet

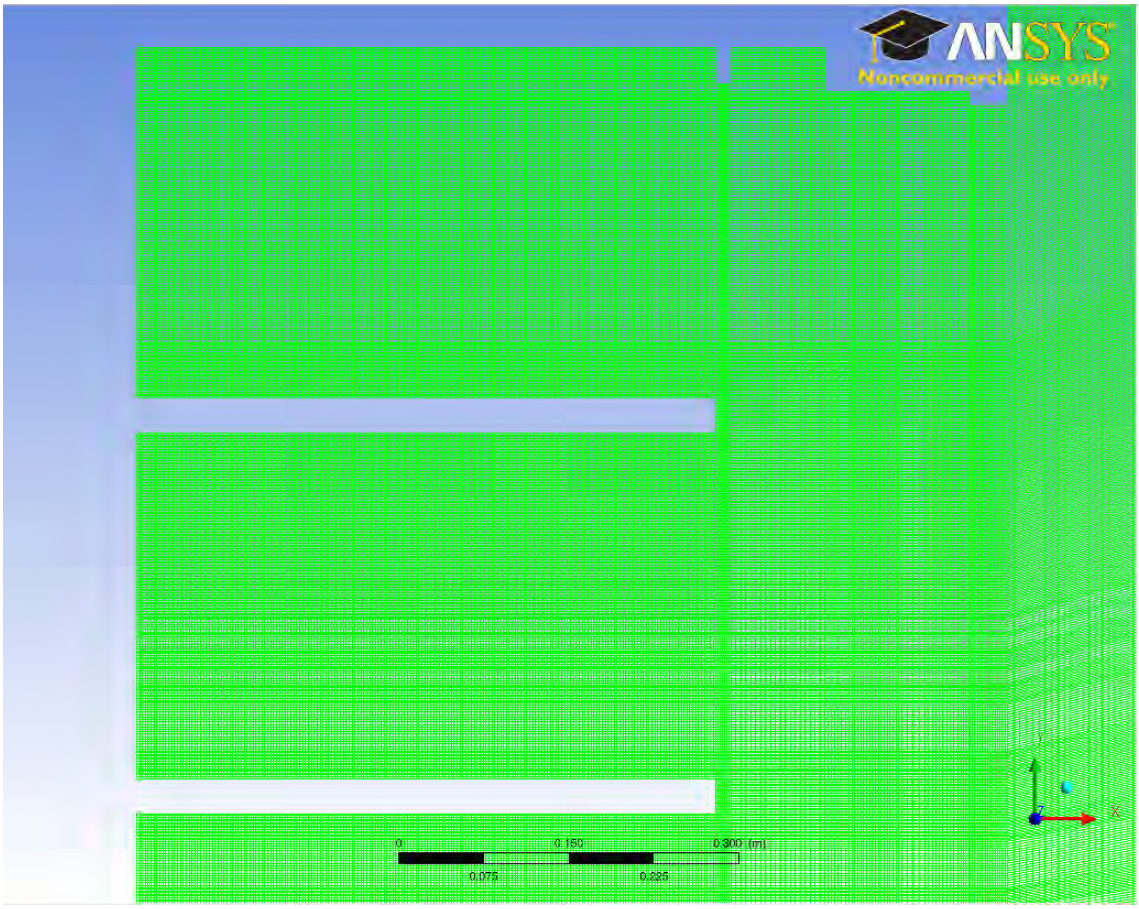

Fig. 13 - Enlarged View of 2D Straight Shelf Mesh for Sections 1 and 2

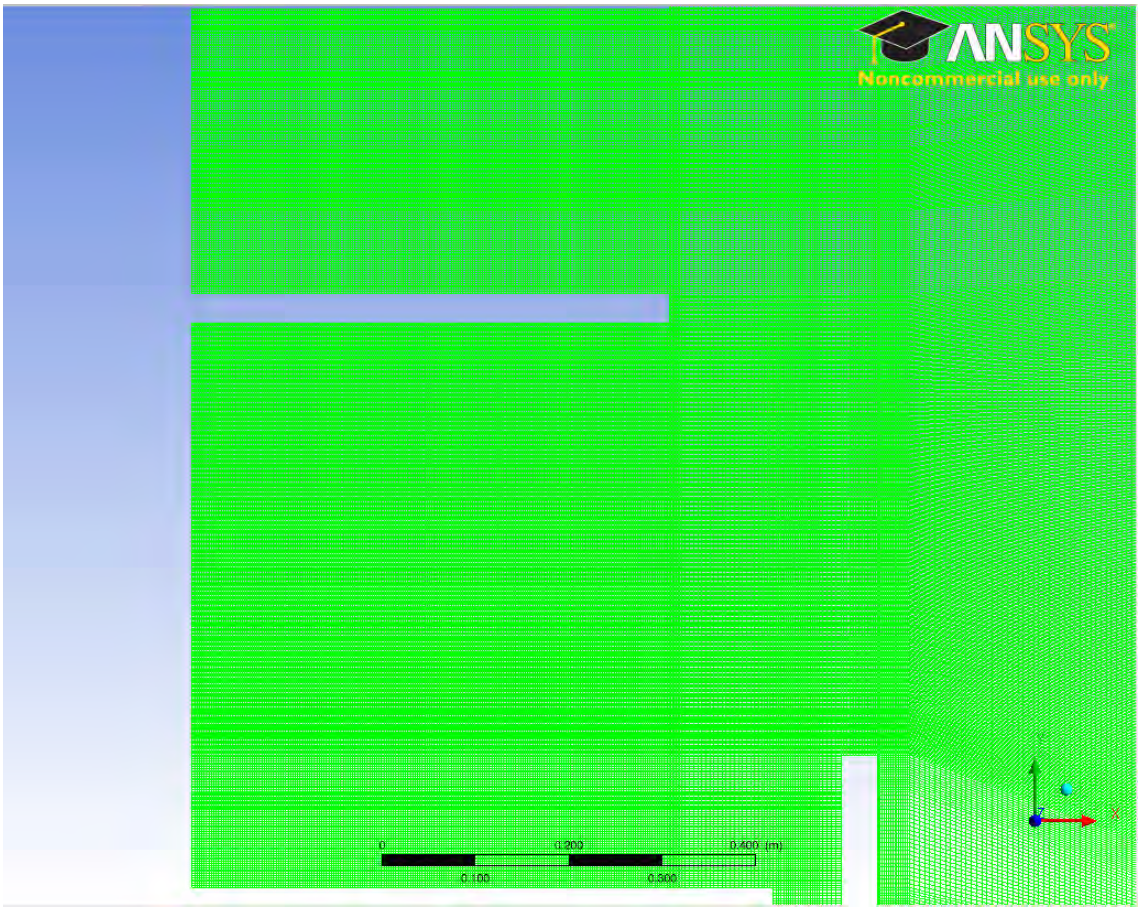

Fig. 14 - Enlarged View of 2DStraight Shelf Mesh for Sections 3 and 4

A two dimensional model was constructed with the mesh count equal to 1.9 million elements. The turbulence model used for steady state and transient state was Sheer Stress Transport for the same reasons as the 3D simulations. The transient time step was set at 0.05s real time with maximum 20 iterations per time step.

For a steady state simulation with 16 cpus and 15 gb of RAM run for 3,000 iterations, the simulation took 6 hours. For transient analysis, a time of 12 hours was set as the limit and the simulation was able to attain 400 iterations per run.

3.5.2 Boundary Conditions for Straight Shelf Two dimensional Model

The side boundary conditions for the 2D simulation were set as symmetry. The velocities and temperatures of the back panel and discharge grill were set at experimental values gathered (as can be seen in Table 1). Both slanted and straight boundary conditions were treated the same as the pressure differences that drive the back panel flow and the fan running the machine was on the same RDC.

3.5.3 Slanted Shelf Mesh

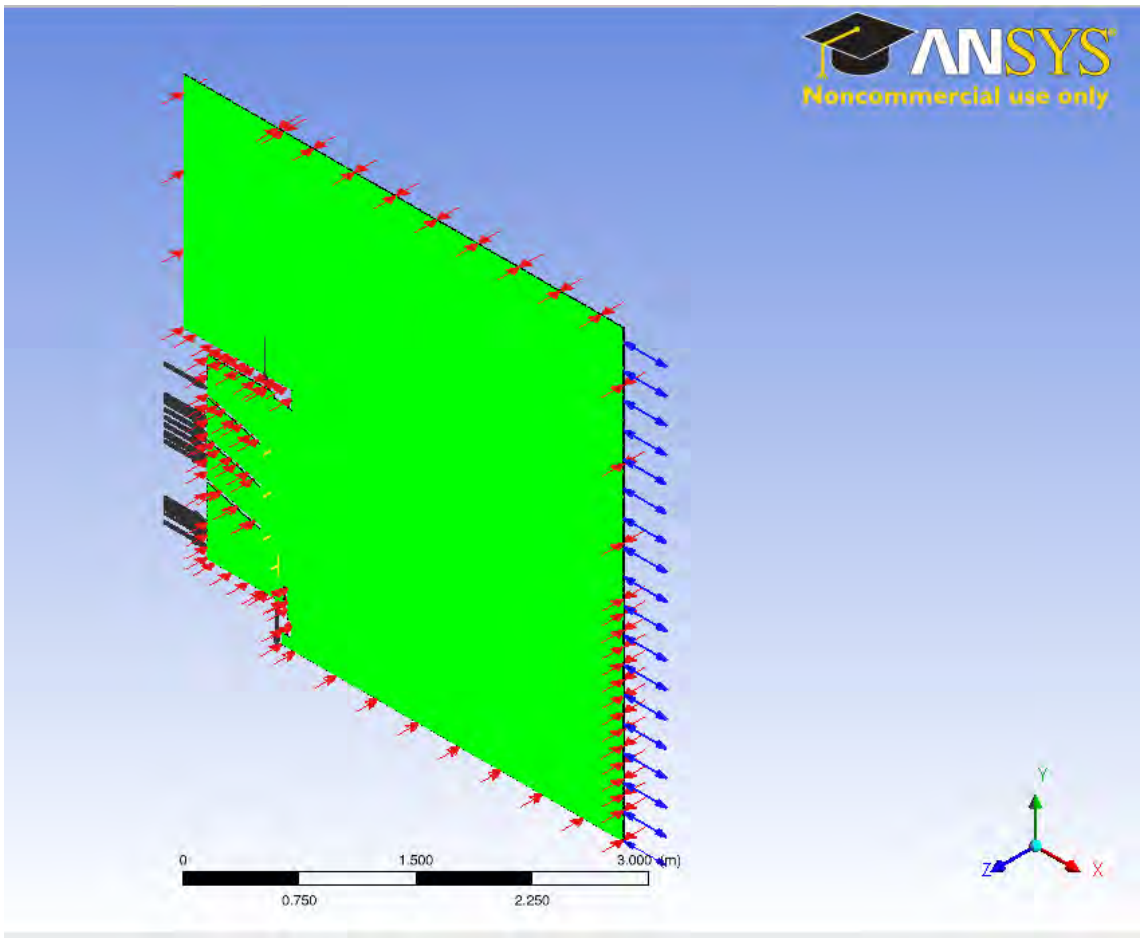

Fig. 15 - Two Dimensional Model of Straight Shelf Open Refrigerated Display Cabinet

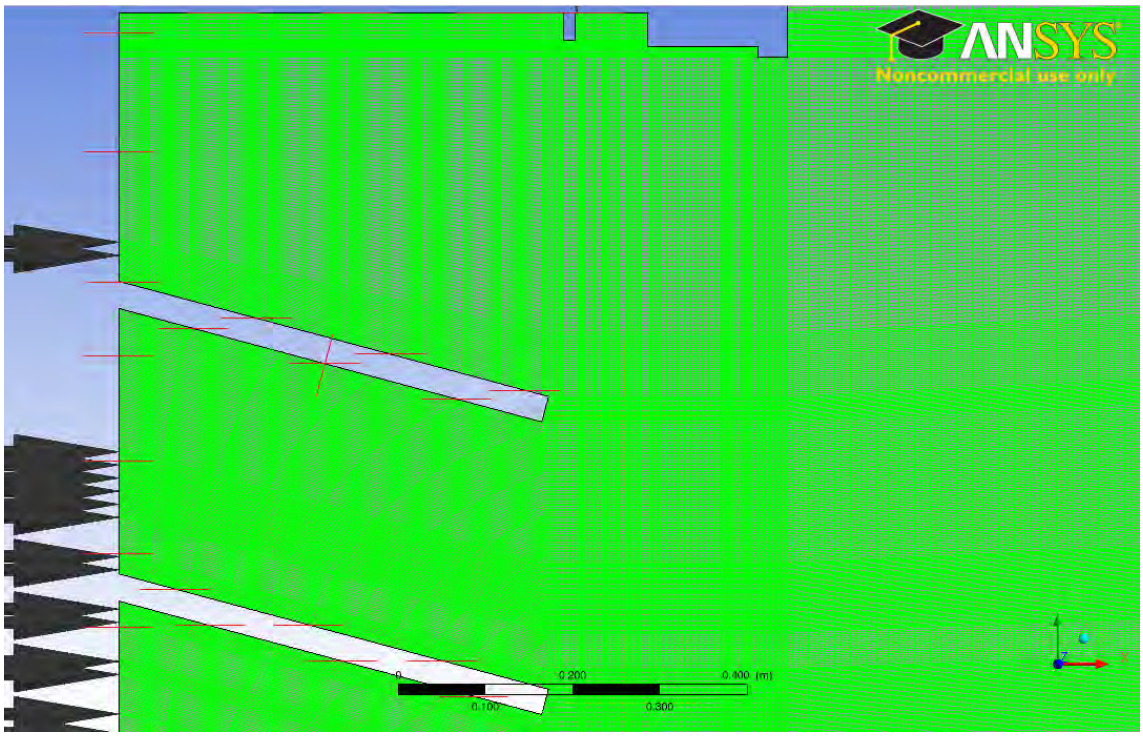

Fig. 16 - Enlarged View of 2D Slanted Shelf Mesh for Sections 1 and 2

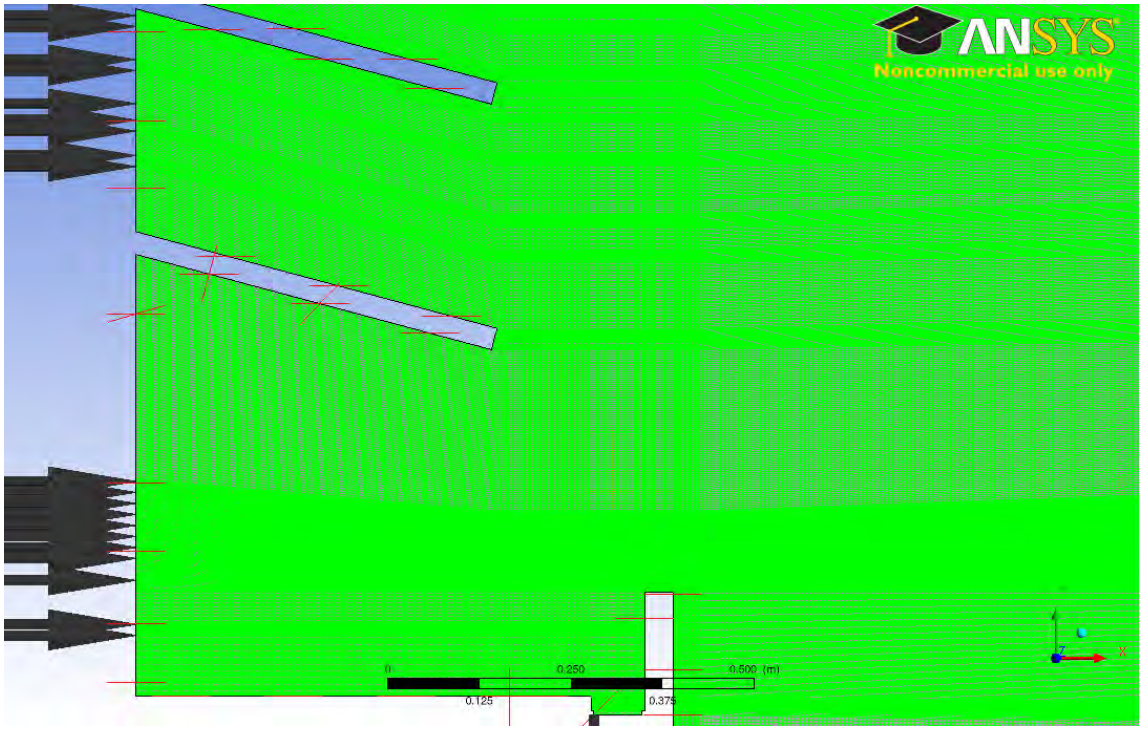

Fig. 17 - Enlarged View of 2D Slanted Shelf Mesh for Sections 3 and 4

The slanted shelf mesh is made up of 2.6 million elements and is run on the same computer. For more information on boundary conditions and run time conditions see section 3.5.1.

3.5.4 Mesh convergence

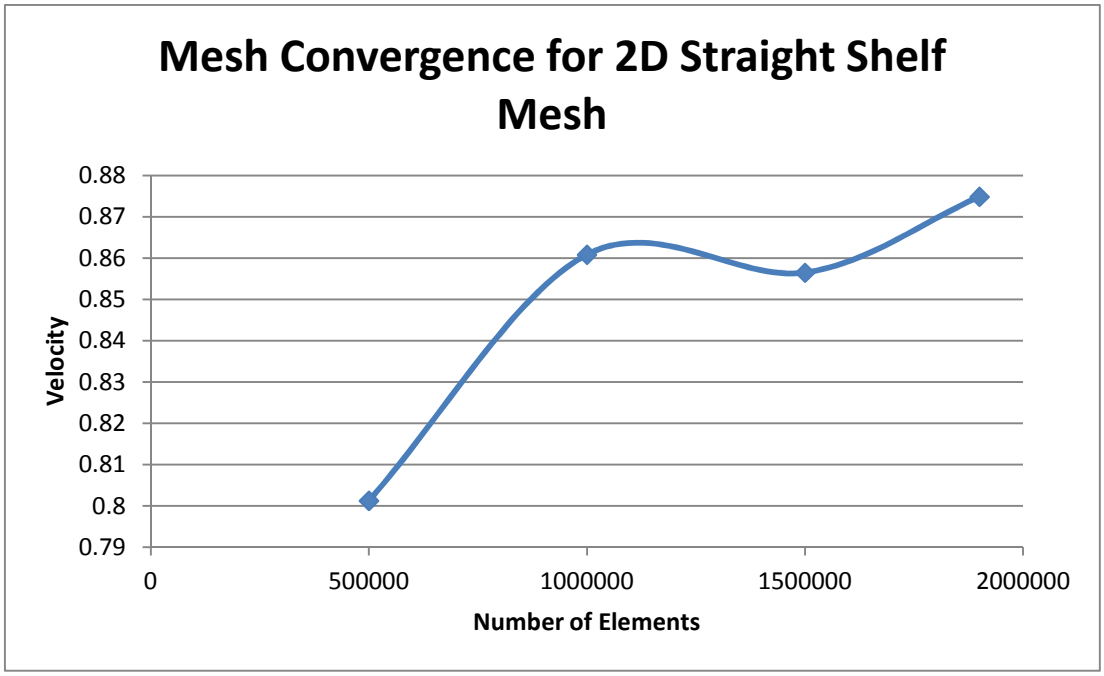

Fig. 18 - Mesh Convergence for 2D Straight Shelf Mesh

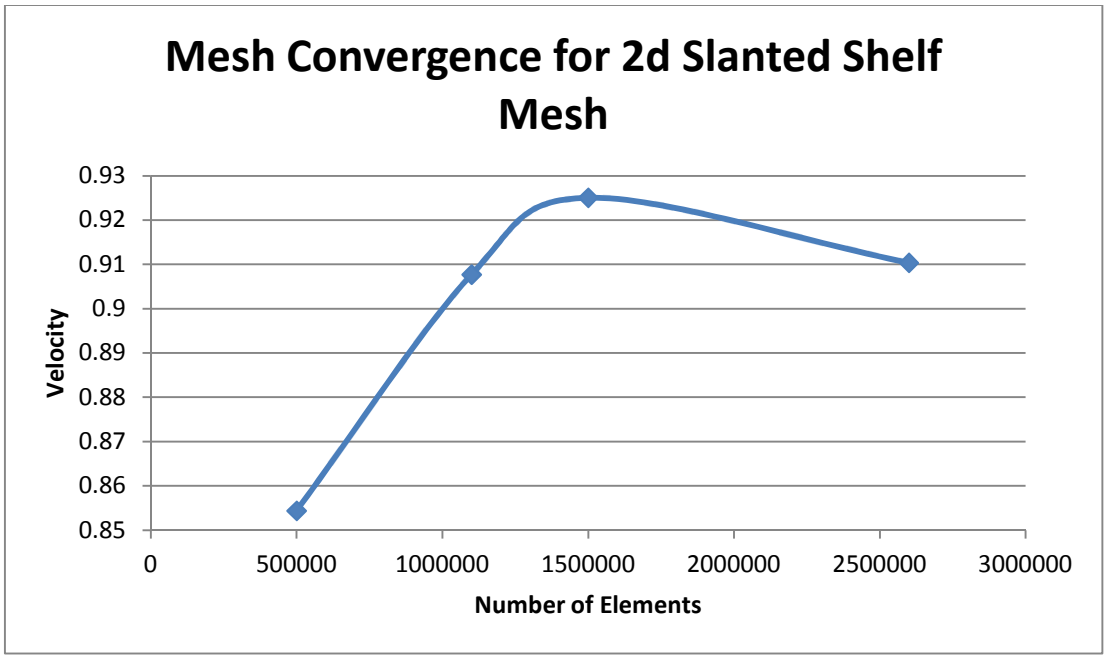

Fig. 19 - Mesh Convergence for the 2D Slanted Shelf Mesh

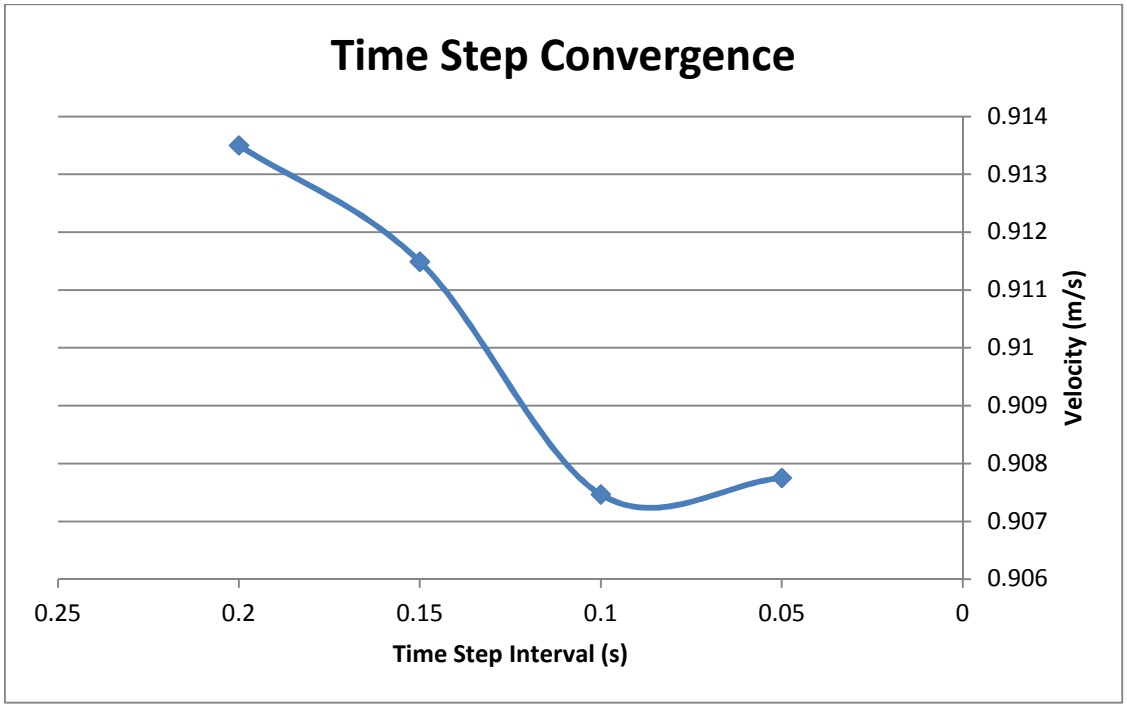

Fig. 20 – Time Step Convergence

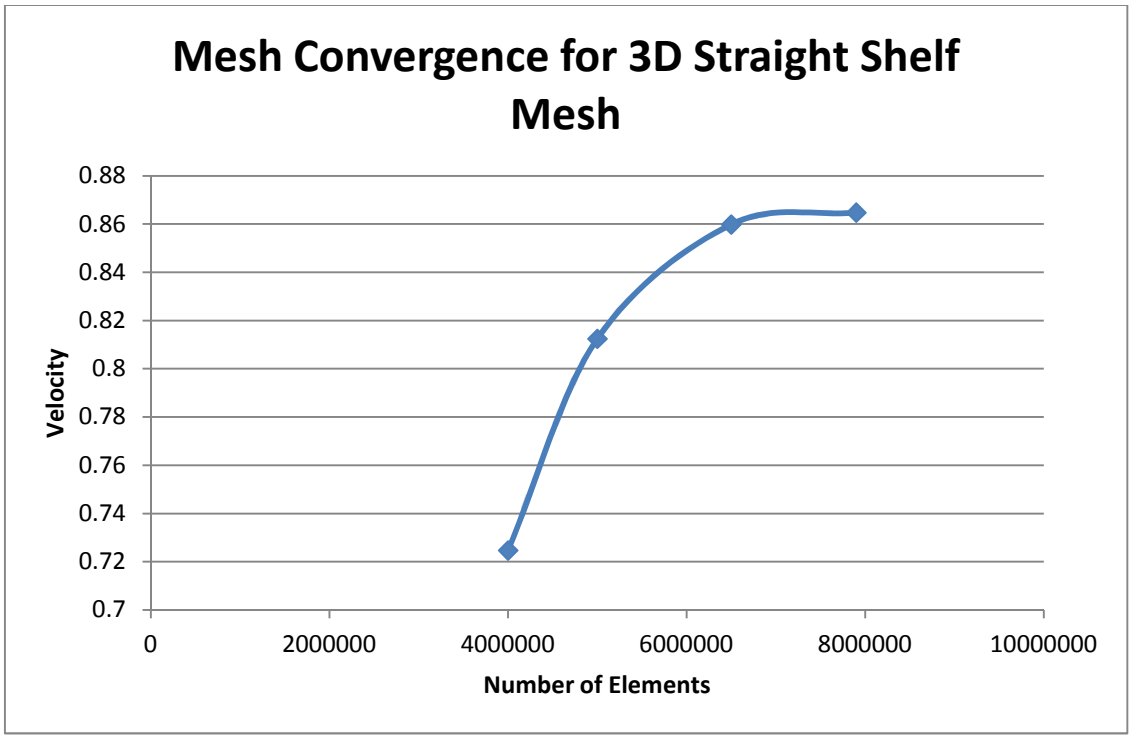

Fig. 21 - Mesh Convergence for 3D Straight Shelf

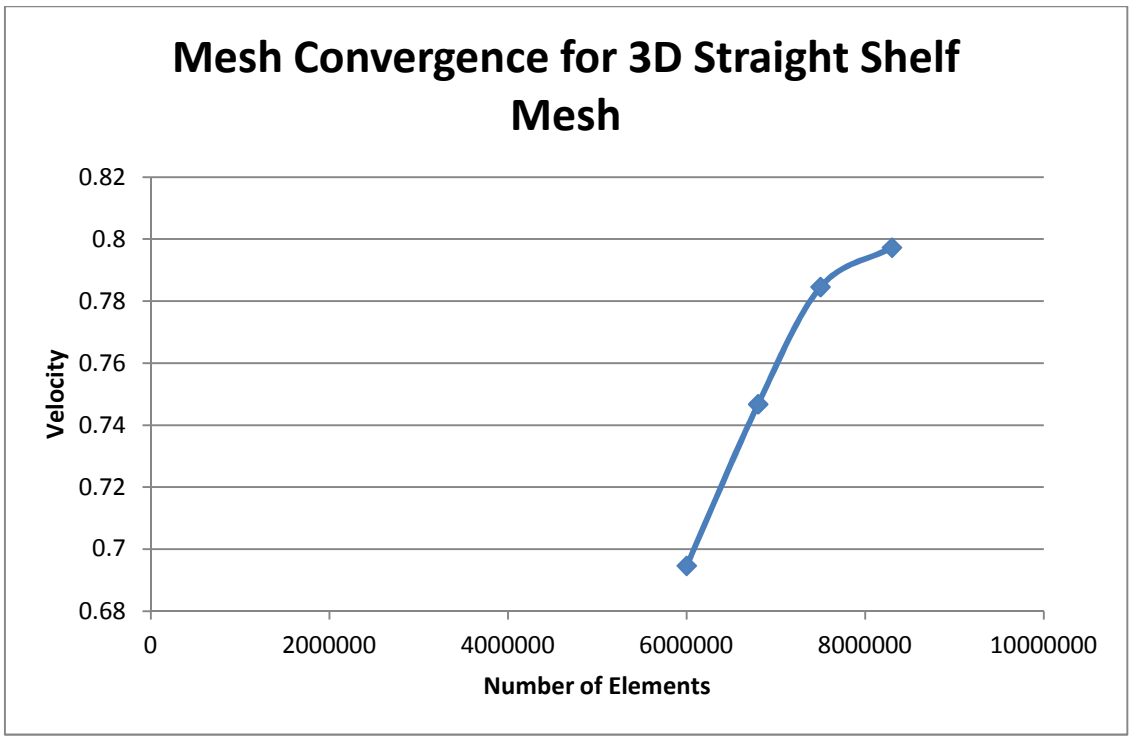

Fig. 22 - Mesh Convergence of 3D Slanted Shelf Mesh

As can be seen from the mesh convergence charts, all the meshes used in this thesis converged to an acceptable level. There was only a time step convergence performed on the 2D mesh because it was decided that transient 3D simulation was outside the focus of this research.

CHAPTER 4 – 2D VERSUS 3D

4.1 Introduction

The following chapter details the results and compares the 2D and 3D models side by side. This is to ascertain whether the models compare well with experimental results and if the increase in computational time in using 3D models is worth the endeavor. The residual errors of the 2D and 3D models are compared followed by the vector plots for qualitative analysis, and finally followed by velocity profiles compared with experimental data. All the following simulation results in this chapter were solved as a steady state problem.

4.2 Residual Errors

Before further investigation of the nature of air curtains, the model has to be verified by comparing different levels of convergence. A number of cases were simulated and the residual level achieved is presented below.

The residual error for the U and V momentum for the 2D slanted shelf scenario converges and oscillates just below the 1e-4 RMS. The mass converges and oscillates around 5e-6 RMS value. The quasi stable nature of the residuals and the high values for a steady state simulation are strong indications for an unsteady system.

The RMS values for the straight shelf scenario are more stable than the slanted shelf case. The oscillations do not appear to be as large and the RMS mass seems to oscillate at a much lower value of 1e-6. The U and V momentum converges and oscillates at 8e-5.

For the 3D the residual values for the U and V momentum oscillate above 1e-4 slanted shelf scenario. The residual values for the 3D slanted shelves are significantly higher compared with 2D case. The residual values are 5e-5 and 8e-5 for mass and W momentum respectively.

The residual value for the 3D straight shelf scenario for the U, V, W and mass are 3.07e-4, 2.1e-4, 1.2e-4 and 2.7 e-5 respectively.

The residual values obtained, for all cases, indicate that the error for the steady state results seems to be too high to produce accurate results but it is still useful to look at the results qualitatively and quantitatively.

4.3 Vector plots

Comparing results on a qualitative scale is an important part in seeing if the flow is behaving realistically despite knowing the convergence level. The vector plots of the slanted and straight 2D and 3D simulation are presented below. A plane side view of each case is provided, for the 3D case for simplified comparison and viewing.

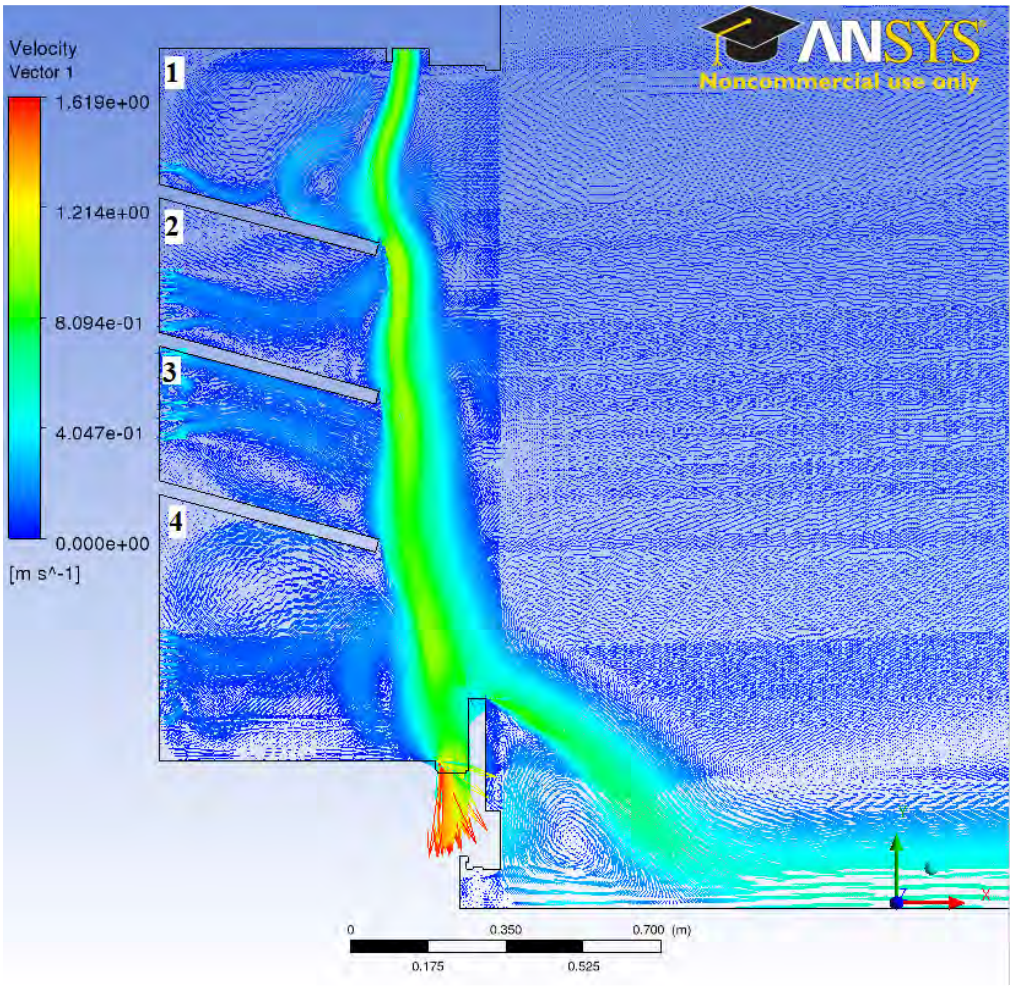

Fig. 23 - 2D Slanted Shelf Vector Plot

The vector plot for the 2D slanted shelf configuration shown in Fig. 23 is qualitatively similar to the flow visualizations performed on the cabinet (see Fig. 53). The numbers refer to the section of the cabinet; these sections will be viewed more closely in the next figures. The air curtain can be seen to move towards the back of the cabinet and the air curtain spreads somewhat towards the bottom of the cabinet. There is clear spillage from the air curtain into the ambient air, as it is with a normal RDC.

There are numerous vortices in the shelf cavities, the space above first and second shelf in particular seem to have a dual vortices formation. This could actually be

assisting or hindering the overall downward velocity of the air curtain depending on where the holes in the back panel are placed. Unless experiments using strict control and variation of the back panel velocities are performed, the exact effect that these back panel jets have on the flow of the air curtain will not be clear and should be a subject of separate study.

There is a slight increase in the velocity after passing the first shelf. This could be the effect of gravity on the system as the air curtain tumble down the sloped shelf back into the system.

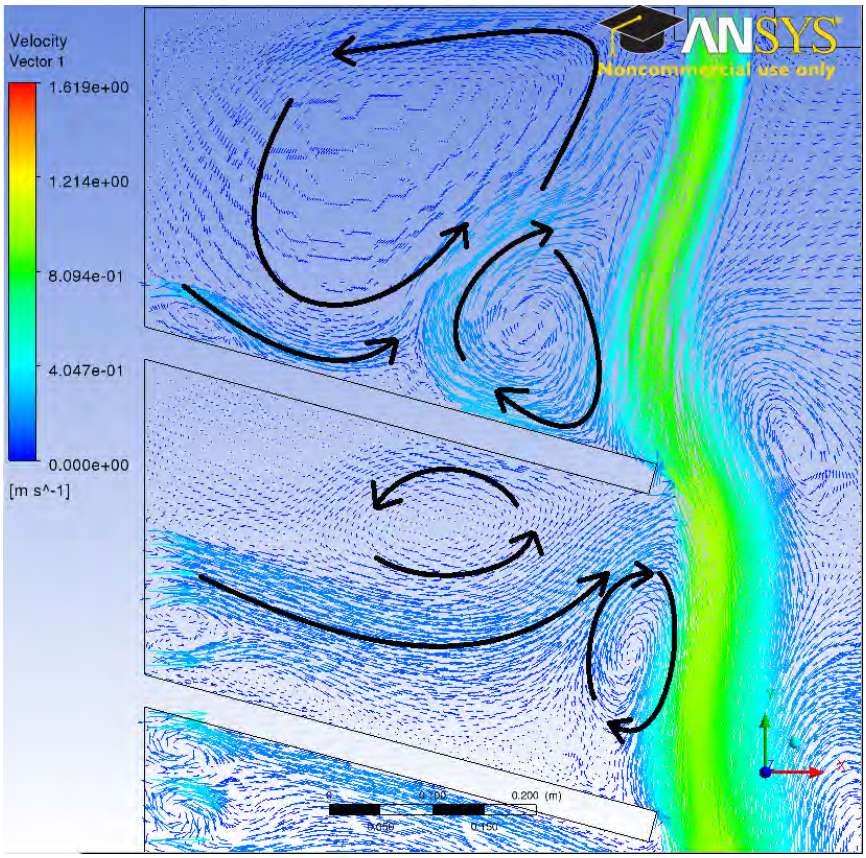

Fig. 24 - Close View of Section 1 and 2 of 2D Slanted Steady State Vector Plot

As can be seen from Fig. 24 the vector plot shows quite a disturbed cavity flow. There are numerous vortices that form and are all reinforced by the back panel flow and kept inside the cavity by the downward flow of the air curtain. In the top section (section 1) there are 2 distinct vortices that form. The vortex at closer proximity to the air curtain is the stronger of the two. They differ greatly in size; the weaker vortex dominated most of the area in section 1 while the smaller, higher velocity vortex only takes up a small place.

The same can be said for the second section. There are two distinct vortices and the vortex closer to the air curtain is the stronger one. Unlike in section 1 the vortices are of similar size.

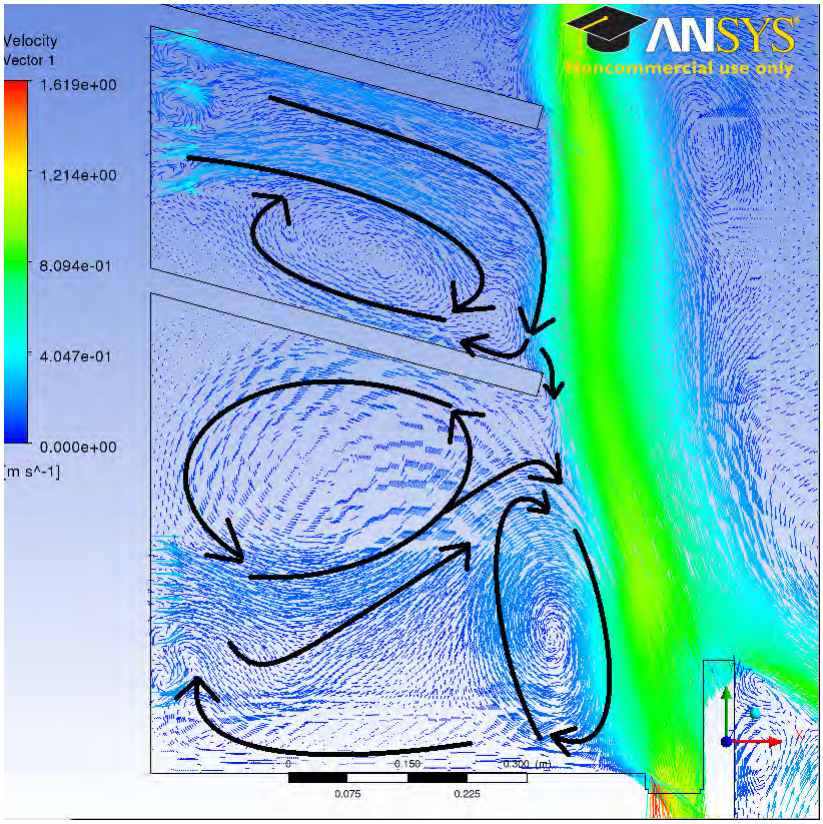

Fig. 25 - Close View of Section 3 and 4 of 2D Slanted Shelf Steady State Vector Plot

Section 3 and 4, seen in Fig. 25 of the vector plot show a similarly complex cavity flow, especially section 4. There only seems to be one major vortex in section 3 and is located a significant distance from the air curtain, unlike in section 1 and 2. Where in section 1 and 2 the cavity flow seems to be trapped, it is not so for section 3 as there is a space for the flow to escape, preventing vortices from forming. This vortex in section 3 takes up a large portion of the cabinet.

In section 4 there is a very complex flow dynamic. 2 main vortices are formed from one main stream of flow from the back panel. The cavity is dominated by a larger low velocity vortex as seen in section 1 and 2 as well.

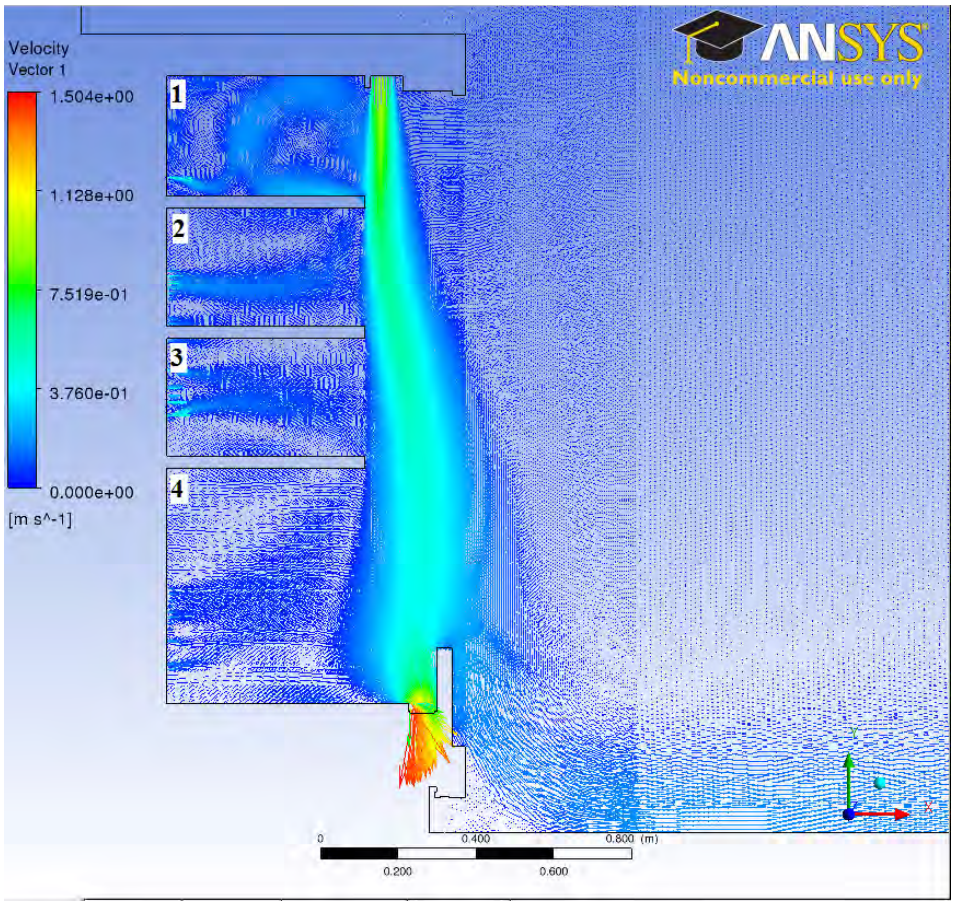

Fig. 26 - 2D Straight Shelf Vector Plot

The vector plot for the 2D cabinet in straight shelf configuration in Fig. 26 shows some different behavior compared to the slanted shelf configuration in Fig. 23. The air curtain is seen impinging on the top shelf as it retreats towards the back. The top shelf stops this and, hence, the impinging can be observed. That air curtain is actually seen to extend out a little more towards the bottom shelf and come back into the cabinet. This is supported by the experimental results as the air curtain moves towards the bottom shelf, it is seen to mix more and move towards the ambient air.

The velocity increase seen past the first shelf in Fig. 23 is not present in this vector plot. The only vortex visible in the straight shelf configuration is in the first cavity, unlike the slanted shelf scenario.

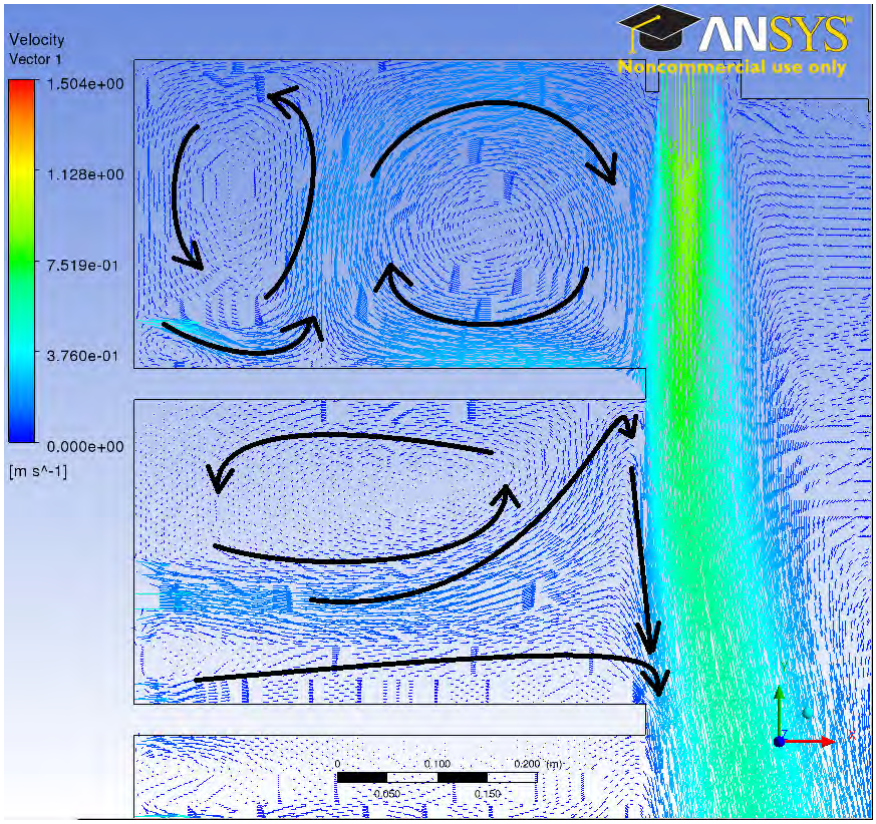

Fig. 27 - Close View of section 1 and 2 of 2D Straight Shelf Steady State Vector Plot

As can be seen from Fig. 27, the cavity flows are much more simpler in the straight shelf configuration. There are two main vortices of similar size but the vortex closest to the air curtain is a bit larger. There is a significant gap at the bottom of section 2, allowing the flow from the back panel to go down into section 3. This prevents a second vortex from forming. A large low velocity vortex can be seen occupying the majority of section 2.

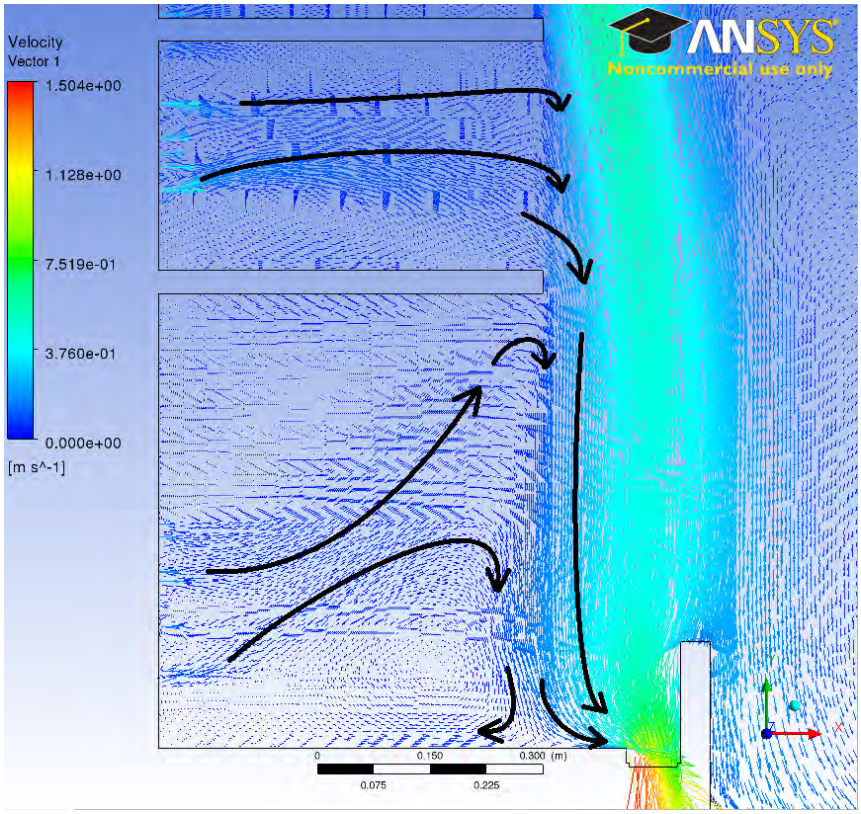

Fig. 28 - Close View of Section 3 and 4 of 2D Straight Shelf Steady State Vector Plot

The behaviour in sections 3 and 4 of Fig. 28 is very similar to 1 and 2. The air from the back panel supports the air curtain by adding to the flow. The extending of the air curtain that was observed in Fig. 26 is caused by this supporting flow from the back panel. There is strangely no vortex formation in section 3 of the cabinet as all the flow

travels down to section 4. Section 4 has a low velocity vortex located at the bottom of the cabinet but most of the air travels to the return grill, instead of being trapped in a vortex.

The behaviour of the flow suggests a much less disturbed system than the slanted shelf case.

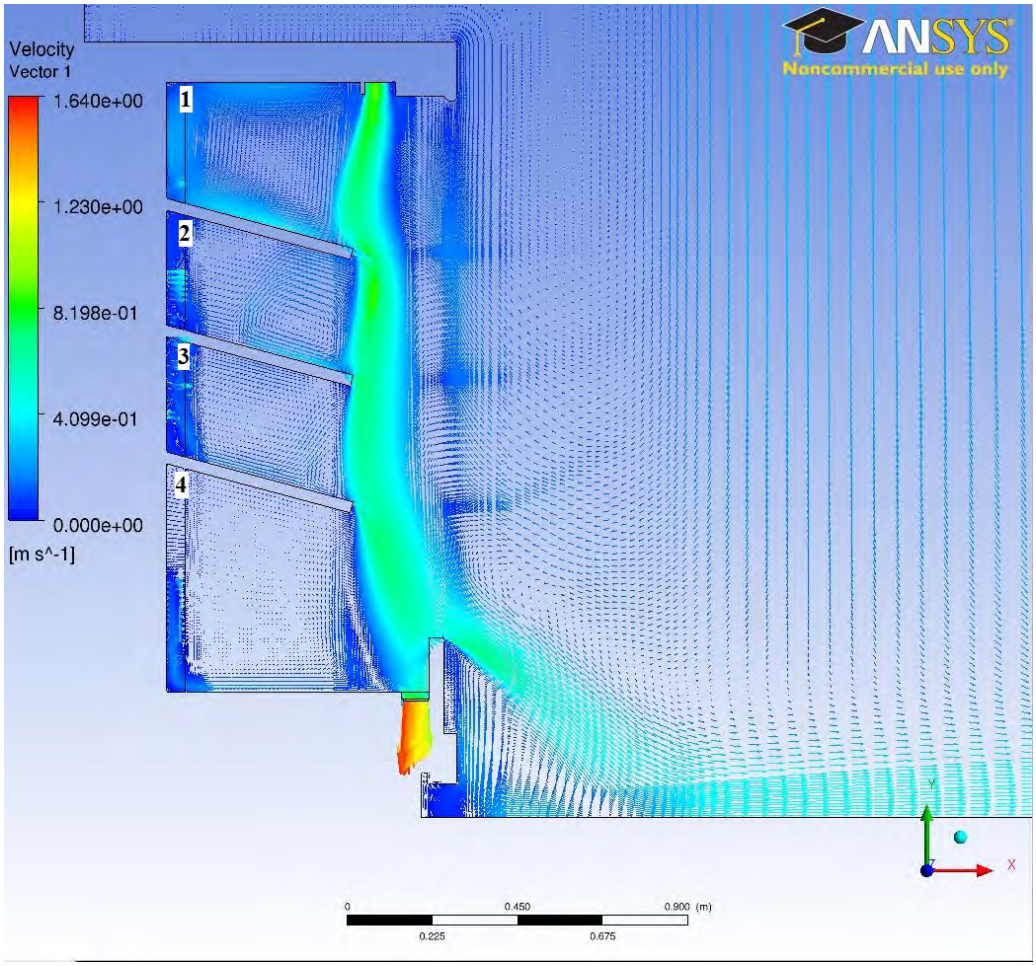

Fig. 29 - 3D Slanted Shelf Vector Plot

The 3D slanted shelf case shown in Fig. 29 is qualitatively very similar to its 2D counterpart in Fig. 23. The negative buoyancy effect seen above the first shelf is almost

identical to its 2D counterpart. The velocity increase is not as apparent in this vector plot but there is a slight increase.

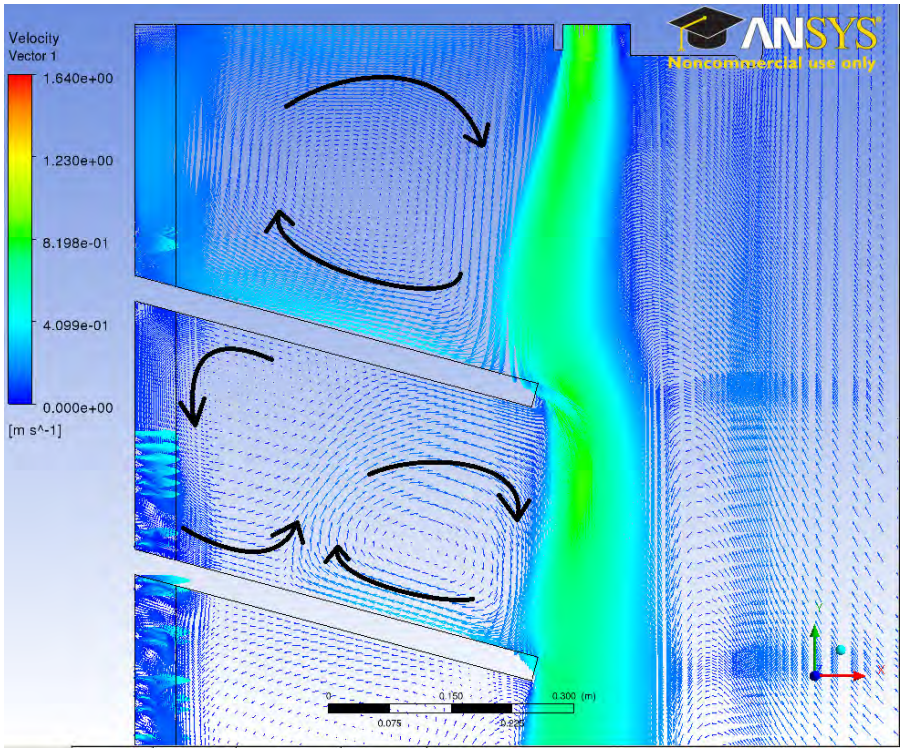

Fig. 30 - Close view of Section 1 and 2 of 3D Slanted Shelf Steady State Vector Plot

The vortices seen in Fig. 30 are very simple compared to the 2D counterpart in Fig. 24. There is only one main vortex in section 1 and it is a much simpler formation. The flow from the back panel is seen to be dominated by the air curtain flow, confining the flow to a very small area at the rear of the cavity. The same can be said of section 2, the formation of both vortices are simple in nature, dividing the cavity into almost 2 equal spaces. There is little room for the back panel flow to support the air curtain and flow down to the next section.

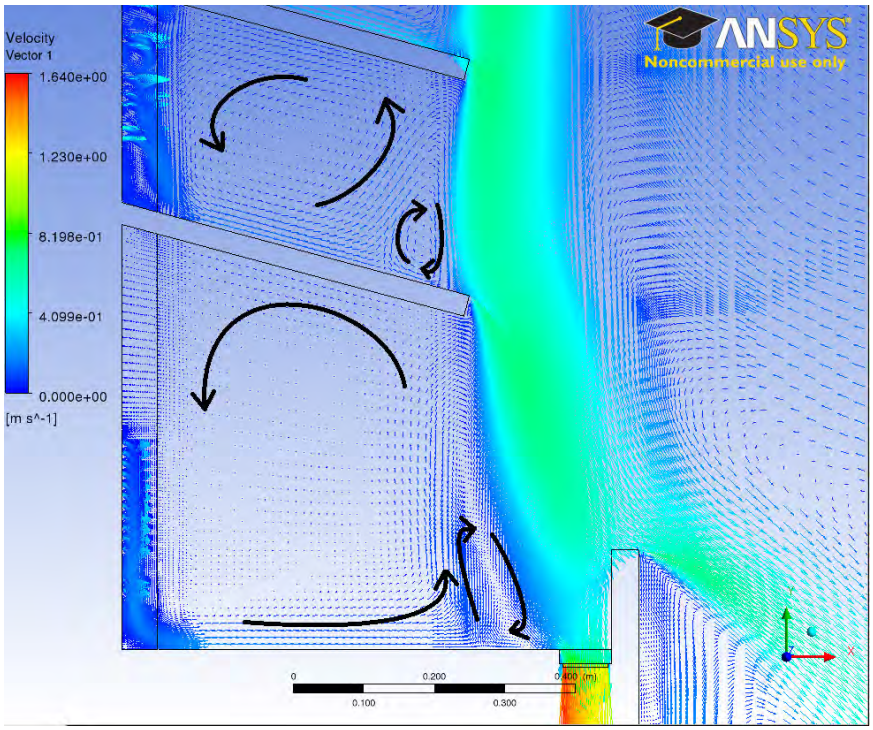

Fig. 31 - Close View of Section 3 and 4 of 3D Slanted Shelf Steady State Vector Plot

Sections 3 and 4 in Fig. 31 are similar to section 1 and 2 in simplicity. Section 3 has 2 main vortices, one of which is close to the air curtain. Unlike in the 2D case, there is no room for the flow in the cavity to proceed to the lower section. This causes a large vortex to occupy most of section 3 cavity.

Section 4 also has 2 vortices similar to section 3 and in similar positions. The magnitude of the larger vortex is much higher in comparison but the small vortex is similar in size.

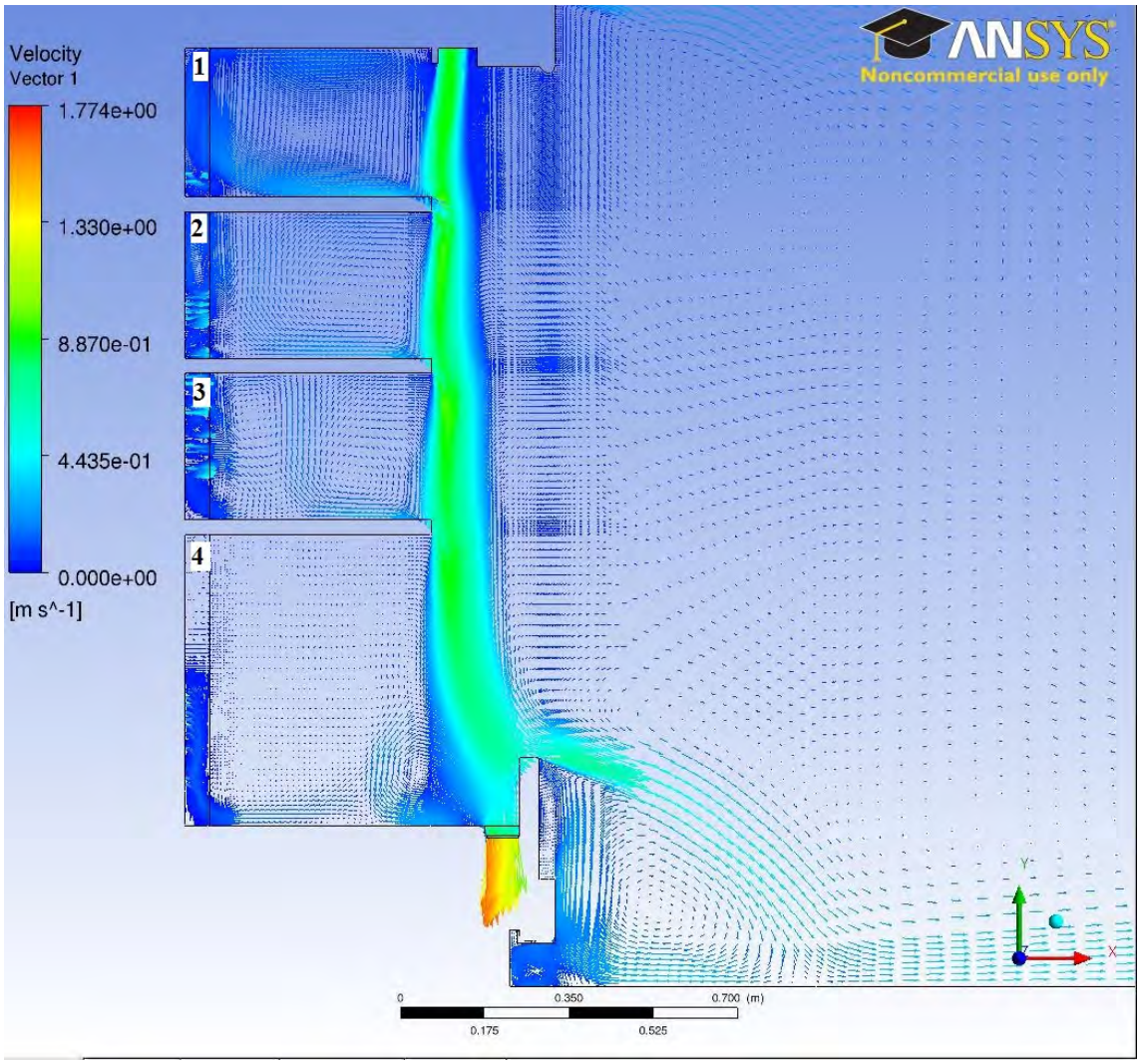

Fig. 32 - 3D Straight Shelf Vector Plot

In contrast to the 2D and 3D slanted configurations, the 2D and 3D straight shelf configurations show a large difference. The extending of the air curtain is simply not present in the 3D straight shelf configuration shown in Fig. 32. The negative buoyancy seen in the slanted shelf vector plots is observed here above every shelf, although not quite as clearly. The large differences between the 2D and 3D vector plots for the straight shelf configurations may be due to the complex mixing in the lower regions of the cabinet.

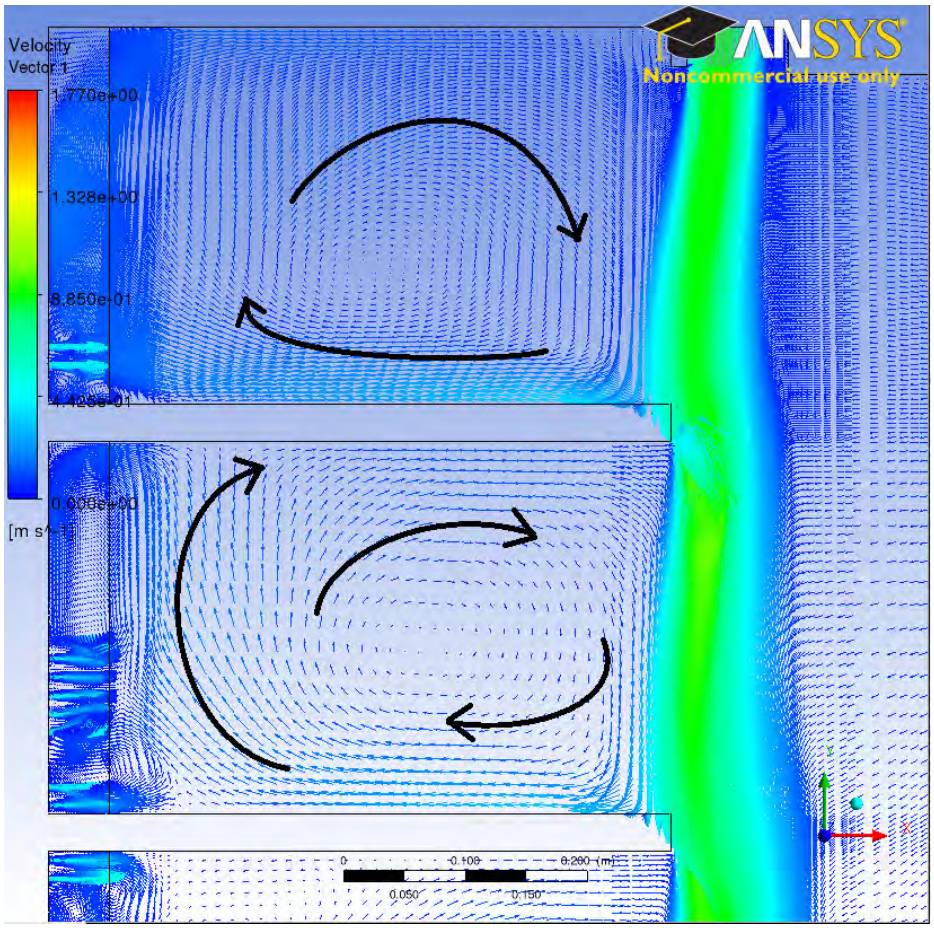

Fig. 33 - Close View on Section 1 and 2 of 3D Straight Shelf Steady State Vector Plots

As can be seen from Fig. 33, the main vortices are very simple, much like in the slanted shelf case. There is also a strong dominance of the air curtain flow versus the back panel flow. One main vortex can be seen in each section.

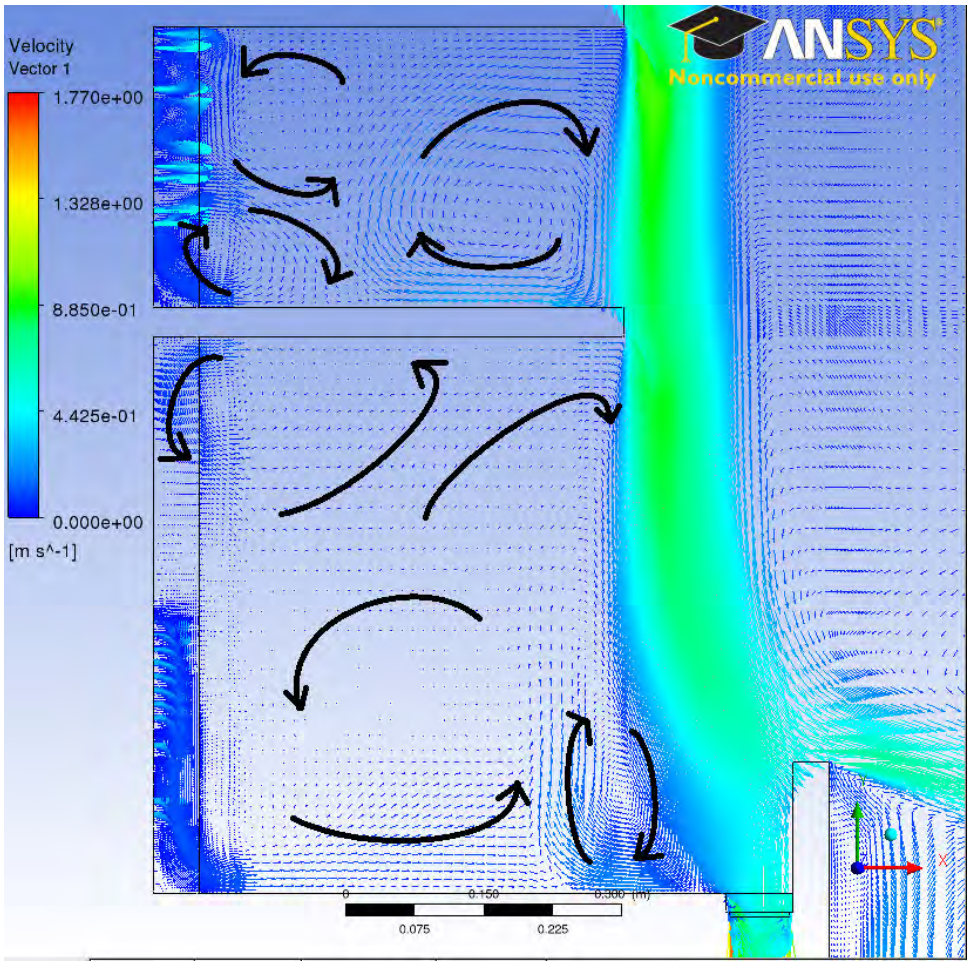

Fig. 34 - Close View of Section 3 and 4 of 3D Straight Shelf Steady State Vector Plot

As can be seen from Fig. 34, there are more vortices visible but most are very weak in magnitude and are very much dominated and defined by the air curtain flow. There are 3 main vortices in section 3 and 4. The back panel flow seems to have very little influence on the formation of the vortices.

4.4 Velocity Profiles

Quantitative analysis is the most accurate and expedient way to determine simulations accuracy with experimental data. Velocity profiles were measured using an LDV in front of each shelf. This region was selected due to the invasive and disruptive

nature of the shelves in such areas. If the simulation is capable of predicting the air curtain behavior in these regions, much confidence can be placed on the simulation methodology. Below are the velocity profiles for the straight and slanted shelves in 2D and 3D models versus the experimental data gathered on the RDC.

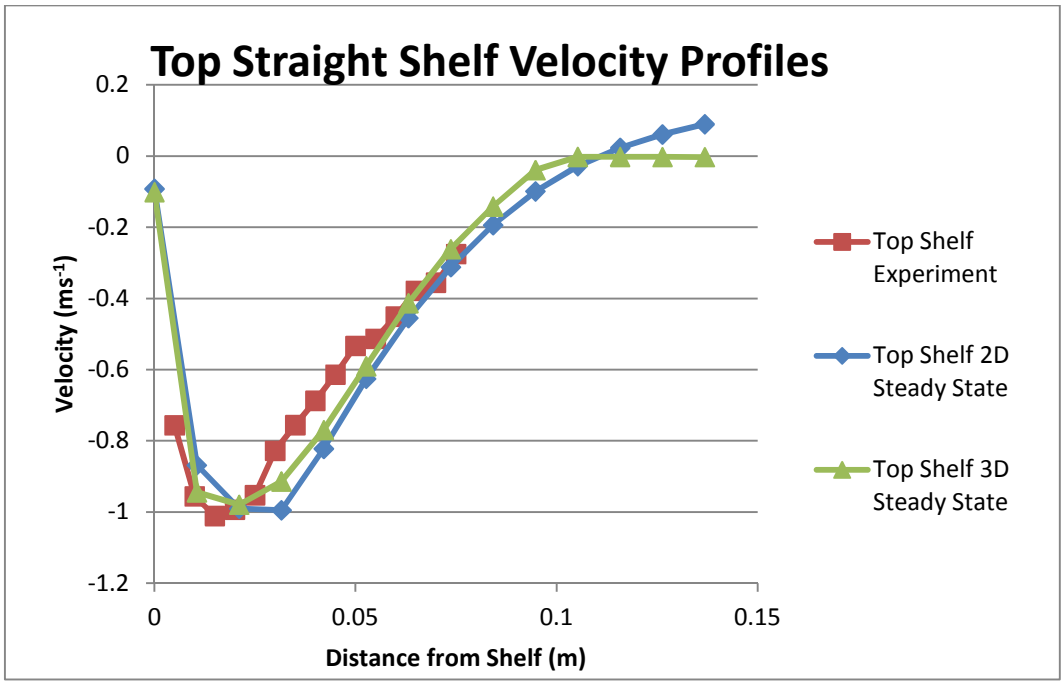

Fig. 35 – Top Straight Shelf Velocity Profiles

Fig. 35 shows the velocity profiles for the 2D and 3D steady state case scenarios. It is apparent that at higher regions of the cabinet, both models predict the air curtain behaviour almost perfectly. There is a slight over prediction of the velocity for the 2D case and the 3D case.

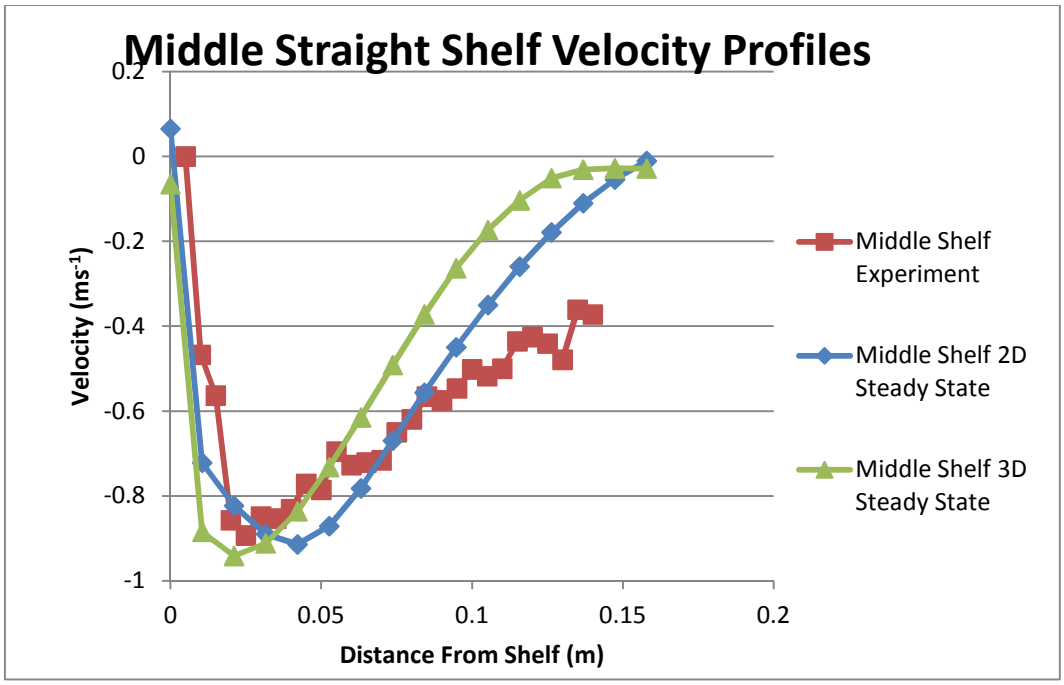

Fig. 36 – Middle Straight Shelf Velocity Profiles

The velocity values in front of the middle shelf show the slight discrepancy between experimental data and both 2D and 3D models particularly in the far distances from the shelf. However it is important that the value of maximum velocity (~0.9ms^{-1}) appears well between for both numerical 2D & 3D configurations with experimental data with slight shift of the maximum to the right for the 2D case. Both models under predict the amount of mass flow out of the cabinet (from x=0.09 m onwards) substantially. While both 2D and 3D models exhibit a gentle decline of the air curtain velocity, the experimental data indicates that the air curtain actually spreads more towards the ambient air than in the simulation. It should be noted that the 2D configuration is slightly more accurate in this case. The reason for this may be due to the removing of the complex 3D behaviours simulated in the 3D case. If 3D is not a good approximation of cabinet conditions, it is more time efficient to focus on 2D cases due to decreased complexity and computational resources needed.

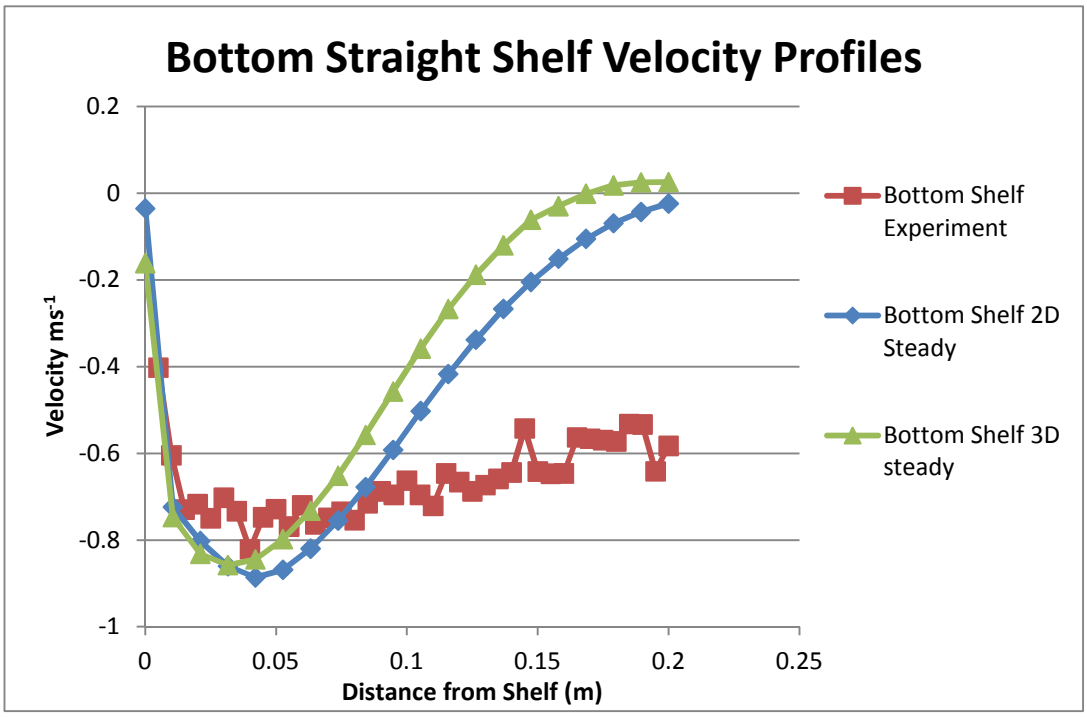

Fig. 37 – Bottom Straight Shelf Velocity Profiles

As can be seen in Fig. 37, in terms of comparison of 2D and 3D configurations, both 2D and 3D simulations are not able to cope with the experimental velocity profile, however, the 2D case shows slightly better agreement compared the 3D. . It is clear to see that the 3D model does not under predicts the effect of entrainment on the lower part of the shelf. The numerical results for the air velocity in front of the bottom shelf agree with experimental data only in close vicinity to the shelf. Beyond 0.07m for the 3D and 0.09m for the 2D, both models under predict the velocity of the air curtain.

Overall the 2D simulation results give a reasonably more accurate picture of the air curtain when compared with the 3D.

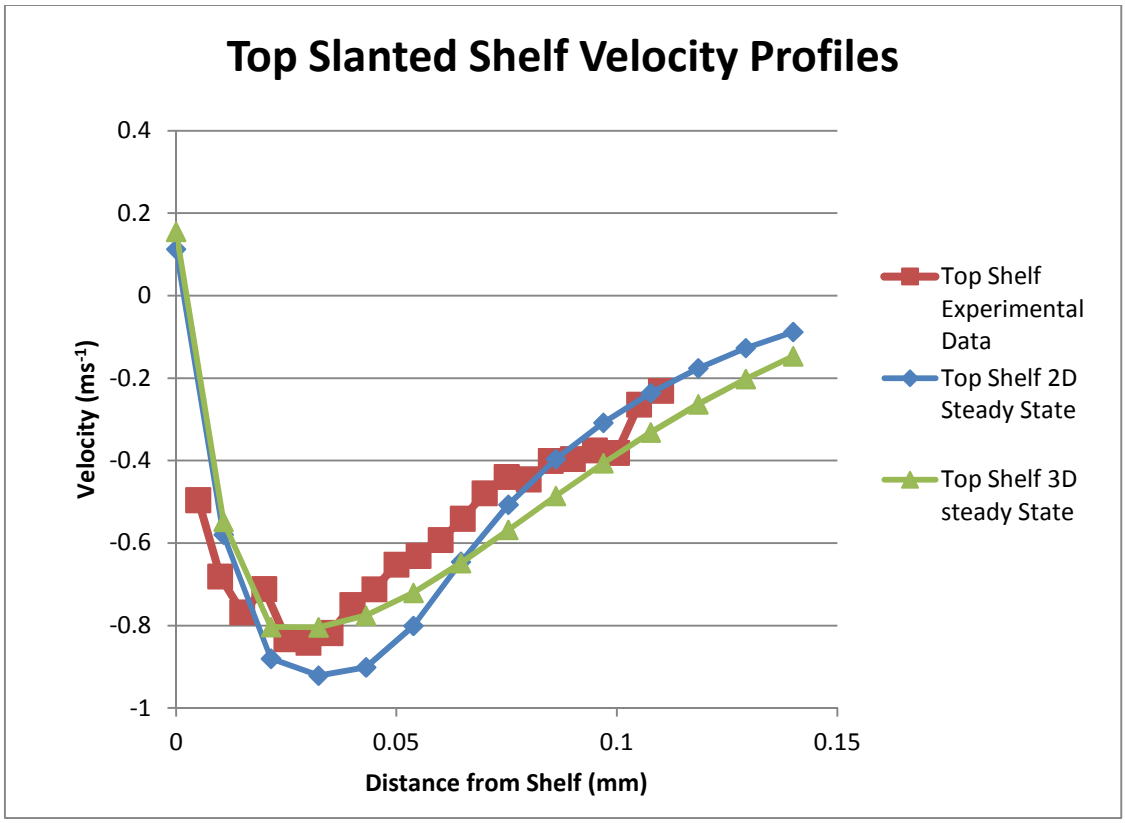

Fig. 38 - Top Slanted Shelf Velocity Profiles

The top shelf slanted scenario in Fig. 38 is much akin to its straight shelf counterpart in Fig. 35. Both 2D and 3D simulations approximate the experimental results well. The 2D, in this case, slightly over predicts compared with the 3D case at the maximum velocity, which agrees very well with the experimental data. As the air curtain velocity location moves further from the shelf, the 3D model slightly over predicts the slope of the velocity as the air curtain ends.

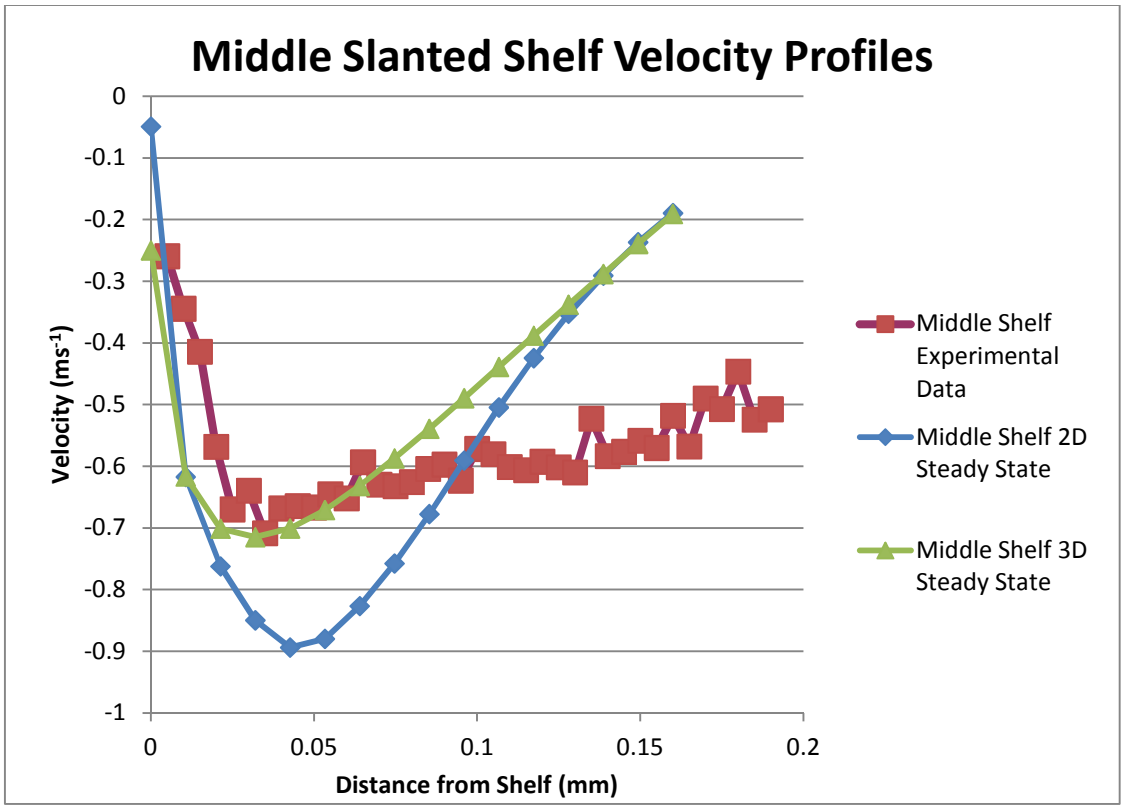

Fig. 39 - Middle Slanted Shelf Velocity Profiles

The middle slanted shelf scenario shows a stark contrast to the straight shelf counterpart. The 2D simulation, in this case, significantly over predicts the velocity at the level of the middle shelf. The 3D simulation shows more agreement with velocity and the entrainment that takes place, particularly in the vicinity of the shelf and predicts the maximum velocity with excellent agreement with experiments. However, as seen in Fig. 37, both 2D and 3D models under predict the air curtain velocity beyond the distance of 0.07m. It seems to be the case that when forced convection is the dominant force, the models predict the experimental results well, as the air curtain moves farther away from the cabinet, natural convection plays a more major role in the behaviour of the air curtain. Therefore, both under estimate the entrainment in this manner but the 3D case makes a much better approximation.

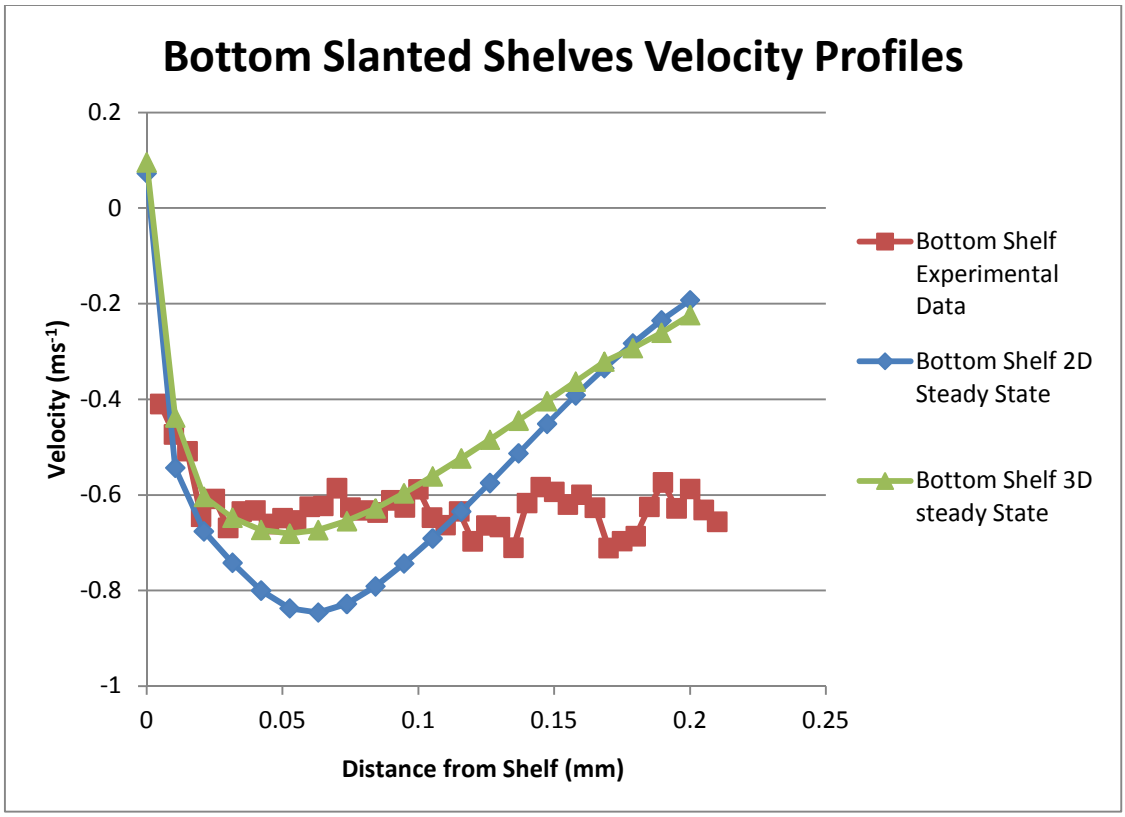

Fig. 40 - Bottom Slanted Shelf Velocity Profiles

The bottom slanted shelf produced similar results to the middle shelf. The 2D simulation over predicts the near-shelf velocity and under predicts entrainment on the outer areas of the cabinet. The 3D case agrees with the near shelf velocity but does not predict the entrainment accurately. Though the slope of the 3D simulation, as the velocity moves further out, is less steep and, therefore, more accurate than the 2D simulation and more adequately predicts entrainment.

As can be seen from the vector plots and velocity profiles, the 2D versus 3D study shows no appreciable differences qualitatively speaking. At the same time the results of the velocity profiles obtained from the 2D and 3D analysis slightly differ in front of the shelves. For the straight shelf case, the result is clear that 2D simulations can produce an accurate picture of the air curtain behavior. For the slanted shelf

scenario, however the 3D simulations results in a better picture of the air curtain. It should be noted, however, that the convergence for all of these cases was not at a satisfactory level. Until the convergence can be improved by more accurate measurements of the boundary conditions, the steady state should not be used to simulate RDCs. If steady state needs to be run due to resource limitations, straight shelf RDCs should be the subject of the simulation if at all possible and limited to the 2D case.

4.5 Summary

A validation study was performed using 2D and 3D numerical models of the slanted and straight shelves configurations. The results showed that the 2D models showed an overall good agreement with the experimental data along with lower residuals. This is compounded by the fact that a large increase in computational power is required to perform a full 3D simulation.

As 2D simulations compare well with the experimental data overall in both the slanted and straight scenarios the remainder of this dissertation will use the 2D version of the numerical models.

As this study was all performed in steady state, a transient analysis is required to see if simplifying an RDC system to a steady state flow is an accurate assumption. This will be the subject of chapter 5 of this dissertation.

..

CHAPTER 5 – STEADY STATE VERSUS TRANSIENT

5.1 Introduction

This chapter details the simulations of the flow field in the refrigeration cabinet with straight shelves in steady and transient states. Due to large computation time required for transient simulations, the results presented in this chapter are all obtained using the 2D model.

5.2 Residual Errors

At first, the residual error values were compared with the steady state version of the simulation to estimate if the transient simulation achieved a lower convergence level. The results of the simulation convergence are detailed below.

The residual error values for the transient simulations converged better than for steady state. For the straight shelf simulation the U momentum and V momentum residual errors converged and oscillated at the residual error value of 1.15e-7 while the mass converged and oscillated at 1.15e-8. This is compared to 8 e-5 for U and V and 1e-6 for mass of the steady state. In all, it can be concluded that transient simulations do achieve a lower level of convergence.

5.3 Vector Plot

Qualitative analysis is important to attain a general idea of flow behavior and analyze how it compares with reality. The vector plots for the transient and steady state are detailed below.

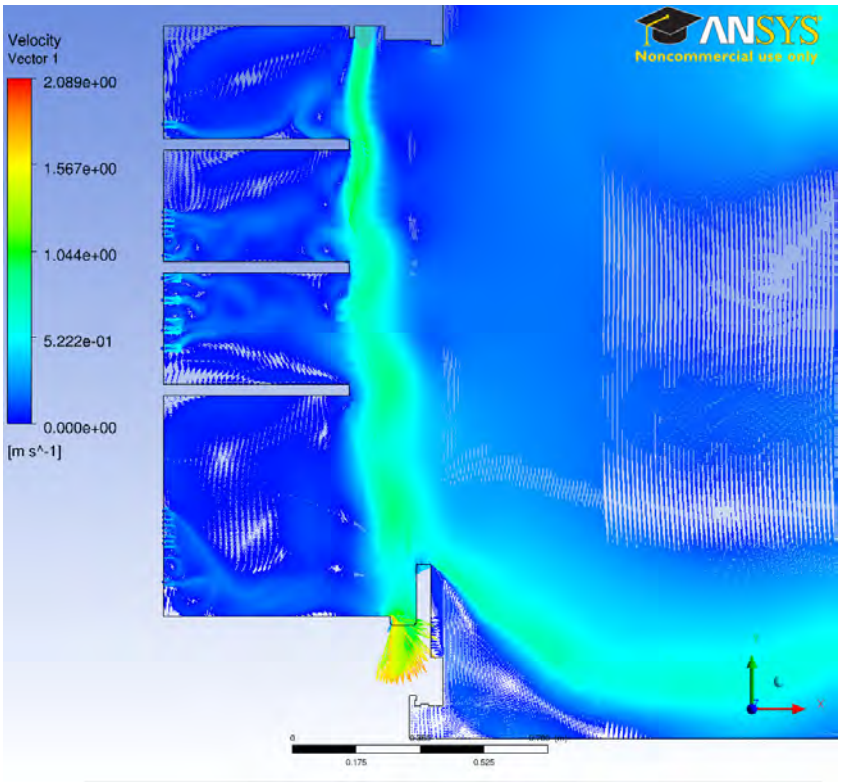

Fig. 41 - Straight Transient Vector Plot

Fig. 41 shows a vector plot of the velocity obtained for the straight shelf. From comparison of this figure and Fig. 26 for the steady state solution it can be noted that there are immediate differences between the steady state and transient versions of the straight shelf simulation. It should be noted that Fig. 41 is only a snapshot in time in the transient simulation. However, some comparisons can still be drawn by comparing results shown in transient and steady (Fig. 41 and Fig. 26 respectively) from the two figures.

There is a general "bowing out" effect seen in both the steady state simulation and the transient case as well. It is more clearly pronounced in the steady state simulation simply because of the less wave like nature of the curtain.

The transient scenario seems to produce more realistic results as it captures the propagation of the wave like phenomena seen in the flow visualizations (see Fig. 53). The flow looks more disturbed than in the steady state and is in a state of flux. The waving behaviour of the air curtain obtained in unsteady simulations results in different flow patterns between the shelves. In addition to that there is a difference on the flow behaviour at the bottom of the cabinet.

5.4 Velocity Profiles

Velocity profiles of the transient and steady state model are important for comparing the simulations to the experimental data. Accuracy in these profiles, in these regions of the cabinet, is key to identifying the most effective numerical models. The velocity profiles are provided below.

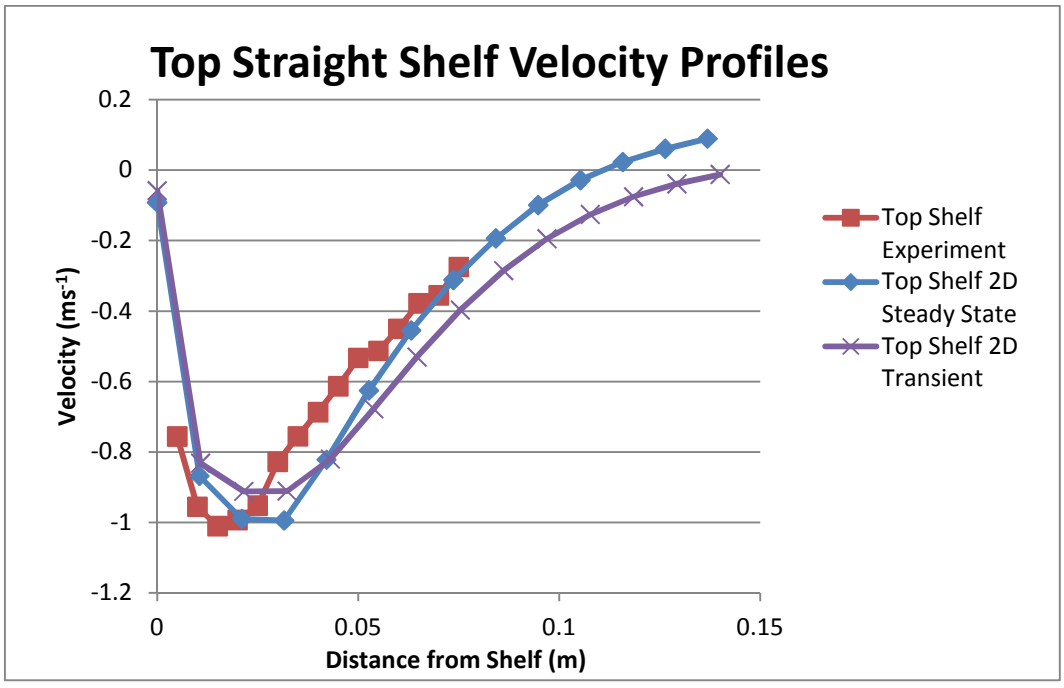

Fig. 42 - Top Straight Shelf Velocity Profiles

It should be noted that all transient velocity profiles are calculated using a time average procedure. As the simulation progressed in time an average value of all the velocity values from the transient simulation was taken and an average value of the velocity was calculated. This was done to ensure a similar procedure to velocity measurement using LDV as the LDV collects an average velocity over time.

The straight shelf velocity profiles for the tops shelf simulation are shown in Fig. 42. The transient velocity profile over predicts the velocity and peak placement of the air curtain. It is also seen to extend further into the ambient air more quickly than the steady state version. Overall, both transient and steady state show good agreement with experimental data. It can be seen at the level of the top shelf; all the models predict very well the maximum velocity of the air curtain and overall profile of the velocity. The transient velocity profile seems to have a slight shift comparing with the experimental data.

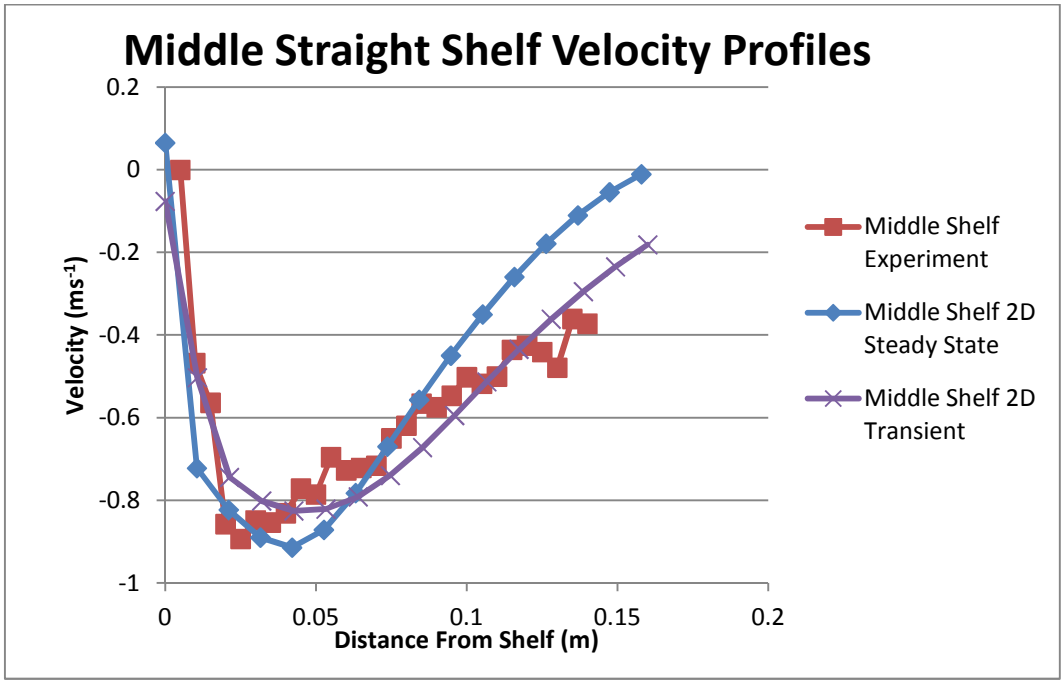

Fig. 43 - Middle Straight Shelf Velocity Profiles

The middle shelf velocity profiles for the steady state and transient simulations are shown in Fig. 43. The steady state simulation from the middle shelf diverges from the experimental values quite early and under predicts the width of the air curtain.

At the same time the transient profile under predicts the peak velocity but almost exactly matches the air curtain width and the slope that the air curtain has at the middle shelf. This is a very large improvement on the accuracy of the simulation as the width of the air curtain and slope of the velocity at greater distances from the cabinet have been shown to be very hard to predict.

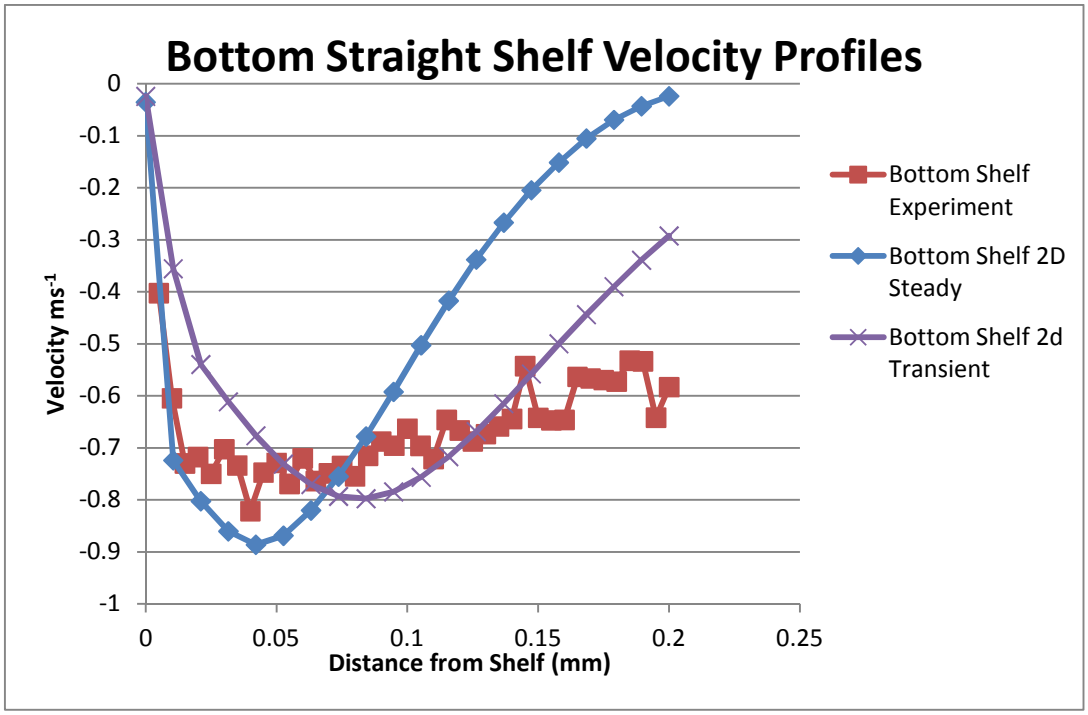

Fig. 44 - Bottom Straight Shelf Velocity Profiles

The bottom shelf velocity profiles for the steady state and transient simulations are shown in Fig. 44. It can be seen that the steady state numerical results do not

accurately predict air curtain width and the peak velocity is misplaced as the profile in the experimental data shows no clear peak.

At the same time the transient velocity profile shows better agreement with experimental data. The air curtain is elongated at this height but does not predict the slope properly. Overall it can be seen as a marked increase in accuracy due to the fact that the transient simulation is showing the lengthening nature of the air curtain.

5.5 Air Curtain Width

The Air Curtain Width (ACW) is analysed in this section for transient and steady state numerical models. Since the solution for the transient simulation is oscillatory, the average ACW is attained by averaging the air curtain width over a typical cycle of the transient solution.

The air curtain width is defined as:

$$\boldsymbol{ACW \equiv (0.4 \cdot V_{max})_{\pm x}} \qquad \text{eq.(9)}$$

Where V_{max} is the local maximum velocity obtained by the air curtain and the subscript ±x is the position in x where that maximum velocity was located, creating the bounds of an air curtain defined by the local maximum velocity. This can be considered the "core" of the air curtain and is different from conventional definition of the air curtain as a simple stream from the discharge grill to the return grill [8, 9, 25]. This conventional definition is not accurate enough as it does not take into account the entrainment from the aisle air or the reinforcement of the air curtain from the back panel.

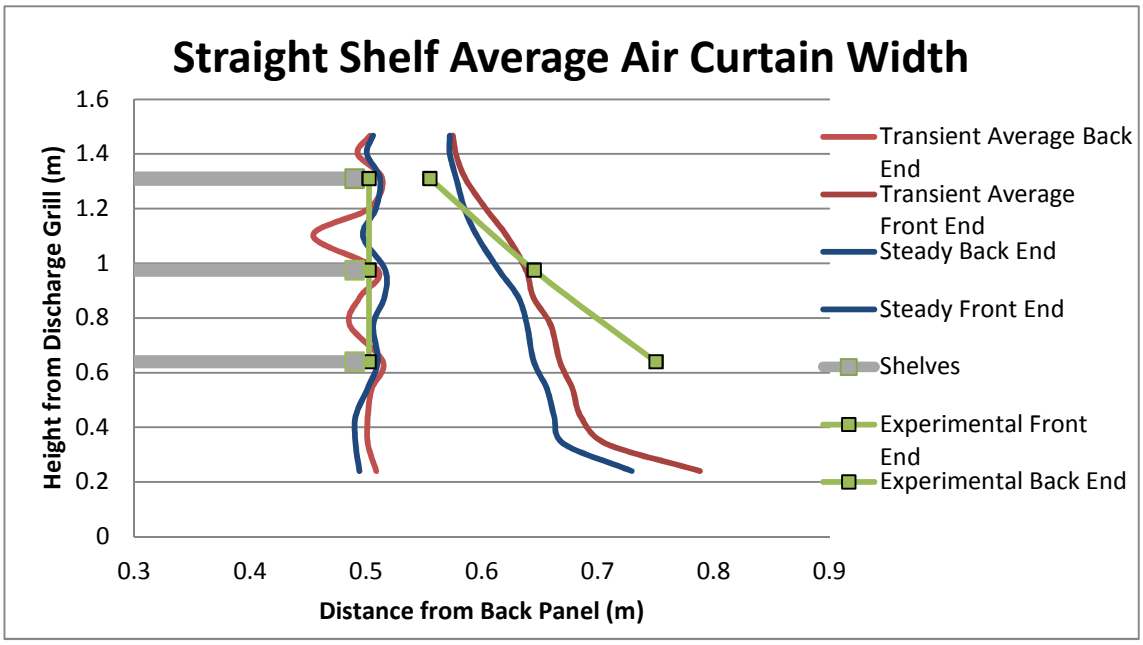

Fig. 45 – Straight Air Curtain Width

The above figure shows the ACW for transient and steady state simulations. As can be seen the transient case is further out of the cabinet than the steady state. As can be seen from the figure the experimental data agree with the ACW model results. The transient case shows very good agreement for the middle shelf; however, it over predicts the result obtained at the top shelf and under predicts the bottom shelf ACW. It should be noted that the transient case results in better agreement with the experimental data than steady one except the lower region which is known as a common problem [12, 13, 34].

5.6 Straight Shelf Turbulent Kinetic Energy Analysis

Analysis of the turbulence kinetic energy will help in observing where the most mixing takes place as well as observations of how the distance from the shelves affects the turbulent kinetic energy. The transient simulation is cyclical in nature and each

period is denoted as a cycle in the following graphs. Each of these profiles are instantaneous turbulent kinetic energy values in a typical periodic cycle. Each cycle consists of one second simulation time and is divided evenly into four instantaneous snapshots and the turbulent kinetic energy value is detailed below. Analysing the cyclical behaviour can give us insight into the quasi stable nature of the air curtain in RDCs.

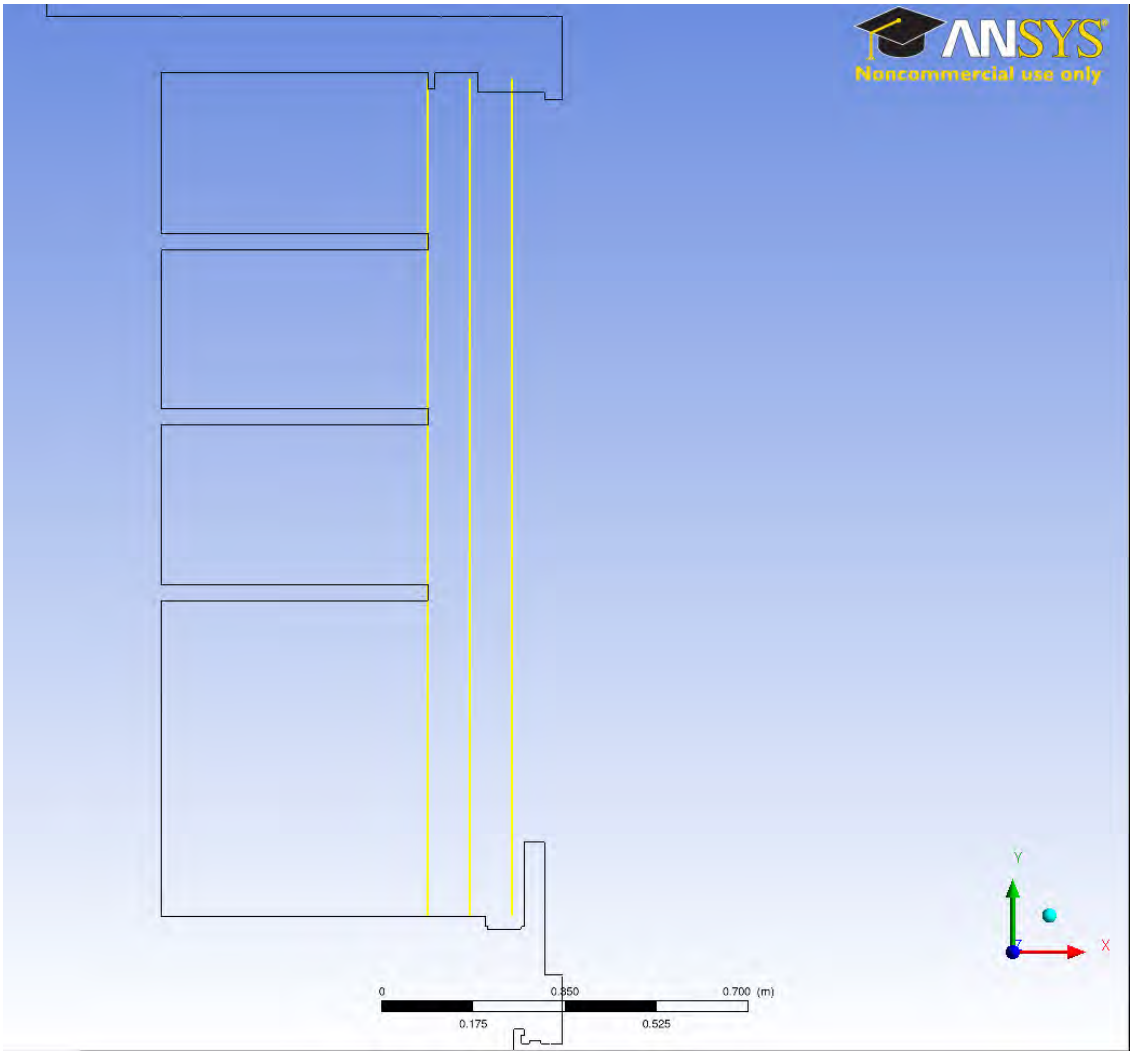

Fig. 46 - Turbulence Kinetic Energy Profile Lines

The above figure gives a visual location to where the turbulent kinetic energy lines are taken. The locations are at 0, 0.08 and 0.16 meters from the shelf from left to right. The shelf location with respect to height from the bottom of the cabinet is as follows. The bottom shelf is at 0.64m, the middle shelf is at 0.975m, and the top shelf is at 1.31m, the horizontal lines in the following graphs denote their locations.

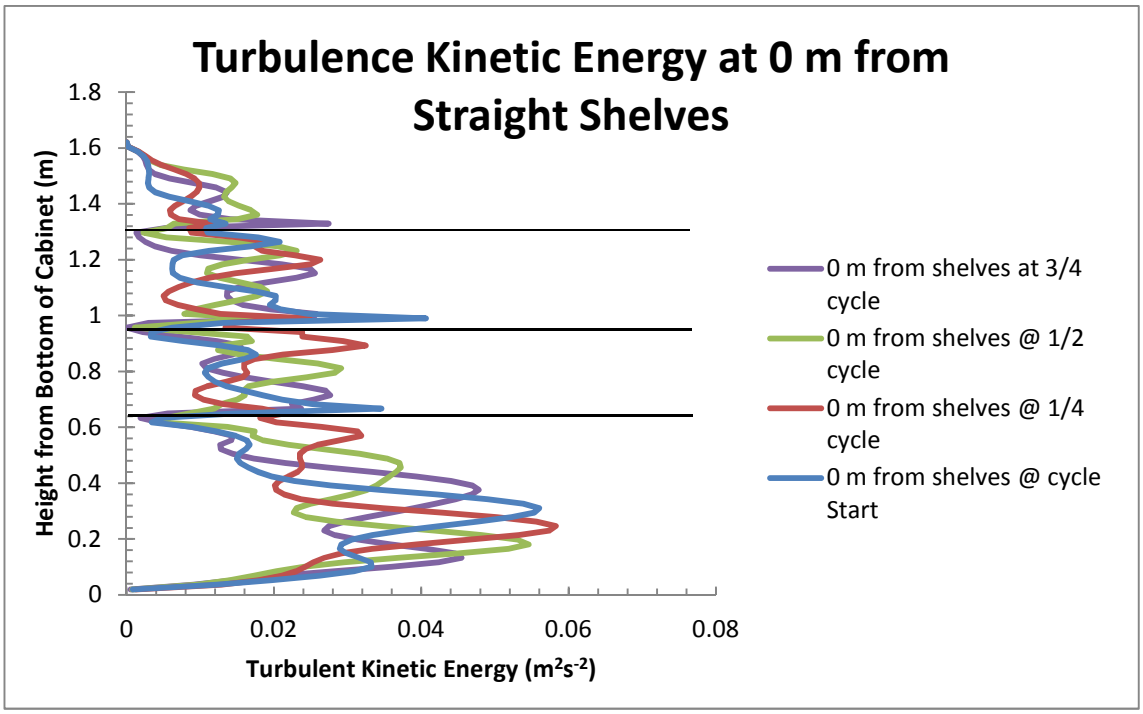

Fig. 47 - Turbulent Kinetic Energy at 0 m from shelves

Fig. 47 shows the turbulent kinetic energy through the cycle at the shelf. It is difficult to recognize any pattern in the top and middle sections, only below the bottom does a clear pattern start to appear. As the cycle progresses (from blue to red to green to purple) there can be seen a rising of the turbulent kinetic energy. The sharp peaks at the cycle start indicate a disturbed flow at the beginning of each cycle. This indicated that at regions very close to the shelf, the flow is greatly disturbed.

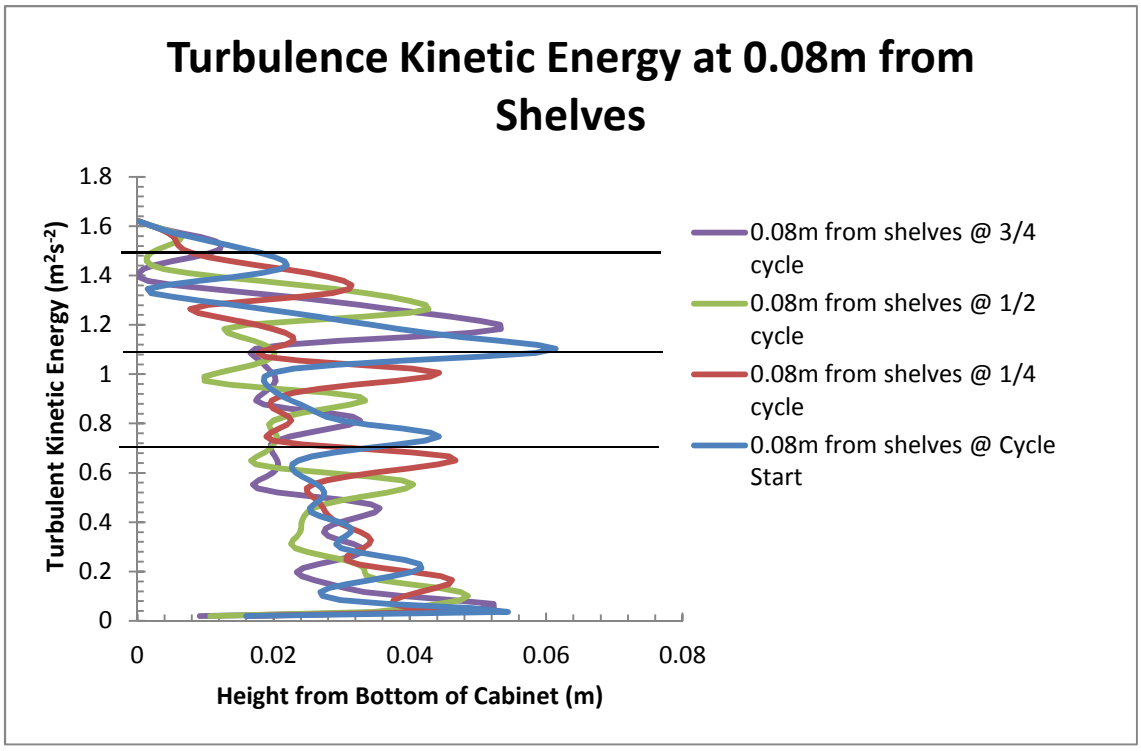

Fig. 48 - Turbulent Kinetic Energy at 0.08m from Shelves

At this distance from the shelves, the turbulence is clearer and less similar to each other cycle. A steady increase in turbulence energy can be observed at the top regions of the shelf. This is followed by a steep drop just after the middle shelf. The high turbulence can be attributed to the disturbance of the flow from the top shelf. The decrease in the turbulence thereafter can be seen and explained by the flow no longer interacting with the shelves in an intrusive manner. The same behaviour can be seen at the line representing the bottom shelf though the jump down in energy is not as high in magnitude.

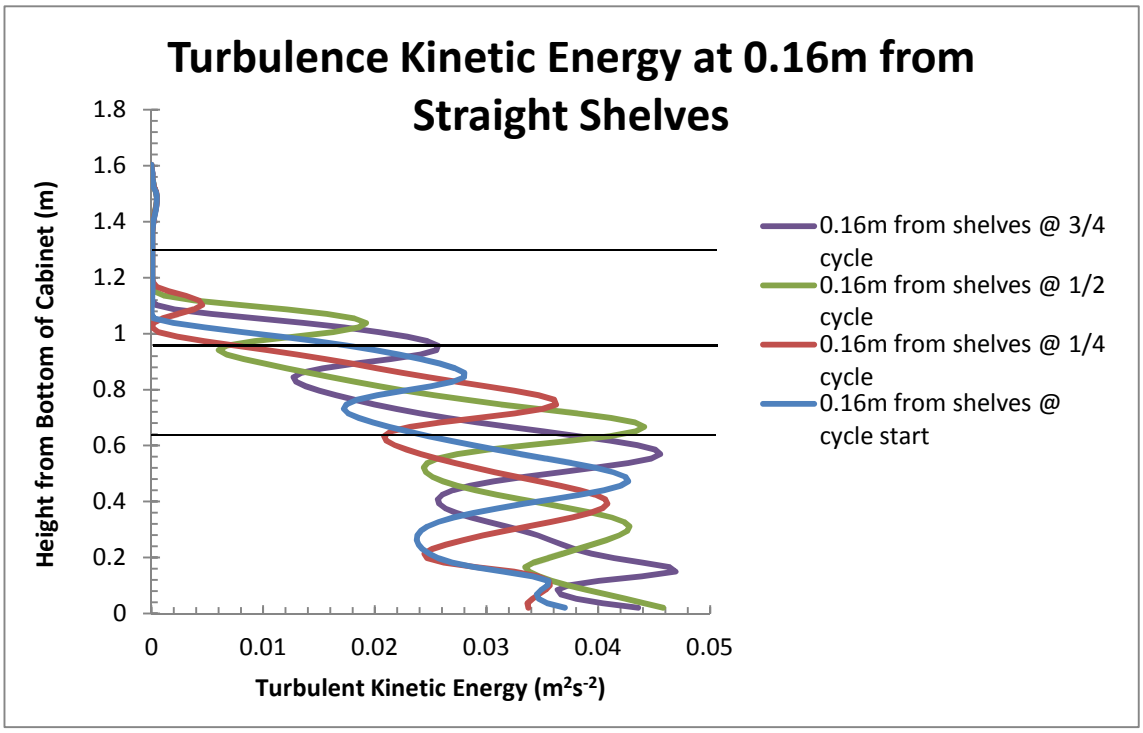

Fig. 49 - Turbulence Kinetic Energy at 0.16m from Shelves

As the turbulence is father away from the shelf, the fewer the disturbances can be attributed to the shelves presence. There is a steady pattern shown in the figure above and the turbulence can be seen to increase on the lower regions of the cabinet at this distance.

5.7 Transient Turbulence Intensity Numerical Analysis

This section details the turbulence intensity from the transient and steady state numerical models in front of each shelf and compares it to experimental data.

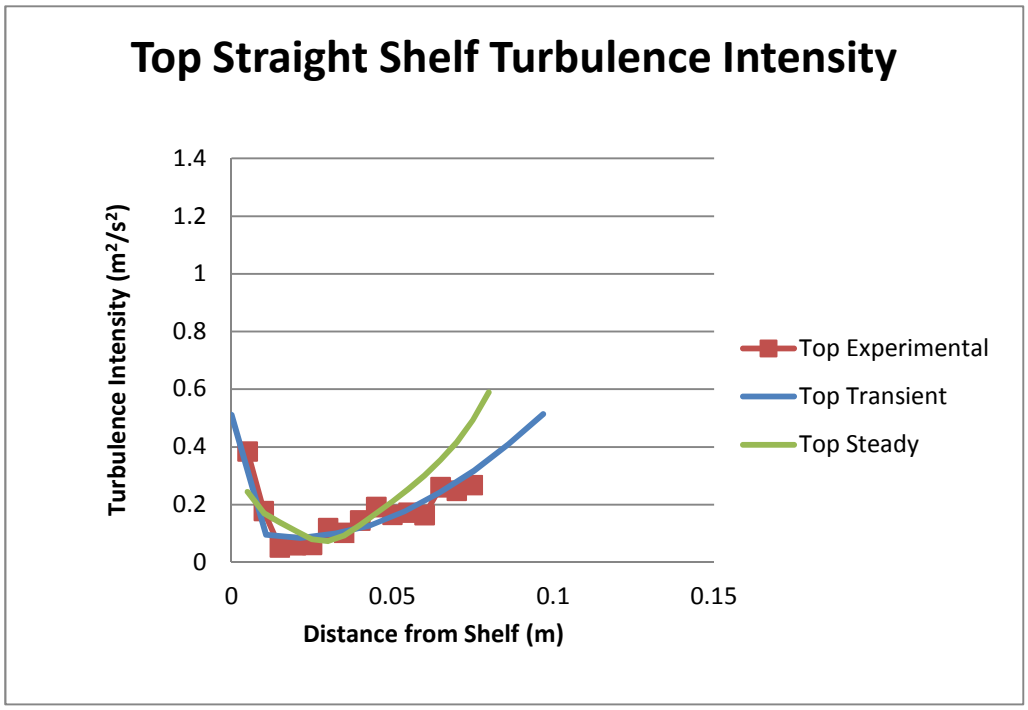

Fig. 50- Top Straight Shelf Turbulence Intensity

As can be seen from Fig. 50, the turbulence intensity for the top straight shelf is very comparable to the numerical experimental data. As the experimental intensity rises, so does the transient and there is good agreement throughout.

The result from the steady state calculations doesn't agree completely and diverges from the experimentally obtained results even at the top shelf location. Typically, all the models tend to predict air curtain flow close to the discharge grill reasonably well, so the discrepancy for steady state model even at distances close to the discharge grill indicates that the model is not performing in this particular case.

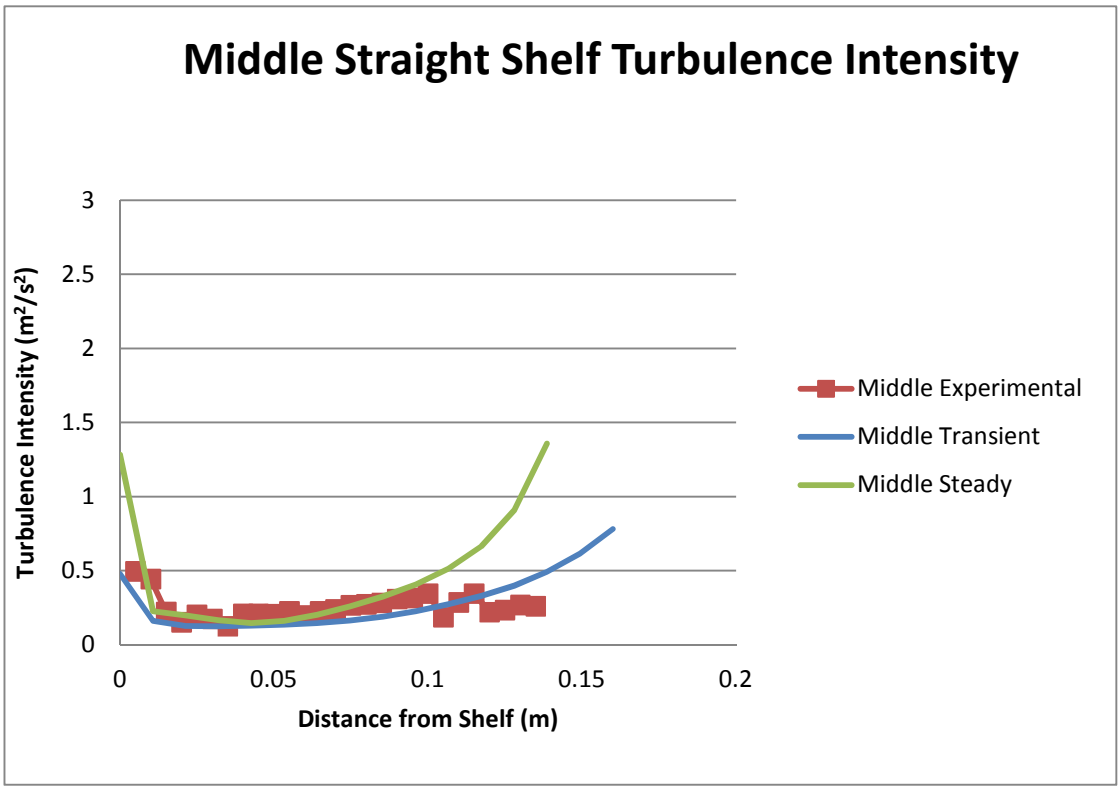

Fig. 51 - Middle Straight Shelf Turbulence Intensity

The middle shelf follows the same pattern as the top shelf. There is a little divergence in the magnitude of the turbulence intensity throughout. The numerical curve for the intensity tends to over predict further away from the shelf. It can be said that the transient numerical result holds well in the middle shelf.

This cannot be said for the steady state solution, however, since the values diverge greatly at 0.1m. The model does a poor job predicting the value of the turbulence in the middle section.

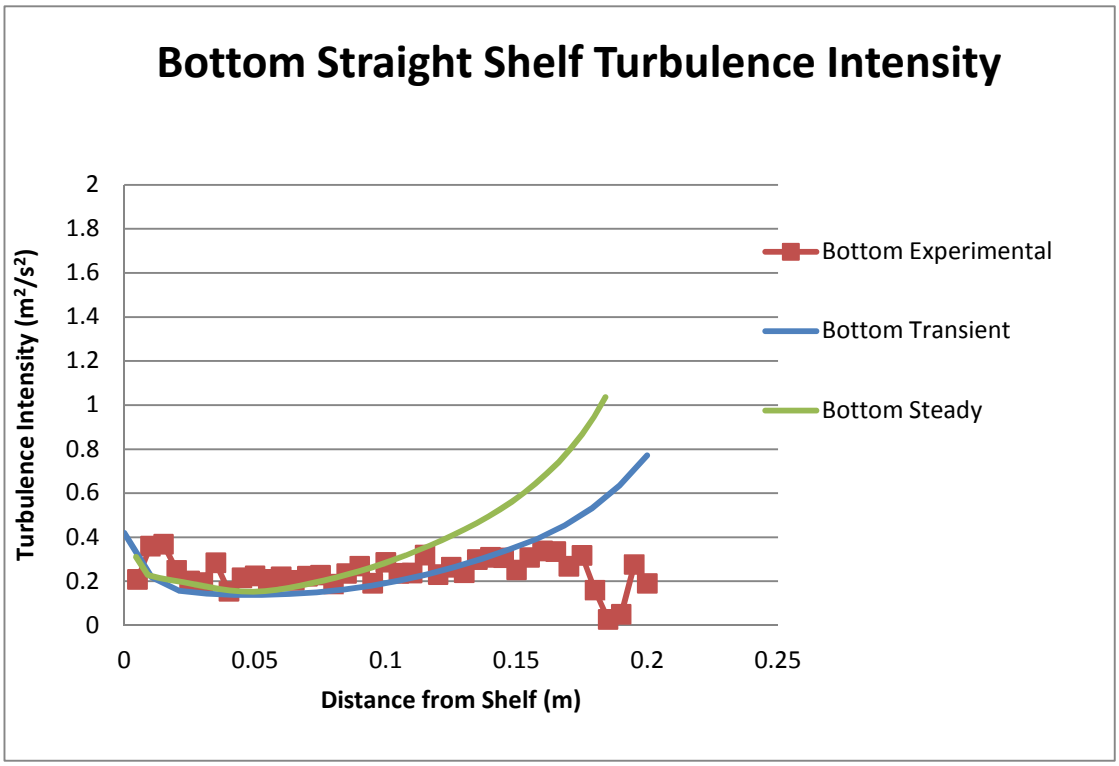

Fig. 52 - Bottom Straight Shelf Turbulence Intensity

Just as with the other shelf graphs, the bottom shelf shows the most divergence with the experimental data. The divergence occurs sooner than with the middle shelf and indicates a definite over prediction compared to the experimental data. The steady state over predicts much sooner and also diverges from the experimental much sooner. At 0.12m the steady state diverges and continues to rise higher than the experimental value.

These plots highlight the difficulty in predicting the nature of the air curtain at lower levels of the cabinet. As can be seen, even though there is even more turbulence predicted in the numerical model as opposed to the physical case, there is a large difference in the resulting velocity profiles and turbulence intensity calculation of the CFD code. Though all care was taken to mitigate any issues that might affect humidity,

this might be attributed to the nature of mixing handled in the CFD code and the humidity of the air curtain and the ambient air. These factors might have played a large role in influencing the prediction capabilities of the code and the behaviour of the air curtain respectively.

5.8 Summary

The results in this chapter show that the air curtain system of an RDC is not a truly steady state system. The periodic behaviour of the system under transient analysis shows the quasi-stable nature of the system. Furthermore, the transient simulations of air curtains attain a higher degree of accuracy than steady state simulations. The results conclude that by running simulations as a transient system, not only do the velocity profiles in the most complex and mixed regions of the cabinet show better agreement, but the turbulence intensity calculated by the CFD is also more accurate at regions lower and farther from the cabinet. For the remainder of the numerical results of this discretion, only the transient results will be shown.

.

CHAPTER 6 – STRAIGHT VERSUS SLANTED SHELVES

6.1 Slanted and Straight Shelf Configurations: Effect on Velocity Profiles

6.1.1 Flow Visualization

Initial results were obtained to determine how the air curtain would behave in the RDC with and without the shelves in the cabinet. This also helped to locate the exact LDV positions for the velocity measurements. The location of the photo is in the upper section of the cabinet near the discharge grill.

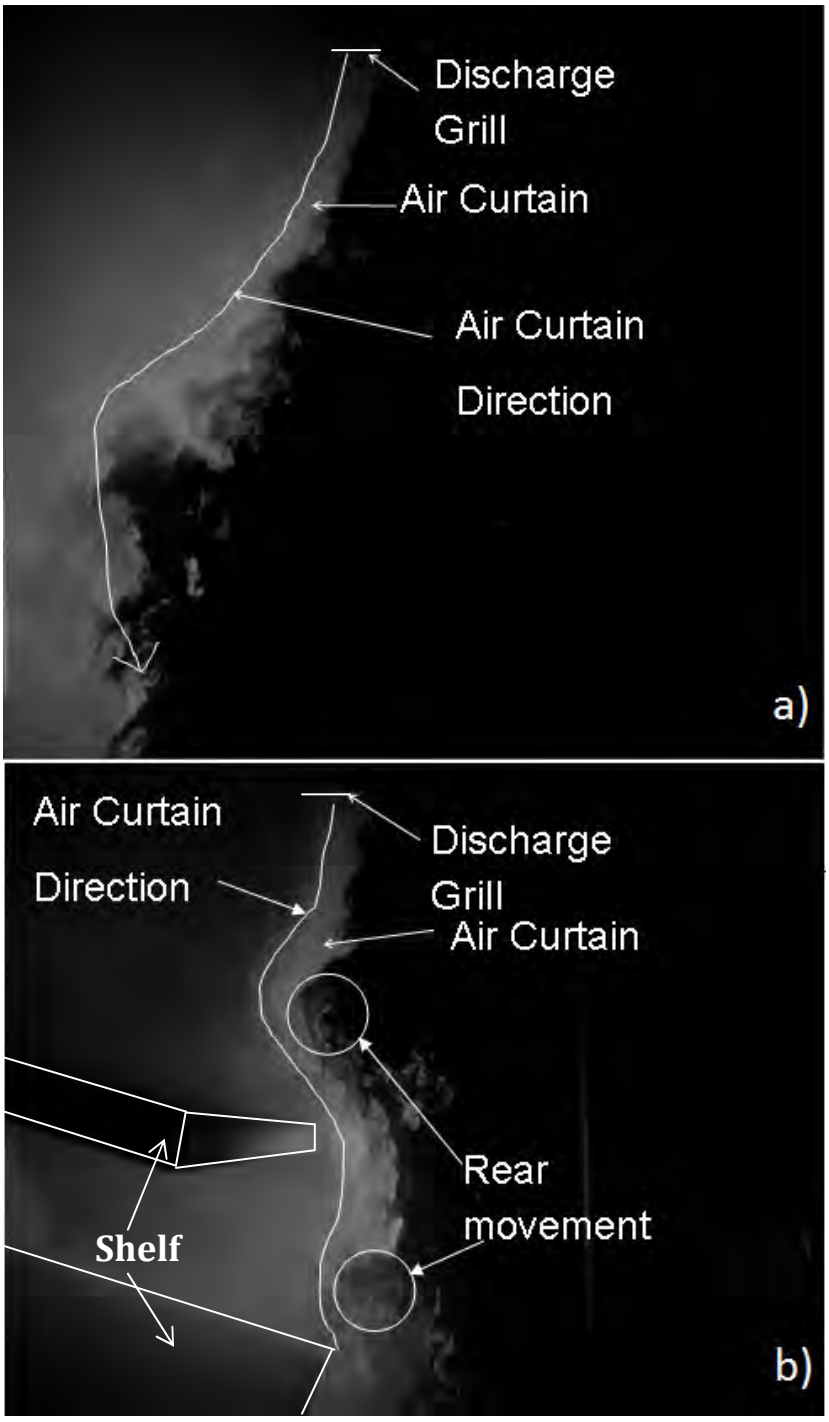

Fig. 53 - Snap shot Flow visualization of RDC a) without shelves and b) with shelves

In Fig. 53 a) the air flow moves to the rear of the cabinet where it proceeds down to the bottom to the return grill. When the flow reaches the bottom of the cabinet, part of the air curtain is recaptured and the remaining part spills over into the ambient air. A high degree of turbulence can be seen as the curtain moves to the back of the cabinet due to negative buoyancy. The turbulence does not seem to diminish after descending a significant distance from the discharge grill.

The photo in Fig. 53 b) is a typical image of the flow pattern with shelves, allowing us to place the position of the air curtain more accurately for the LDV measurements. The air curtain is pushed out by the shelves of the cabinet, causing a more solid air curtain to form over the front of the RDC. The slanted shelves allow the air curtain to "fall" over the edge, causing turbulence due to the tumbling over the edge, tripping eddy flows. This agitation of the flow, however, does not prevent the air curtain from moving toward the back panel. There are two sections in Fig. 53 b) that shows the tendency for the air curtain to move to the back panel, even with shelves in place. From a qualitative standpoint, there does not seem to be any more turbulence generated with or without the shelves in place.

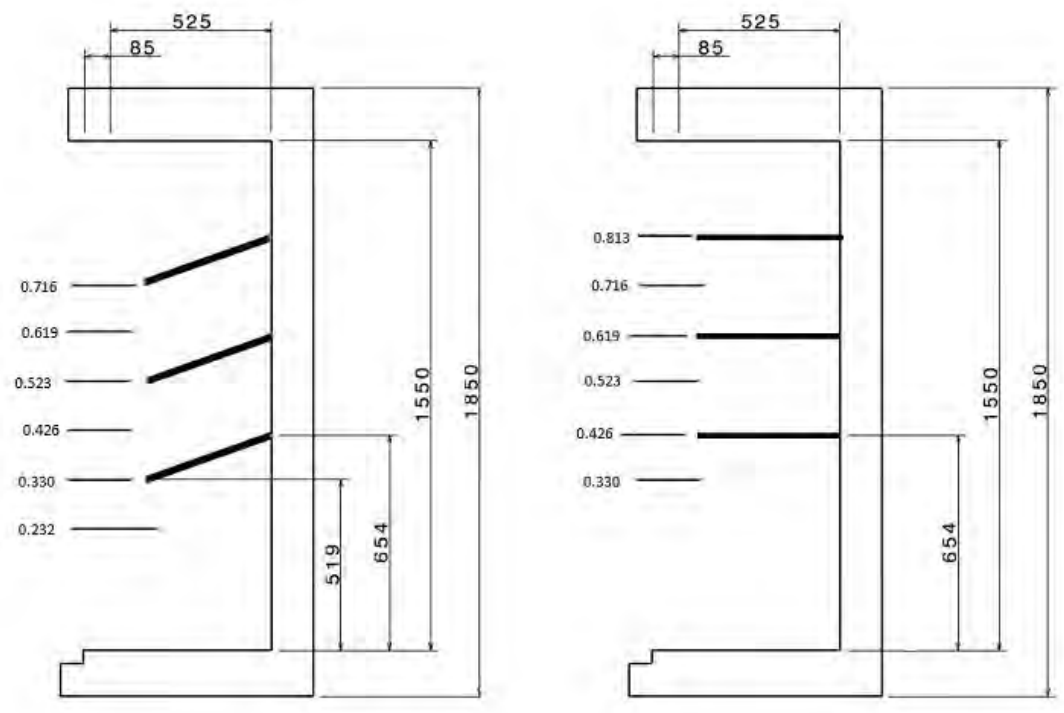

Fig. 54 - Cross sections of RDC in mm with numbered locations of relative heights and origin

The cross section of the RDC is presented in Fig. 54 where the dimensions of the cabinet (on the right side) are given in mm. The locations where the velocity measurements were taken (on the left) are non dimensionalized as h/H. Where h is the height from the return grill and H is the height of the cabinet cavity. The velocity measurements on figures below are presented as a function of *l* or non dimensional air curtain width (NDACW) where:

$$\boldsymbol{l} = \frac{\boldsymbol{ACW}}{\boldsymbol{Width\ of\ Discharge\ Grill}} \qquad \text{Eq. (10)}$$

Where $l = 0$ is the edge of the shelf in both the slanted and straight shelf scenario and ACW is the air curtain width as defined by Eq. (9).The negative direction is defined as into the cabinet and the positive direction is defined as out.

The width of the discharge grill was fixed at 85mm. The width of the air curtain is not fixed and is based on the LDV data as opposed to at least one previous study where the air curtain was describes as fixed in width [25]. The seeding of the flow, however, shows that the air curtain actually changes in width. The relationship between this width change and entrainment is not fully understood. The non dimensional number l provides a useful comparison with other cabinets while giving us valuable insight to the air curtain width with respect to the slanted and straight shelves.

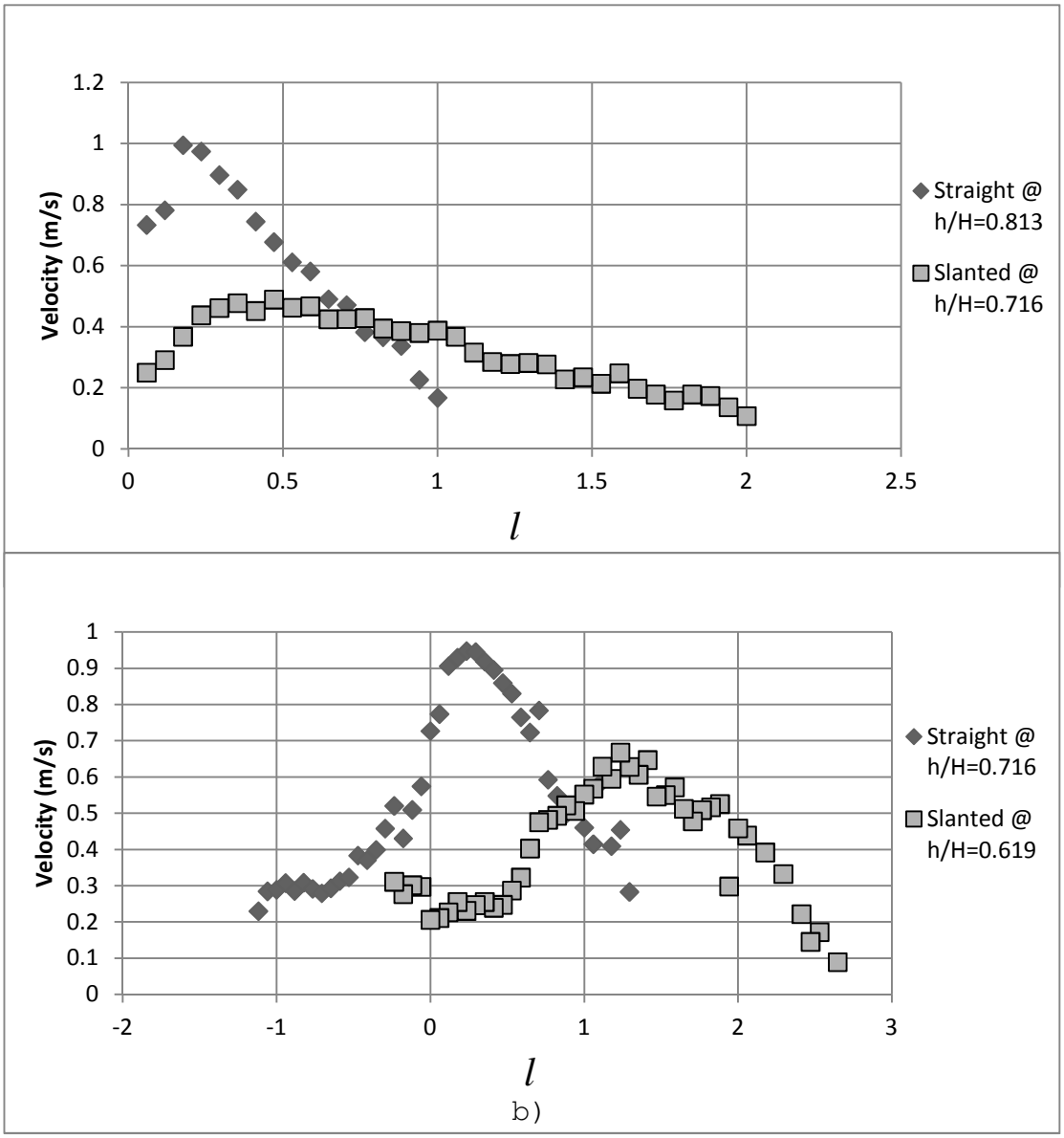

Fig. 55 – Velocity profiles representing a) top shelf and b) cavity between bottom shelf and top shelf

6.1.2 Upper Cabinet Results

It can be clearly seen from the top shelf profile in Fig. 55 a) that the straight shelf configuration does not cause the air curtain to extend out of the cabinet as far as the slanted shelf. This is most probably due to the air curtain going back into the cabinet due to negative buoyancy (as can be seen in Fig. 53 a) and b)) and flowing down the incline of the slanted shelf, causing the air curtain to proceed farther beyond the cabinet. The slanted shelf non dimensional air curtain width extends to twice the amount of the straight shelf air curtain, 2 to 1 respectively.

At the same time, the maximum velocity is a little more than twice as large for the straight shelf comparing with the slanted one, 1.0 m s-1 and 0.47 m s-1 respectively. This happens not only because the location at which the straight shelf measurement was taken was higher but also due to less overall disturbance of the flow in the case of the straight shelf configuration. In the slanted shelf scenario, where the flow encounters the slanted shelf due to negative buoyancy, causing significant disturbance and slowing down the overall flow. The maximums in the slanted and straight shelves are in slightly different areas away from the shelf. The straight shelf maximum appears at $l = 0.17$ while the slanted maximum appears at $l = 0.47$. The small difference between the areas in which the maximums appear is largely due to the proximity to the discharge grill. As seen in subsequent figures, the maximums are shown to diverge from each other.

The velocities for the slanted and straight shelves degrade at very different rates. From the edge of the shelf the velocity starts at zero and quickly climbs to its peak velocity for the slanted and straight. There is a noticeable jump in velocity early in the

profile from the second to third point in the straight shelf configuration that is not observed in the slanted shelf counterpart. The degrading of the velocity profile is steeper for the straight shelf, implying a more intact and less disturbed air curtain. The velocity for the slanted shelf configuration, on the other hand, degrades far more slowly, extending relatively far out of the cabinet as compared the straight shelf configuration.

In Fig. 55 b) the maximum velocities are more comparable, 0.95 and 0.68 m s-1 for straight and slanted respectively. This is due to an increase in velocity of the slanted shelf profile, from 0.48 to 0.68 m s-1. This is caused as the air curtain proceeds past the first slanted shelf into the cavity just below the top shelf; a slight increase in velocity is seen, or "recovering". This recovering of the velocity can be seen throughout the air curtains interaction with the slanted shelves but it is most prominent at the top shelf height. This recovering becomes less prominent in subsequent shelves. In comparison, the straight shelf velocity decreases slightly from 1.0m s-1 to 0.95 m s-1. The locations of the maximum velocities are $l = 0.23$ and $l = 1.24$ for straight and slanted respectively. This is a difference of one characteristic discharge grill length. This marks one of the key differences between slanted and straight shelf behavior, the location of the middle of the velocity profile. This determines where the center of the flow is for each situation and it shows that the center flow of the air curtain for the slanted configuration is farther out of the cabinet.

The straight profile in Fig. 55 b) also intrudes into the cavity area more than the slanted profile, reaching to l values of -1.1. The slanted shelf only intrudes into the cavity up until $l = -0.24$. As also can be seen from Fig. 55 b) the slanted shelf pushes the air curtain outwards much further than the straight shelf, reaching l values of 2.65

while the straight shelf only reaches *l* values of 1.29.The cause of the extension, being more prominent in the slanted shelf than in the straight shelf configuration, is the same reason the straight shelf retreats further into the cavity between the top and bottom shelf. The slant of the shelf not only causes disturbance of the air curtain flow but pushes the air curtain out of the cabinet significantly. The straight shelf retreating into the cavity is just an effect of negative buoyancy, while the slanted shelf velocity profiles does go into the cabinet slightly, the predominant force is the potential energy gathered by the air curtain interacting with the slanted shelf. It should be noted that the slanted shelf velocity is slightly higher just under the shelf (negative *l* values). This may be due to a separate recirculated flow within the cavity.

The slopes in each of these configurations are different but are more similar than in Fig. 55 a). In Fig. 55 b) the slopes of the slanted shelf increase and decrease at a larger rate than the slanted shelf. The slanted shelf velocity profile shows a gentler increase and decrease from maximum velocity to the end sections of the air curtain.

The slight choppiness of the data in the slanted shelf profiles suggests that entrainment starts already to play a role in the development of the air curtain. In comparison the straight shelf shows little signs of unsteadiness within the flow regime.

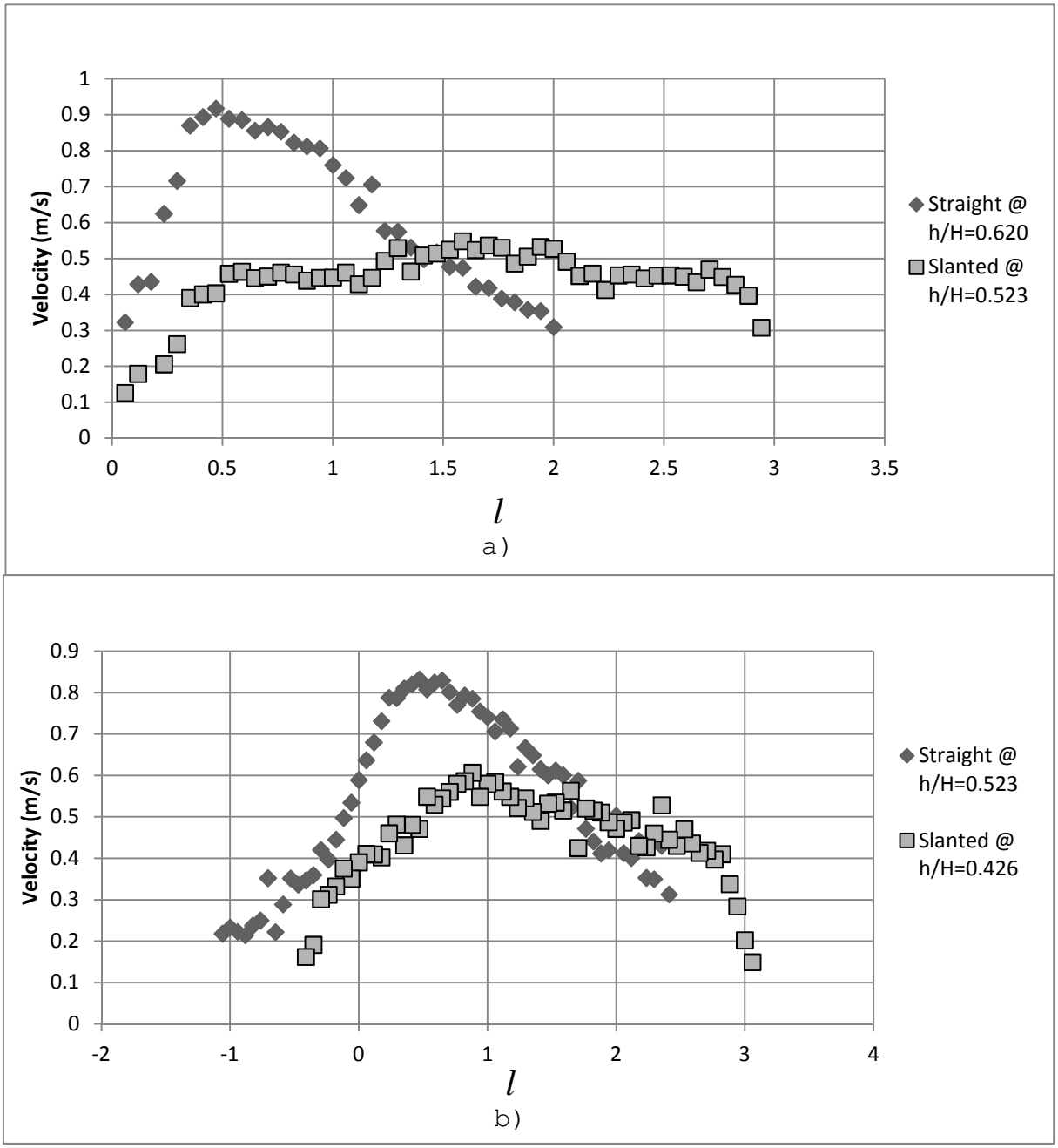

Fig. 56 - Velocity profiles representing a) the middle shelf and b) the cavity below the middle and bottom shelf

6.1.3 Mid Cabinet Results

It can be seen in Fig. 56 a) that the middle shelf shows the same disparity on the maximum velocities, 0.92 m s-1 and 0.55 m s-1 for straight and slanted respectively. The slanted shelf shows an interesting dip in the peak velocity as compared with Fig. 55 b), showing the disturbance that the shelf has on the peak velocity. The peak velocity dips to 0.55m s-1 from the value of 0.67 seen in Fig. 55 b). The maximum velocity for the straight shelf only dips a small amount, from 0.95 to 0.92 m s-1 from Fig. 55 b) to Fig. 56 a).

The slope of the slanted shelf is very similar to the slanted shelf velocity profile at the top shelf in Fig. 55 a). The profile is very flat and shows little variation in velocity once attaining a velocity value close to the peak. The velocity on Fig. 56 a) for the slanted shelf stays steady around the peak velocity for a much longer time. It also ends at an *l* value of 3.05 versus 2 in Fig. 55 a). It should be noted that the peak velocity for the middle shelf in the slanted configuration is higher than in Fig. 55 a) but not Fig. 55 b). This is mainly due to the disturbance that the middle shelf causes to the recovering of velocity and the forces of entrainment acting on the air curtain.

The straight shelf velocity, on the other hand, is almost twice the magnitude of the slanted shelf profile. The air curtain profile can be seen to be more intact for a longer period of time with the straight shelves. The shape of the profile on the straight shelf is very similar to Fig. 55 a) straight shelf profile. The velocity increases very quickly to peak and degrades relatively quickly compared to the slanted shelf

configuration. In comparison to Fig. 55 b) the air curtain has extended from an *l* value of 1.29 to 2. This is due to the increasing entrainment as the air curtain descends farther from the discharge grill.

In Fig. 56 b) the slanted shelf maximum velocity recovers slightly to 0.61 m s-1 at *l* = 1 from 0.55 m s-1 in the previous profile. The change in slope is also more poignant on either side of the peak velocity value. The peak velocity is also noticeably closer to the cabinet at an *l* value of 0.88. The slanted shelf also retreats slightly more into the cabinet cavity than in Fig. 55 b), from an l value of -0.24 to -0.41. The air curtain only slightly extends from Fig. 56 a). This either shows that the disturbance from the middle shelf is still prevalent or potential energy gained from sliding down the slanted shelf is not enough to extend the curtain significantly. The velocity profiles seem to drop off at the same rate at roughly the same *l* value in the positive *l* direction.

The straight shelf velocity degrades slightly from 0.92 m s-1 to 0.83 m s-1 from Fig. 56 a) to b). The slope on either side of the peak seem to remain in the same state as with Fig. 56 a); the only difference being that the air curtain enters into the shelf cavity. As can be seen, the air curtain in the straight shelf configuration enters the cavity slightly less than in Fig. 55 b), *l* = -1.05 and -1.1 for Fig. 56 b) and Fig. 55 b) respectively. The outer edge, compared to Fig. 55 b), can also be seen to reach out more, to *l* values of 2.41 while it was 2 and 1.29 for Fig. 56 a) and Fig. 55 b) respectively. This shows the tendency for the air curtain to expand out of the cabinet as the distance from the discharge grill increases.

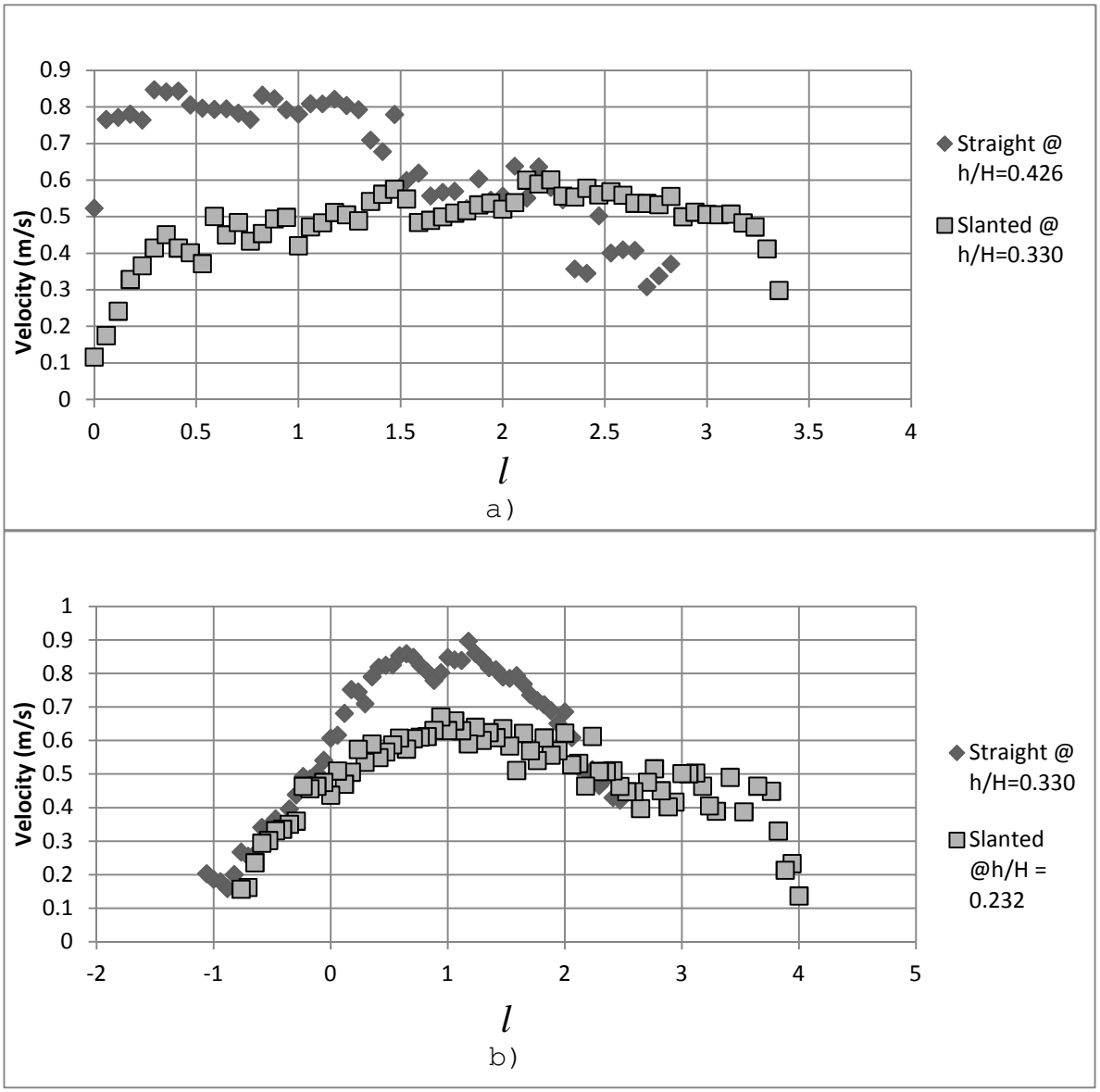

Fig. 57- Velocity profiles representing a) the bottom shelf and b) the cavity below the bottom shelf

6.1.4 Lower Cabinet Results

It can be seen in Fig. 57 a) that the gradient in the positive *l* direction for the straight shelves is lower as compared to the areas above this. As expected, the *l* value for the straight shelf reaching out of the cabinet increases slightly from 2.41 to 2.86. The maximum velocity in Fig. 57 a) for the straight shelf stays at around the same value of 0.85 m s-1. The more sporadic data in Fig. 57 a) shows that the air curtain is not as contained as it was at higher levels in the cabinet. The continued entrainment coupled with the disturbance from the shelf is the main cause of this disturbance.

The profile of the velocity for the slanted shelf shows almost no qualitative change from Fig. 56 a) to Fig. 57 a) as the gradient and general shape are very similar.. This is probably due to the consistent disturbance from the shelves at these locations. The maximum velocity for the slanted shelf is a little higher than in Fig. 56 a); the recovering factor seems to take precedence over the disturbance in this instance, if only slightly. The air curtain can be seen to spread more out of the cabinet from Fig. 56 b) Fig. 57 a), from *l* values of 3.05 to 3.35 respectively. The gradients around the peak velocity lessen greatly, as seen with previous shelves for the slanted configuration. The maximum velocity only decreases slightly from Fig. 56 b) to Fig. 57 a), showing that the shelf disturbance is not that significant in perturbing the maximum velocity. The same cannot be said, however, of the perturbation of the entire profile as there are significant changes in the shape and behavior. The peak velocity *l* location seems to moves from 0.88 to 2.12.

The disturbances caused by the straight shelves do not perturb the flow as much as with the slanted configuration. Therefore, it can be concluded that by putting shelves in the slanted position, the disturbance to the flow and entrainment rate increases significantly as compared to the straight shelves.

As can be seen from Fig. 57 b) velocity for both slanted and straight shelves configuration recovers little, changing from 0.6 m s-1 to 0.7 m s-1 and 0.85m s-1 to 0.9 m s-1 for slanted straight shelf respectively.

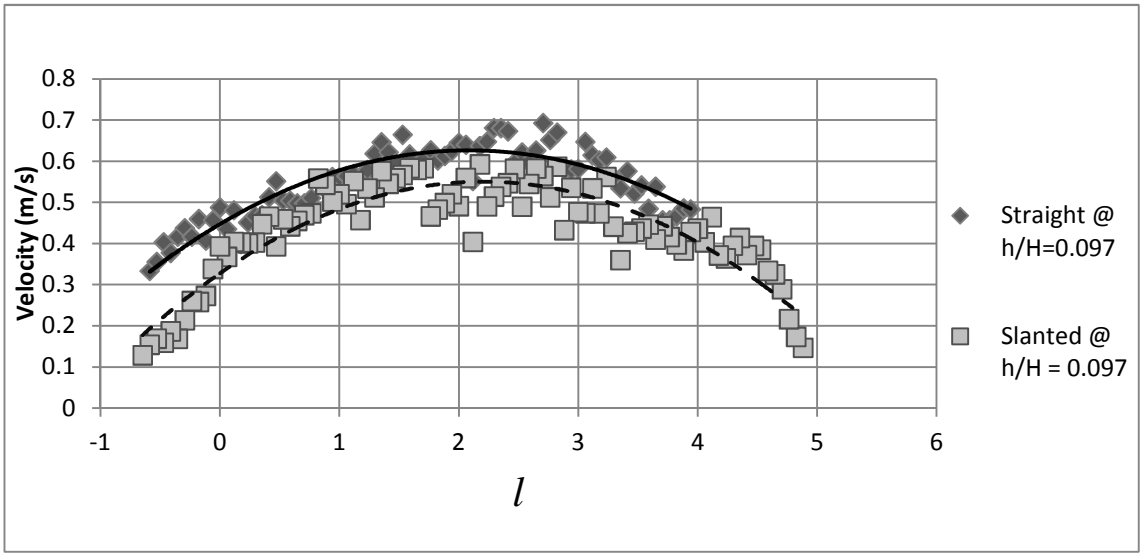

Fig. 58 Velocity Profiles above the Return Grill

6.1.5 Results Above Return Grill

As can be seen from Fig. 58, the unsteadiness of the flow has caused both slanted and straight configuration profiles to look very similar to each other. The main difference being the velocity of the straight shelf profiles is markedly higher than the slanted shelf configuration. It is interesting to note that even with these profiles taken so low down the cabinet, the entrainment doesn't seem to overpower the effect that the

straight shelves have on the flow, such as higher overall velocity. This information can be useful in analyzing not only the effect that the straight shelves have on a cabinet but also on the flow past the shelf section.

The peaks of each velocity are in the same area and the degading of the velocity on each side of the peak is consitent with slanted and straight shelf configurations.

6.2 Non Dimensional Air Curtain Width Results

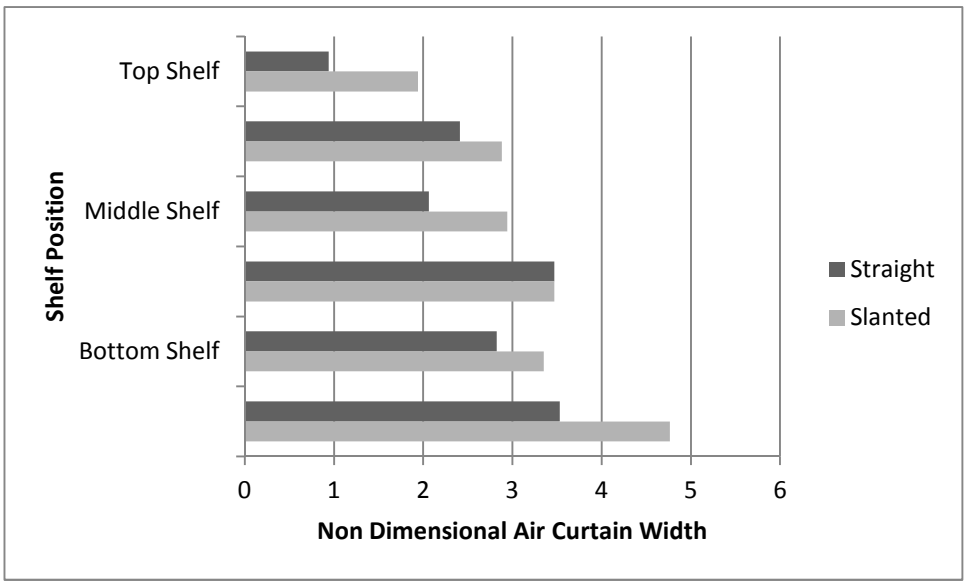

Fig. 59- Non Dimensional Air Curtain Width Versus Shelf Position for Slanted and Straight Shelves

The labels in Fig. 59 on the x-axis denote which shelf the measurements were taken. The blank bars in between top and middle denote the non dimensional air curtain width in the cavity between the top and middle shelves.

As can be seen from Fig. 59 the non dimensional air curtain width has a steady increasing trend from top to bottom for both straight and slanted configurations. There

is a large gap between the two values at the location taken below the bottom shelf. The fact that there was no shelf below the third may have played a factor in the air curtain becoming largely widened. This is, however, not the case for the straight shelf scenario where the increase in the width is not significant from the bottom shelf further down the cabinet.

It is also clear to see from the data that the slanted shelves have, on average, a larger width than the straight shelf case. The middle bottom cavity seems to be a numerical exception in this case and can be concluded to be a statistical anomaly.

The straight shelves go by a specific predictable pattern. Where there is the shelf to support the air curtain, the width is low. In the cavity between the shelves the air curtain expands into the cavity, increasing the width. This can clearly be seen at the top shelf and the top middle cavity. When it encounters the middle shelf, the width lowers again to below its previous value in the cavity and expands again when reaching the middle-bottom cavity. Each subsequent shrinking and lengthening of the air curtain becomes lessened and greatened respectively. In comparison, this behavior is not seen in the slanted shelf case. The only reduction in width is slight from the middle-bottom cavity to the bottom shelf.

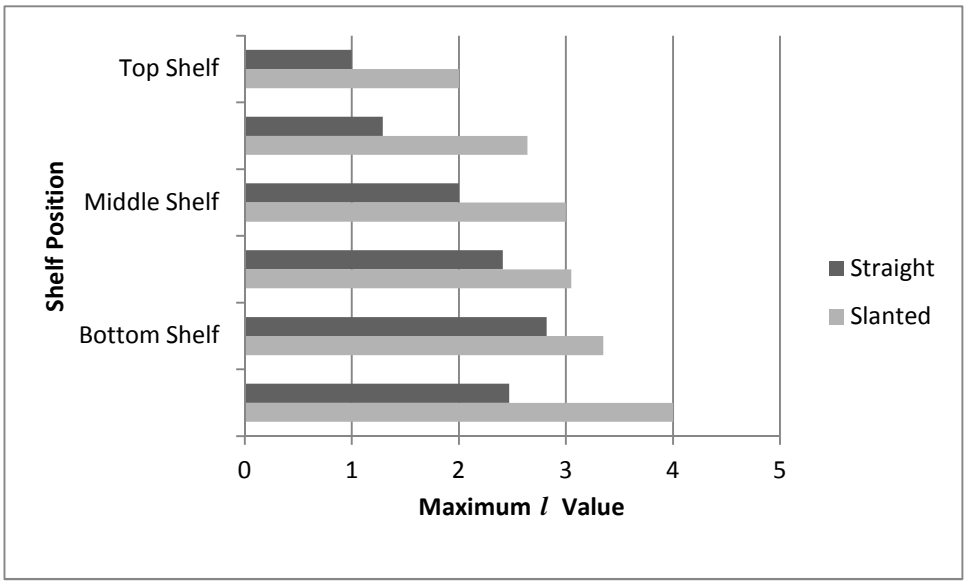

Fig. 60 - Non-Dimensional Extension of Air Curtain from the Shelves Versus Shelf Position

Fig. 60 shows the maximum non dimensional distance the air curtain reaches out of the cabinet; this is generated by taking the largest positive *l* value and comparing it to position. As Fig. 60 shows, there is a distinct gradual increase in non dimensional air curtain width value as the air curtain travels from top to bottom for both configurations, except for the last point for the straight shelf configuration. Even in this case, the decrease is small and an overall trend can be seen of increasing propagation of the air curtain out of the cabinet.

It can also be seen that the air curtain propagates significantly further with the slanted shelves than with the straight shelves. This increases the amount of ambient air interacting with the air curtain and, therefore, increases entrainment. This chart clearly shows the straight shelves are a far more efficient in storing chilled goods.

Upon further examination of the results, several observations can be made from the experimental data. The air curtain width is shown to expand greatly as the air curtain falls from the cabinet. This could be due to the large turbulence intensity caused by the introduction of the first shelf; this introduces mixing and entrainment and, eventually, increases the air curtain width as the air curtain falls to the lower regions of the cabinet. The NDACW provides a useful tool in understanding entrainment. Turbulence intensity helps us to see when entrainment happens and the NDACW shows us the results of the introduction of entrainment downstream. The effect of entrainment is not immediate and takes time to manifest in physical characteristics such as increasing the buoyancy of the air curtain and, therefore, increasing the air curtain width.

There are numerous differences between slanted and straight shelves. The ACW and NDACW for the slanted are larger, if only slightly in the ACW case. This does show a general trend that the slanted shelf air curtain extends farther from the cabinet, which is a negative characteristic.

6.3 Kinetic energy difference

Table 2 - Percent velocity difference between slanted and straight shelves

	Slanted Maximum Velocity (m/s)	Straight Shelf Maximum Velocity (m/s)	Difference (%)
Top Shelf	0.48	0.99	0.51
Top-Middle Cavity	0.64	0.95	0.32
Middle Shelf	0.55	0.92	0.40
Middle-Bottom cavity	0.61	0.83	0.27
Bottom Shelf	0.60	0.85	0.29
Below bottom shelf cavity	0.67	0.90	0.25

As can be seen from the table above, the velocity change is of a significant nature. At the least, the velocity change is at 25% and it reaches as high as 51% for the top shelf. It cannot be questioned that all things remaining the same, the changing the angle of the shelf has a significant effect of the velocity and, therefore, the kinetic energy of the system. It should be noted that the Re (72,000) and Ri (13.3) of the system does not change with the introduction of a slanted shelves as it does not affect the main geometries of the system (discharge grill width, height of the cabinet etc).

6.4 Slanted and Straight Shelf Numerical Comparison

In this section, the slanted and straight shelf numerical results are analyzed and compared. This section will help us understand the differences between the slanted and straight configurations using a varying number of parameters to analyze both cases.

6.4.1 Vector Plots

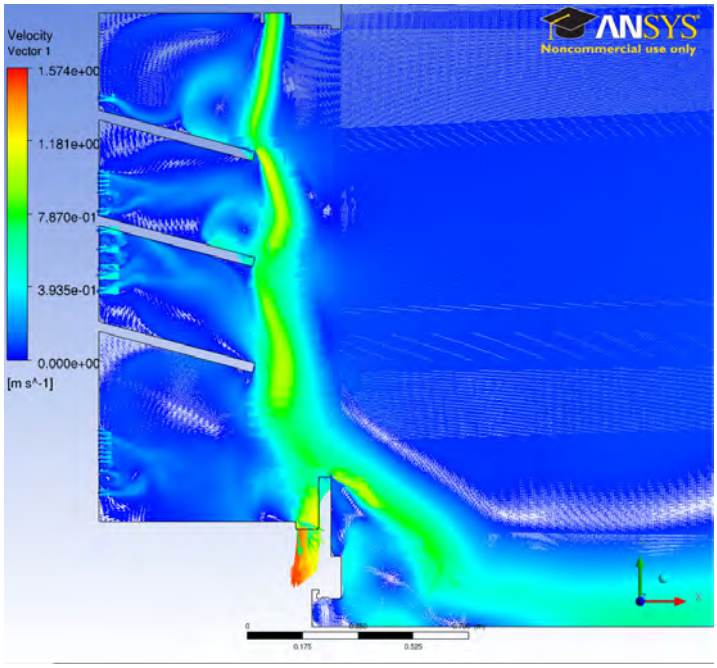

Fig. 61 - Slanted shelf instantaneous Vector Plot

The velocity field obtained from transient simulations for the slanted shelf is shown in Fig. 61. The negative buoyancy that shifts the air curtain towards the back of the cabinet is similar to what was observed in the steady state case in Fig. 23. The wave like nature of the air curtain obtained from transient simulation is more comparative with flow visualization results and therefore it can be concluded that transient simulation produces realistic results.

6.4.2 Velocity Profiles

The slanted and straight velocity profiles are detailed in this section. Velocity profiles in front of the shelves are useful in judging the differences between the configurations.

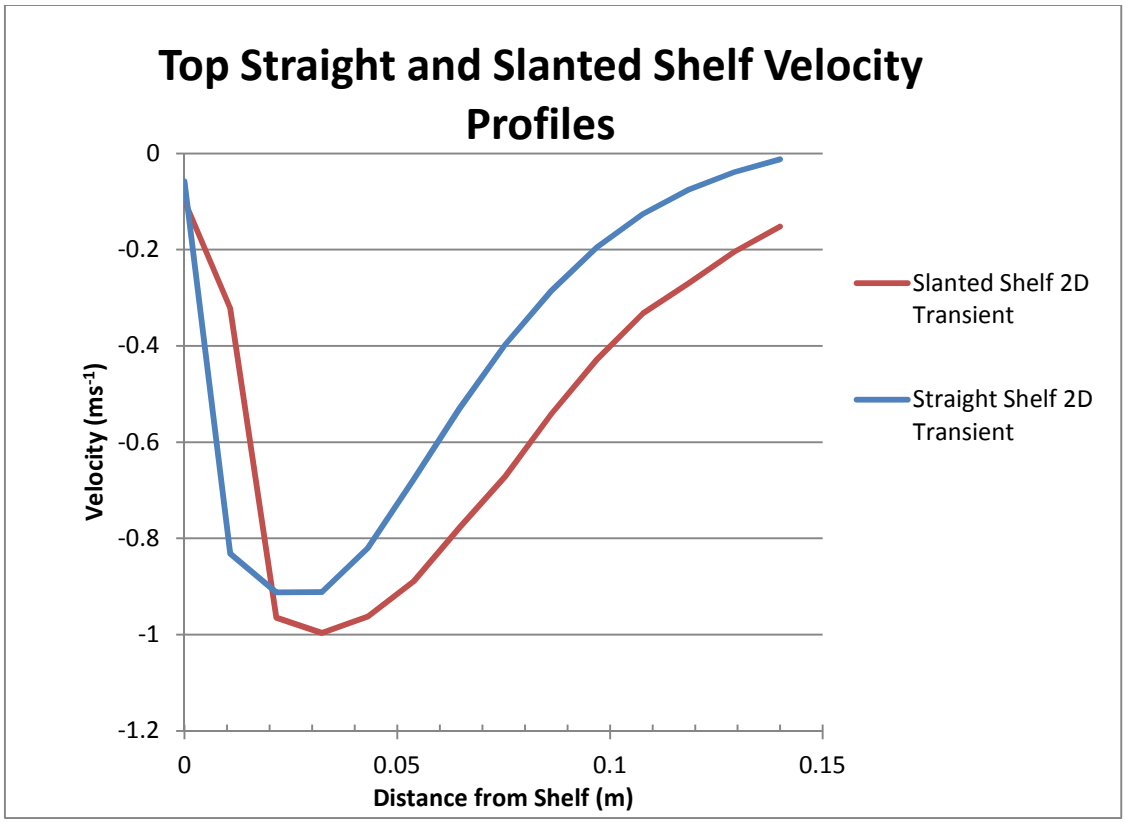

Fig. 62 - Top Straight and Slanted Shelf Velocity Profiles

The slanted and straight state velocity profiles for the top shelf shown in Fig. 62 are almost identical in structure; however, the slanted simulations predicts the air curtain velocity to be about 0.1 ms^{-1} faster at peak velocity of the slanted shelf and after peak, while before the peak velocity, the straight shelf has a higher velocity.

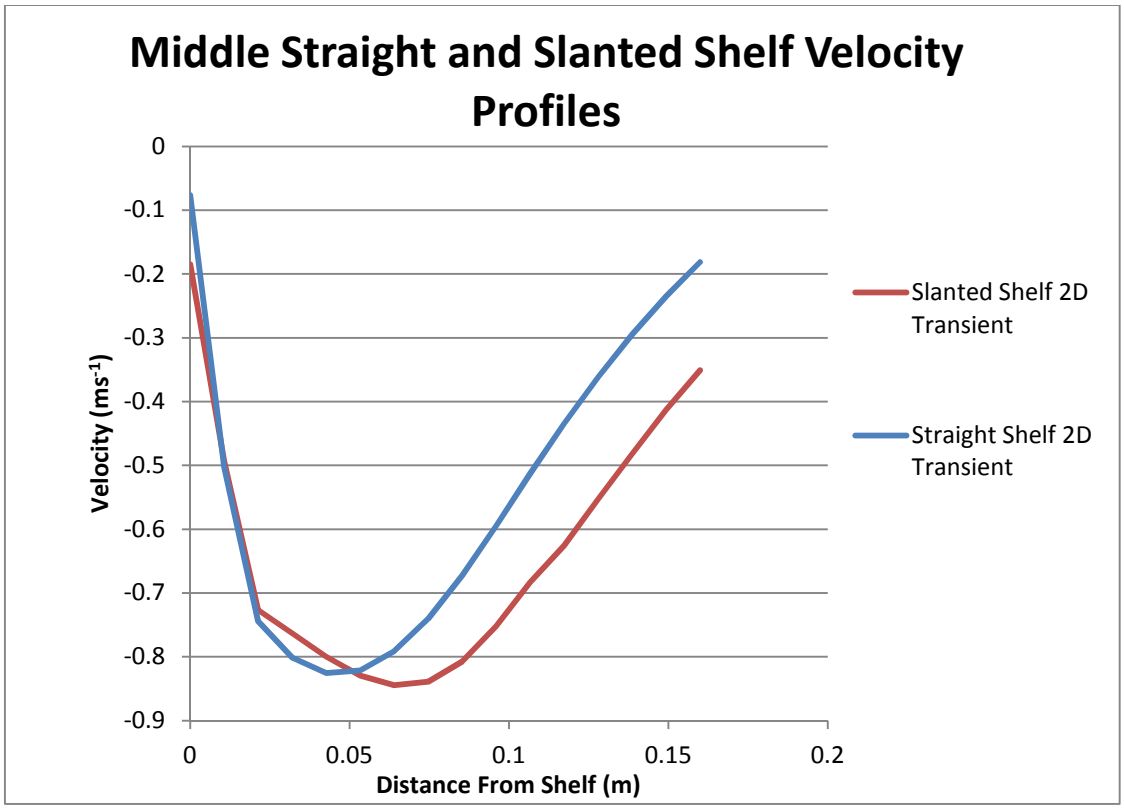

Fig. 63 – Middle Straight and Slanted Shelf Velocity Profiles

The middle shelf velocities for the straight and slanted simulations are shown in Fig. 63. The steady state predicts and high peak close to the shelf at about 0.04 m away from the cabinet. The peak for the transient profile shifts slightly farther from the cabinet to 0.06 m away from the shelf. Both peak velocities are high compared to the peak experimental velocity. The peak experimental velocity is 0.7 ms^{-1} and the peak velocity for the steady state and transient are 0.9 ms^{-1} and 0.85ms^{-1} respectively.

The transient results, for the middles shelf profile, are more accurate at predicting the width of the air curtain.

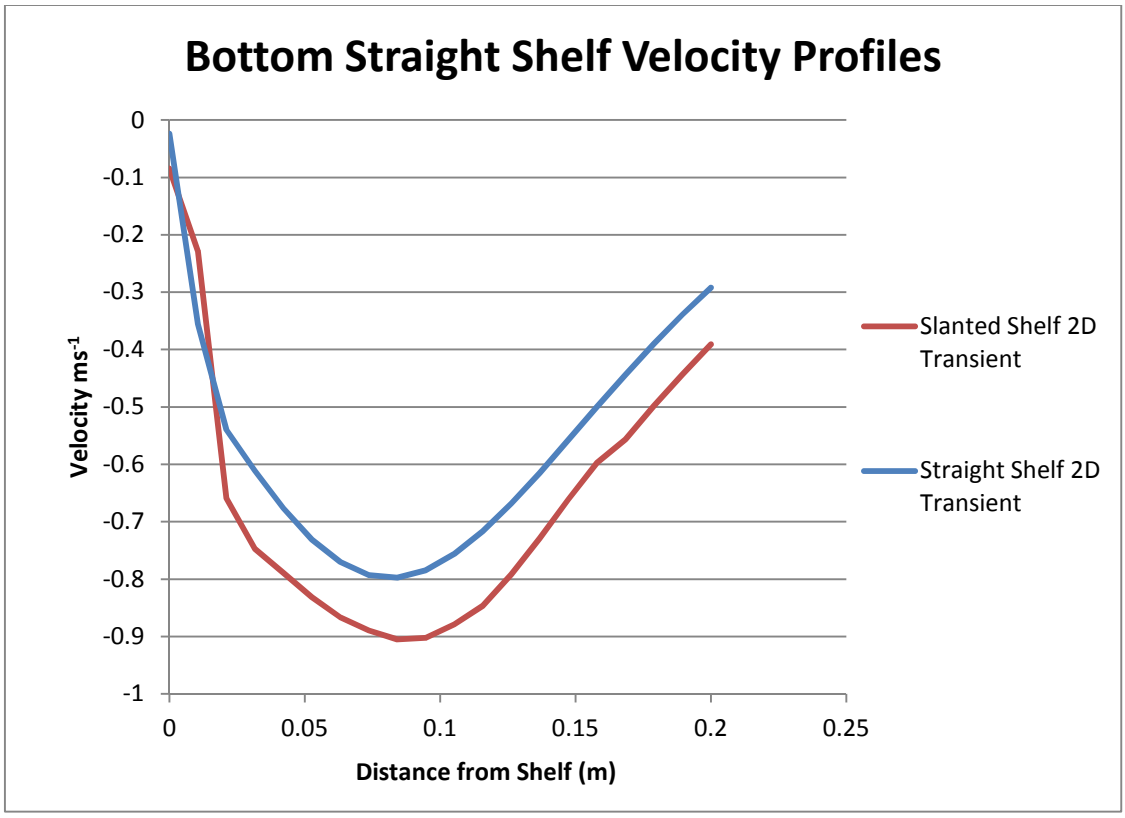

Fig. 64 – Bottom Straight and Slanted Shelf Velocity Profiles

The numerically obtained straight and slanted for the bottom shelf are both similar for the slanted shelf scenario shown in Fig. 64. The velocities are only very close to the shelf. Then the slanted shelf velocity magnitude increases compared with the straight shelf and maintains a 0.1 ms^{-1} higher velocity than the straight throughout the profile. Both profiles peak at about the same location at 0.08m.

6.4.3 Air Curtain Width

Air curtain width is a useful tool in seeing how far the air curtain reaches in relation to one another and how the shelves affect the width of the air curtain.

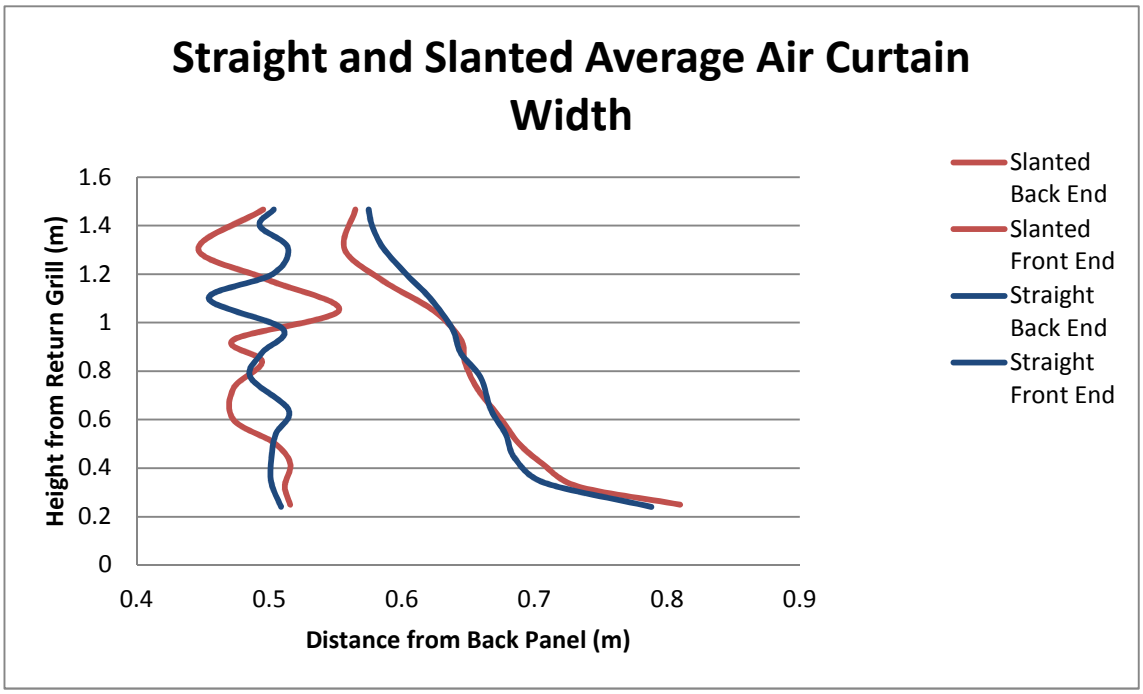

Fig. 65 – Slanted and Straight Shelves Air Curtain Width

As can be seen from Fig. 65, the air curtain extends out of the cabinet at about the same distance. However, on average, the slanted shelf extends farther than the straight shelf at lower regions of the cabinet. It can also be observed that the slanted shelf is heavily influenced by the angled shelves as can be seen at the height of 1.1m from the return grill. The negative buoyancy effect can also be seen with the straight shelf case at the same height.

6.4.4 Slanted Shelf Turbulence Kinetic Energy Analysis

The results for the turbulence kinetic energy can give a further insight on the characteristics of the flow in the cabinet. The profiles presented in this section have been calculated at the same relative location with respect to the shelf as with the straight shelf scenario (Refer to Fig. 46). The bottom shelf is at 0.34m, the middle shelf is at

0.675m, and the top shelf is at 1.01m. The horizontal lines in the following graphs denote their locations.

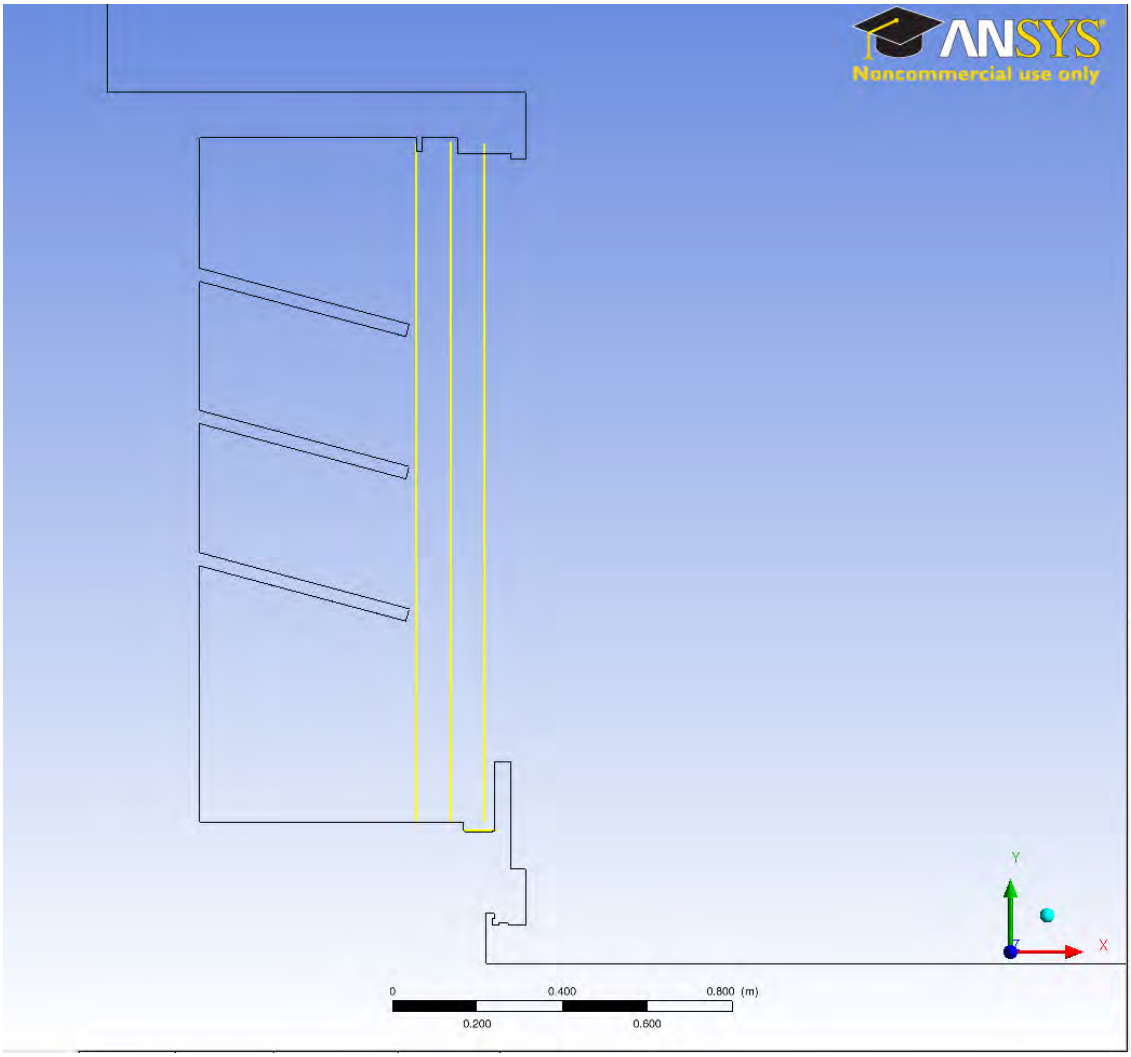

Fig. 66 - Location of Slanted Turbulent Kinetic Energy Lines

In Fig. 66 the locations of the turbulence intensity profile lines for this section are shown. Analysing the kinetic energy gives us an indication how far from the cabinet the shelves have an influence on the flow in terms of turbulence.

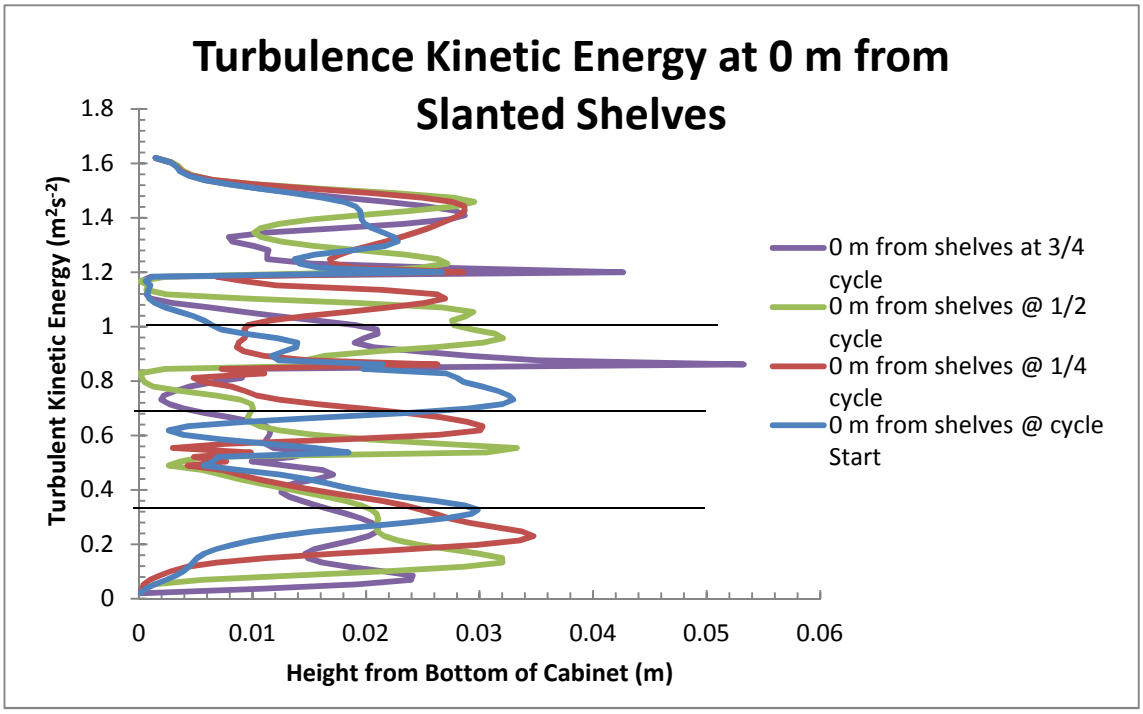

Fig. 67 - Turbulence Kinetic Energy at 0 m from Slanted Shelves

The values for the kinetic energy next to the shelves show that the flow is very turbulent and chaotic. There seems to be no pattern at this distance during the cycle except there is peak at the end of the cycle that reduces in intensity as the wave of the air curtain propagates down.

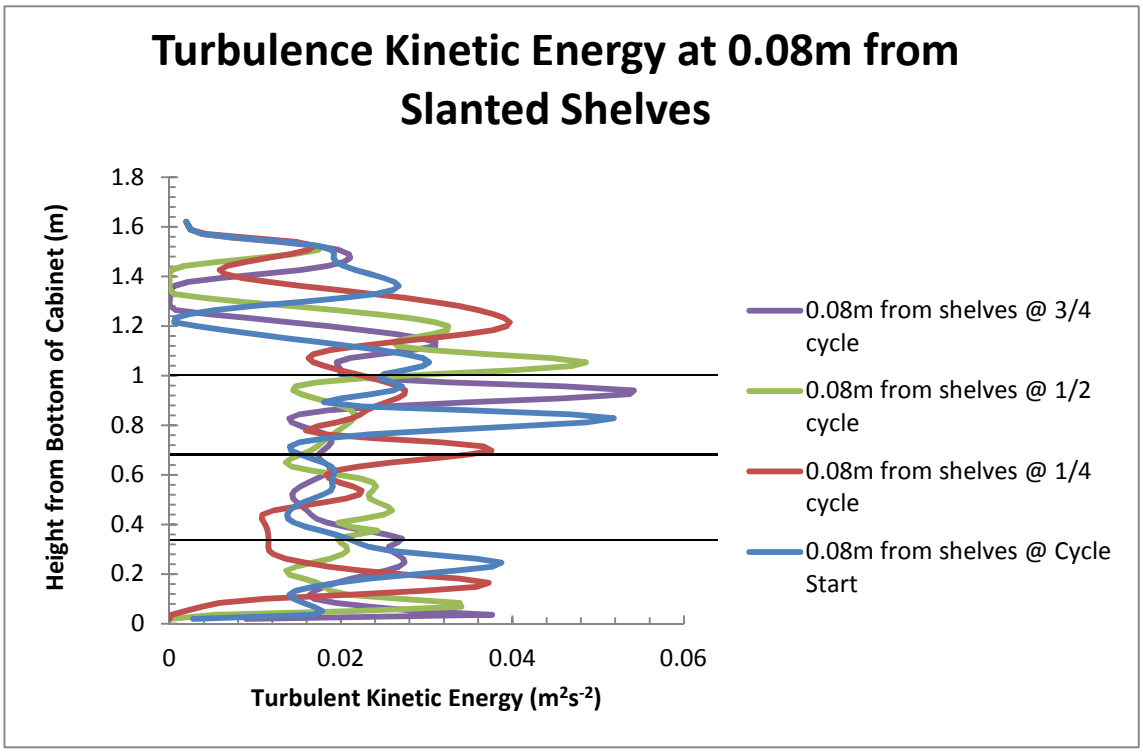

Fig. 68 - Turbulence Kinetic Energy at 0.08 m from Slanted Shelves

At 0.08m from the shelf the profiles are less jumbled and clear peaks can be seen. The turbulence gradually rises and falls compared to Fig. 47. The turbulence is highest after the middle shelf and lowers. It then rises again at the bottom part of the cabinet.

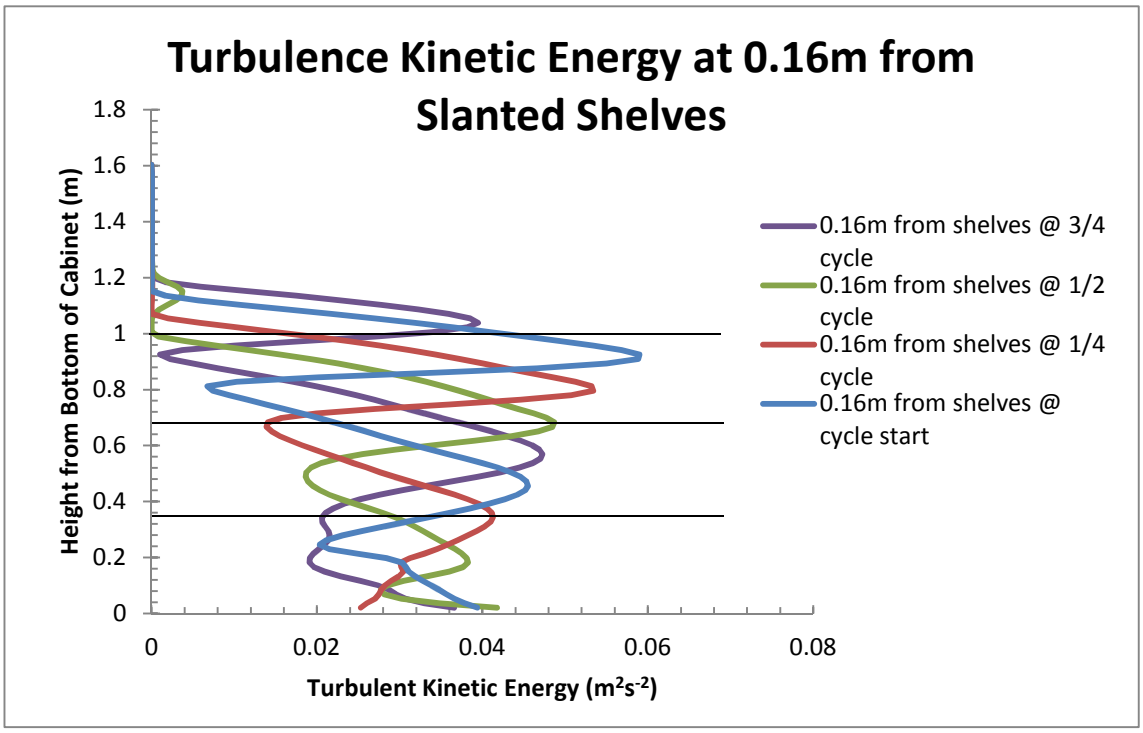

Fig. 69 - Turbulence Kinetic Energy at 0.16m from Slanted Shelves

The kinetic energy is quite high at 0.16m from the shelves. The turbulence is highest just below the top shelf region and slightly lowers from there. A wave pattern can be seen to emerge as the cycle continues.

Turbulent kinetic energy can be seen as high at 0.16 m from the cabinet in the slanted shelf scenario and is significantly higher than with the straight shelf scenario. This region is the area where the aisle air is on the cusp of the RDC and turbulence in the region should be avoided as much as possible.

In the area right next to the shelf both slanted and straight cases seem to be equally chaotic as high degrees of turbulence kinetic energy can be found with no real connection to the shelf placement or pattern through the overall cycle.

6.4.5 Slanted and Straight Shelf Turbulence Intensity Analysis

The analysis of the difference in turbulence intensity can help identify the areas where the turbulence is at the highest value. If a correlation can be established of the angled shelves having a greater effect on the turbulence intensity, then, at the very least, a conclusion can be made of high turbulence intensity with respect to slanted shelves.

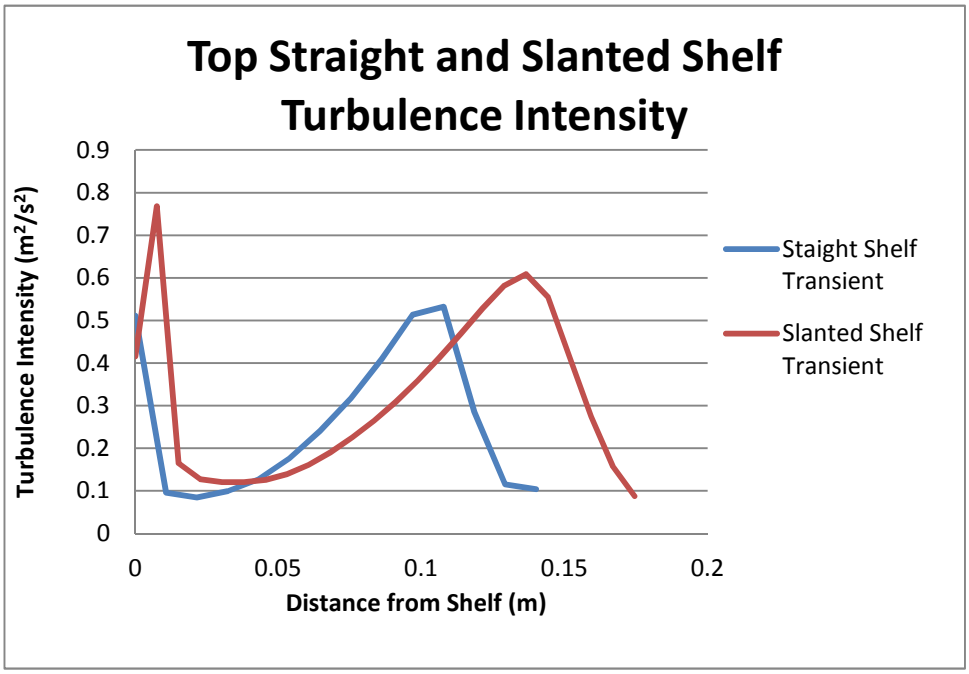

Fig. 70 – Top Straight and Slanted Shelf Turbulence Intensity

As can be seen from the figure above, the slanted shelf turbulence intensity profile has a lower magnitude compared to the straight shelf overall. However, in regions close to the shelf the turbulence is much higher. This is most probably due to the air curtain mixing in the region just in front of the slanted shelf. This behaviour is caused by the slanted shelf, in which case the air flow goes down, hits the shelf and then changes the direction following the slope of the shelf. As the profile reaches beyond 0.04 m the slanted shelf turbulence shows a lower magnitude until 0.14m where the

turbulence intensity peaks higher than the straight shelf turbulence. The peak of the slanted shelf turbulence intensity is markedly further than the straight shelf; this is another effect of the slanted shelf geometry, the increasing of turbulence and pushing the mixing region farther from the cabinet.

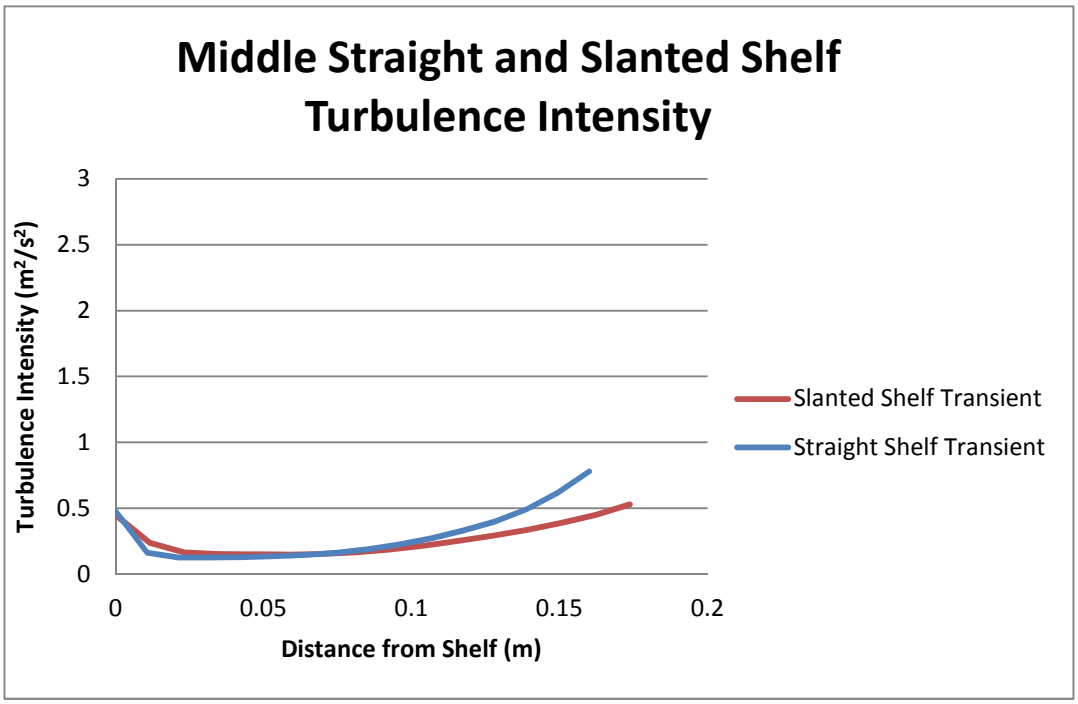

Fig. 71 - Middle Straight and Slanted Shelf Turbulence Intensity

The slanted and straight shelves velocity magnitudes match with each other quite well. The values only diverge from each other at about 0.11 m from the middle shelf. Again, as in Fig. 70, the slanted shelf shows slightly lower turbulence intensity than the straight one farther away from the shelf.

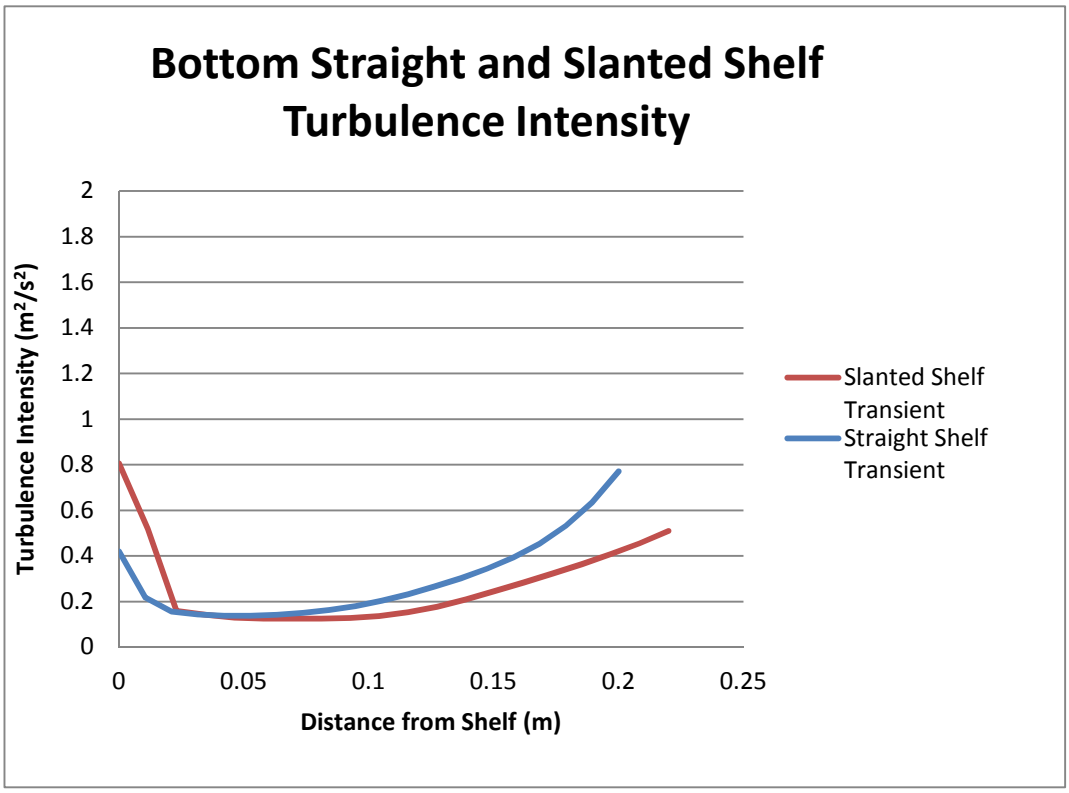

Fig. 72 - Bottom Straight and Slanted Shelf Turbulence Intensity

At the level of the bottom shelf it is clear from Fig. 72 that the turbulence is greater with slanted shelves close to the shelf than with straight shelves. In particular, the difference in the values of turbulence intensity increases at 0.05m from the shelf and continues to increase far away from the shelf. It can be said that increases in turbulence produced higher up in the cabinet and in close proximity to the shelf can lead to large increases in turbulence in the lower regions of the cabinet.

The turbulence intensity is slightly higher overall away from the shelf but in regions close to the shelf, the turbulence intensity is much higher with the slanted case than with the straight shelf scenario case. In almost all aspects related to entrainment and turbulence, the slanted shelf is inferior to the straight shelf scenario.

6.5 Vortex Diagrams

Through observation of the transient simulation, simple diagrams were produced indicating the location of the vortices in the slanted and straight shelf scenario. This can be a good indication of what is happening behind the air curtain as the cycle moves from start to finish. AS stated before each cycle represents one second in real time. Each section (refer to Fig. 9) will be discussed and comparisons will be made from slanted and straight shelves.

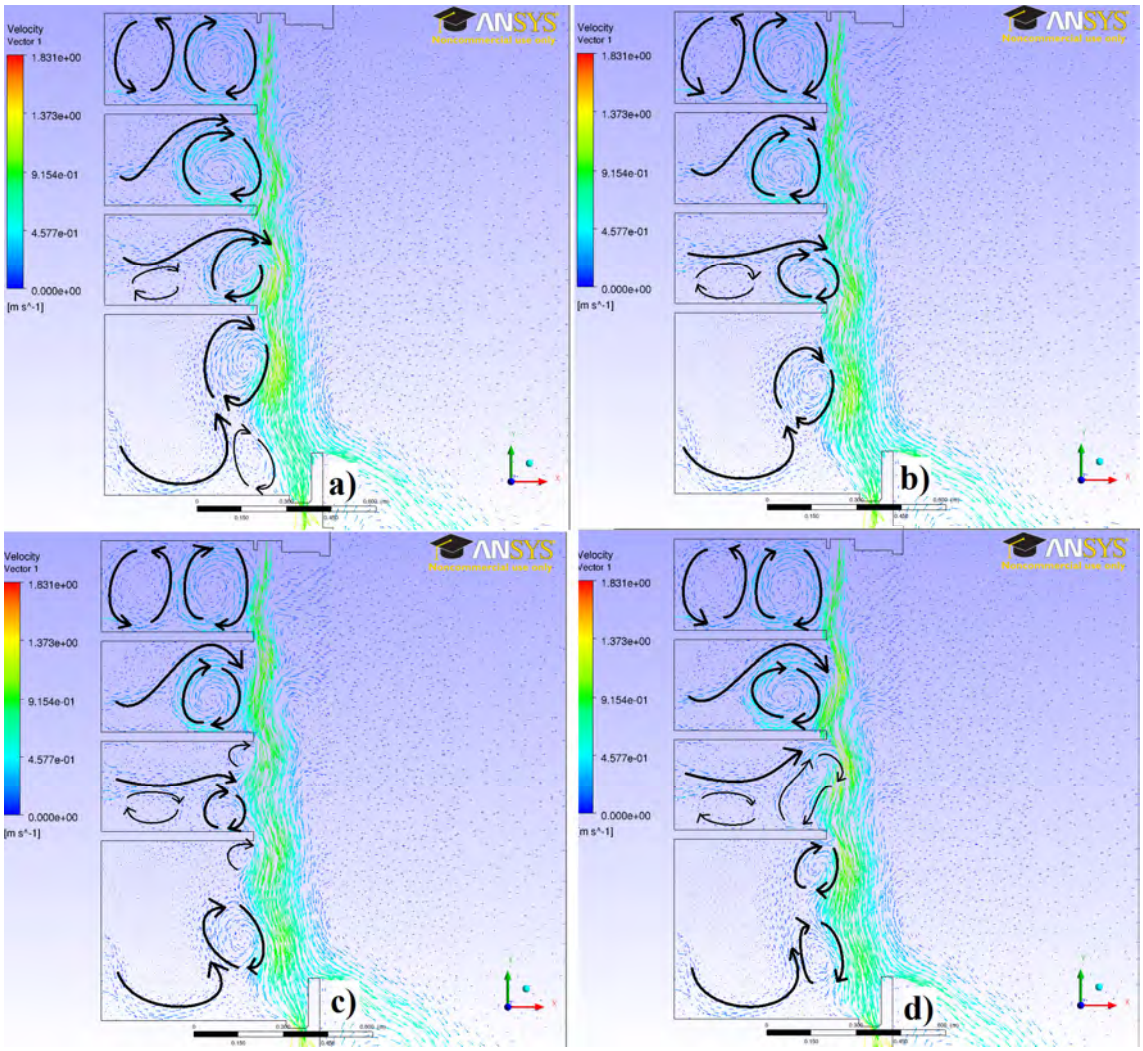

Fig. 73- Vortices Diagram for Straight Shelves at a) Cycle start b) quarter cycle c) Half Cycle d) three quarter cycle

As can be seen for the straight shelves scenario, the vortices are at typically at the edge of the shelves and adjacent to the air curtain. Section 1 and 2 do not change over the course of the cycle and represent a very stable cavity vortex. In sections 3 and 4, however, changes can be seen to take place over the course of the cycle. In Fig. 73 c) a small second vortex is seen forming and in d) the second vortex disrupts the first altogether. In section 4 you can see how a vortex begins to form at the top of the shelf in c) and moves downward until it is absorbed by the return grill at a) and b). It should be

noted that during the formation of one vortex at the top of the shelf there is already a secondary vortex firther down the air curtain soon to be absorbed by the return grill.

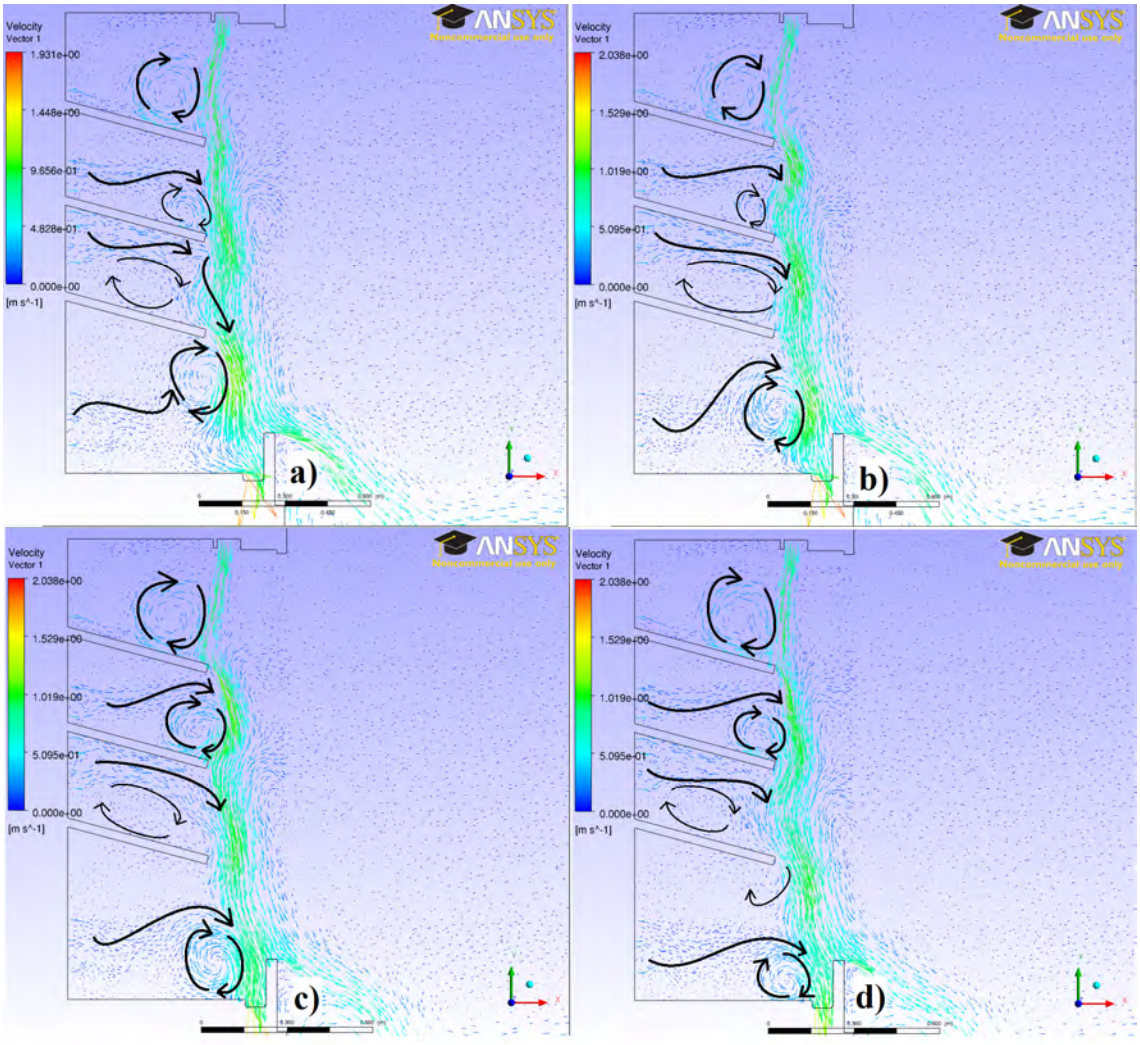

Fig. 74 - Vortices Diagram for Slanted Shelves at a) Cycle start b) quarter cycle c) Half Cycle d) three quarter cycle

For section 1 and 2 in Fig. 74, there appears to be no differences when the cycle continues, much like in Fig. 73. However, in the straight shelf case there are 2 vortices in section 1, there is only one in the slanted shelf section 1. Section 3 also shows very stable behaviour over the course of the cycle by the formation of only one vortex.

Section 4, though having a distinct cycle, is not as complex as with the straight shelf configuration. Only a single vortex is formed per cycle in the slanted shelf case. Only the very beginnings of a vortex can be seen forming in Fig. 74 d) As can be seen from Fig. 73 and Fig. 74, the vortices formation is different but only in sections 1 and 4. Only one vortex in the section 4 of the slanted shelf case could be an argument for the stability of the system. It can be seen that there is only one vortex formation per cycle unlike the straight shelf case where 2 are seen to be formed in the same cycle. From observation of the cycles, the back panel flow seems to support the air curtain in a more stable fashion in the straight shelf case. The formation of the two vortices allows for the back panel flow to move in the same manner throughout the cycle. In the slanted shelf case, the back panel flow moves from supporting the vortex to moving over the vortex and into the air curtain. It is unclear which is more beneficial to a RDC but fewer fluctuations in the cavity of the cabinet should be a goal. Component Velocity Analysis

In this section the differences between the effects of the straight and slanted shelves on the u and v velocity components are discussed and analysed.

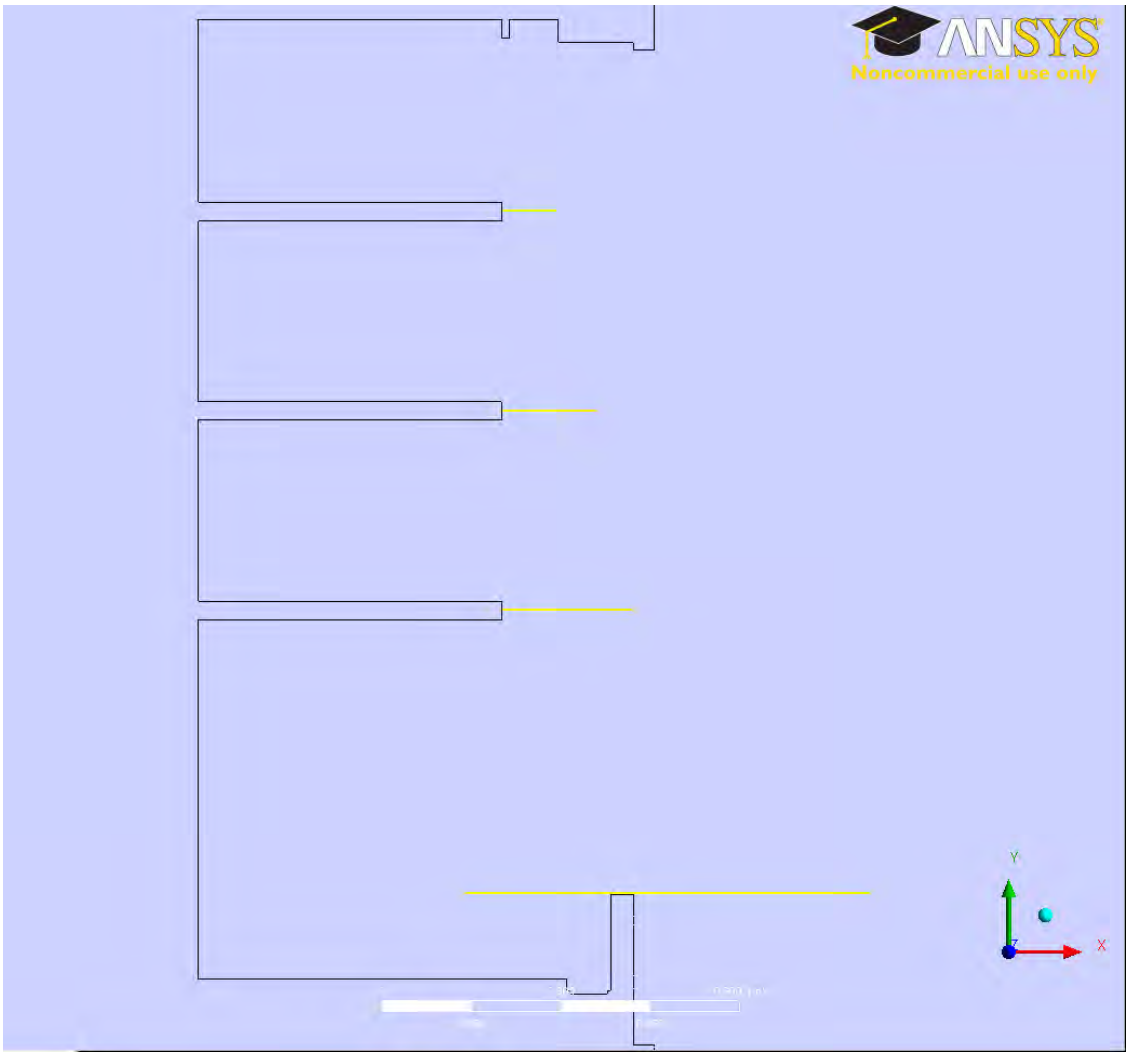

Fig. 75 – Straight Shelf u and v Component Velocity Profile Locations

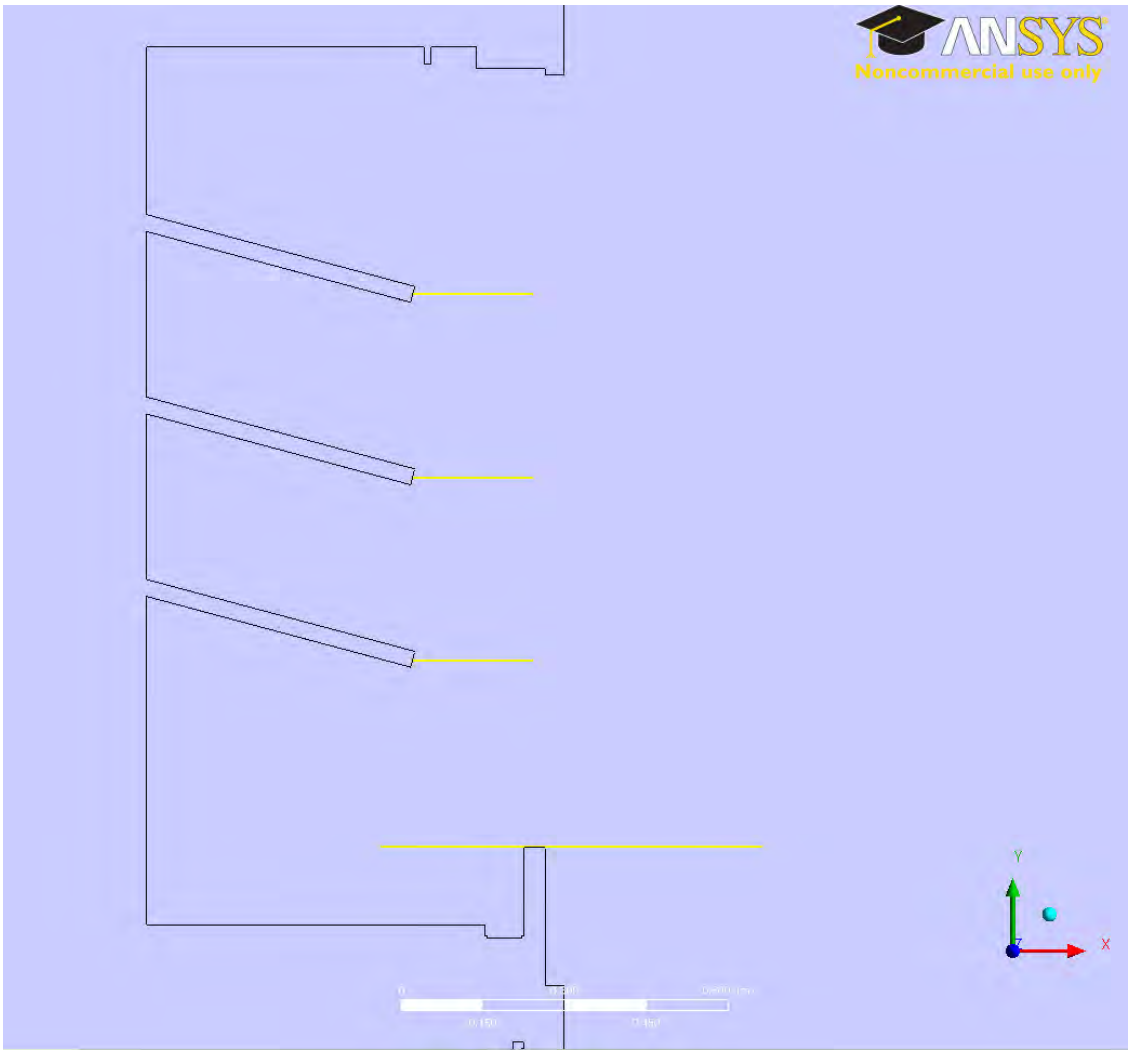

Fig. 76 – Slanted Shelf u and v Velocity Profile Locations

Fig. 75 and Fig. 76 show the locations where the u and v velocity component profiles were calculated. The u component is parallel to the shelves where positive u velocity is denoted out of the cabinet and negative u velocity is denoted into the cabinet. In the same respect, positive v velocity is denoted as up the cabinet and negative denoted as down. There are four locations noted and studied, the top middle and bottom shelves along with the length just above the return grill guard denoted as “above guard” in the chart.

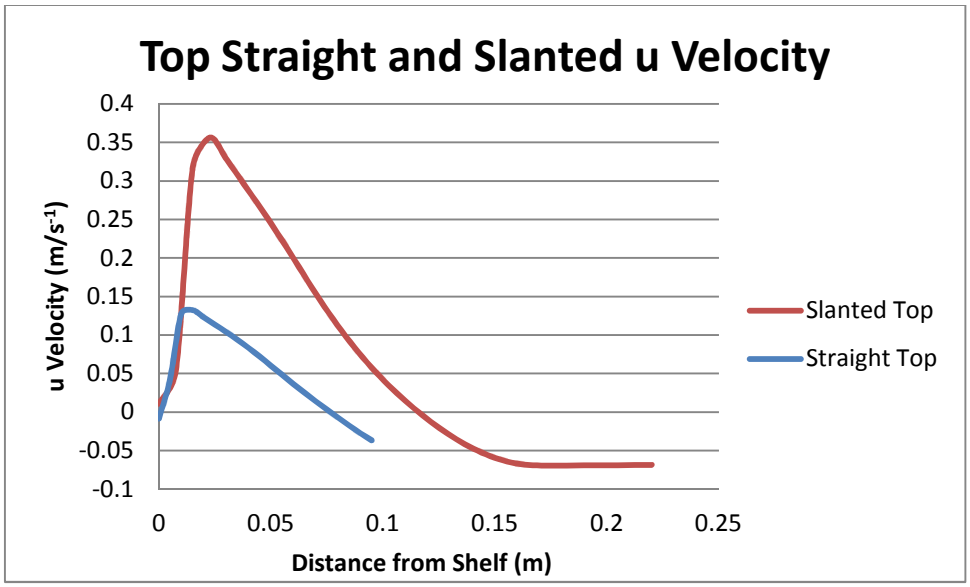

Fig. 77 - Top Shelf Straight and Slanted u Velocity Profile

As can be seen from Fig. 77, the slanted shelf has a much higher velocity out of the cabinet than the straight shelf. This is easily explained by the angle of the shelf and the fact that the air curtain hits the shelf on the way down towards the discharge grill. The angle of the shelf provides a ramp so that more forward momentum velocity can be generated than with the slanted shelf case.

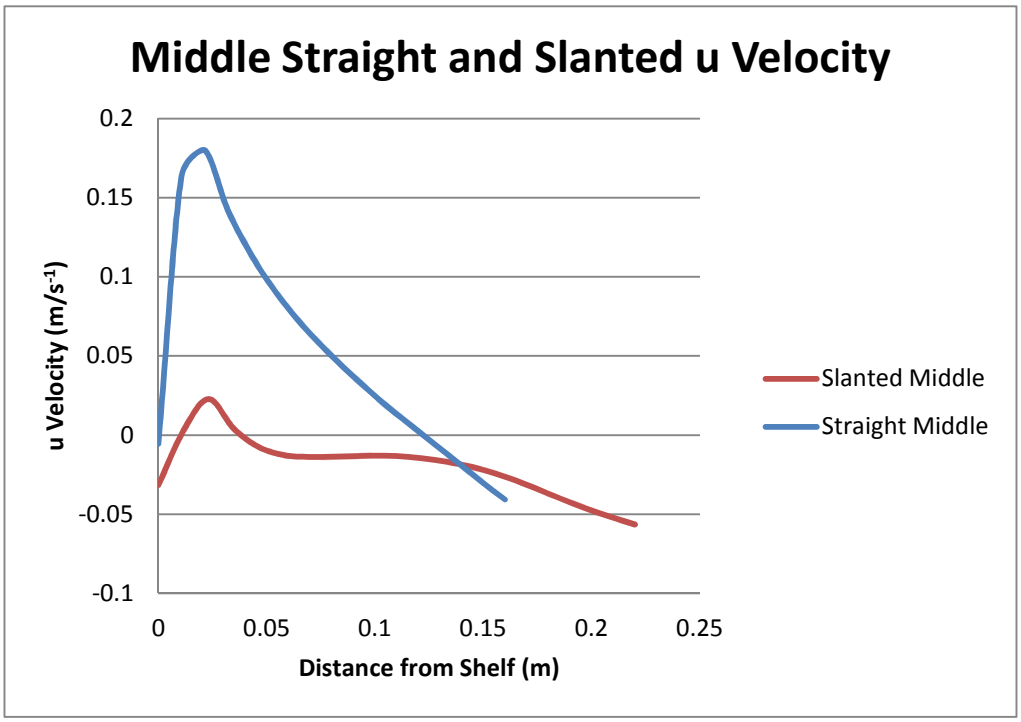

Fig. 78 - Middle Straight and Slanted Shelf u Velocity Profile

The case seems to be reverse for Fig. 78 comparing with Fig. 77. As can be seen from the figure above, the slanted shelf has produced a large reduction in u velocity while the flow in the case of the straight shelf has remained at relatively the same velocity. This decrease in outward momentum for the slanted shelf may be explained by the redirection of the flow caused by the presence of the top shelf. As flow passes this top shelf it changes the direction and start to move along the slanted shelf so that the main stream of the flow is getting father away from the middle shelf. This phenomenon is not occurring in the case of the straight shelf where air flow is not changing direction and remains close to the shelves.

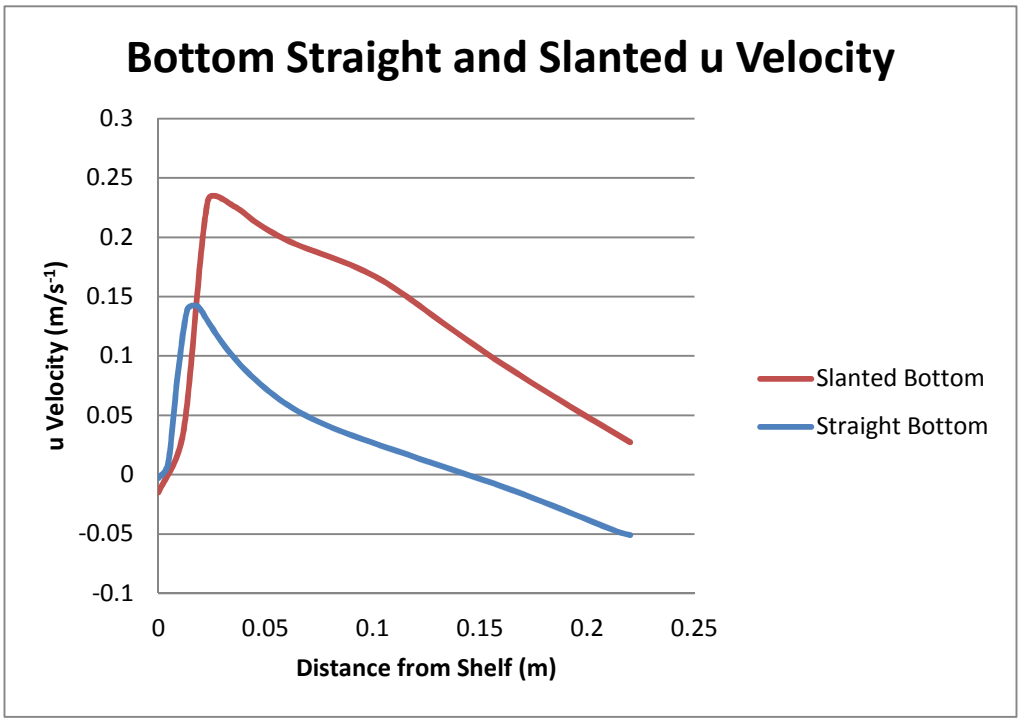

Fig. 79 - Bottom Straight and Slanted Shelf u and v Velocity Profile

As seen in the top shelf scenario, the outward velocity continues to be dominated in the case of the slanted shelf. After recovering from the outward disturbance caused by the top shelf, the air curtain now returns back to the bottom shelf due to negative buoyancy effect and increases the outward momentum from the incline edge of the shelf. At the same time the u velocity for the straight shelf remains relatively the same in the magnitude and the shape.

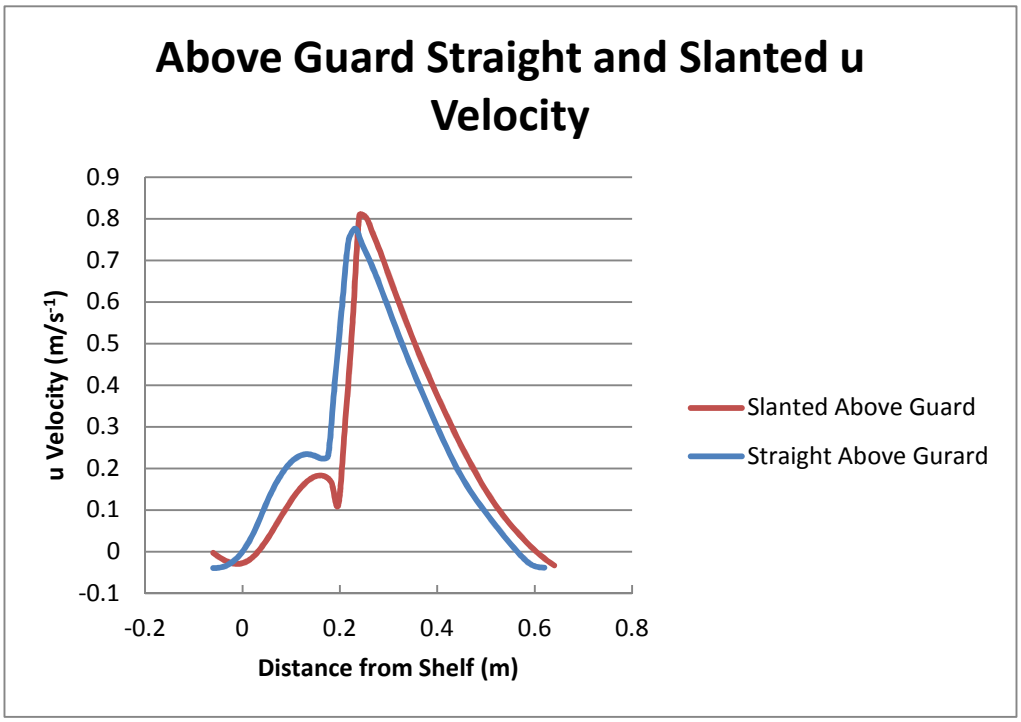

Fig. 80 - Above Return Grill Guard u Velocity Profile

Just above the return grill guard the data is almost identical except a slight shift and magnitude difference. The outward velocity is large compared to any of the previous profiles but it is of note that the slanted shelf still retains a higher magnitude of exiting velocity from the cabinet.

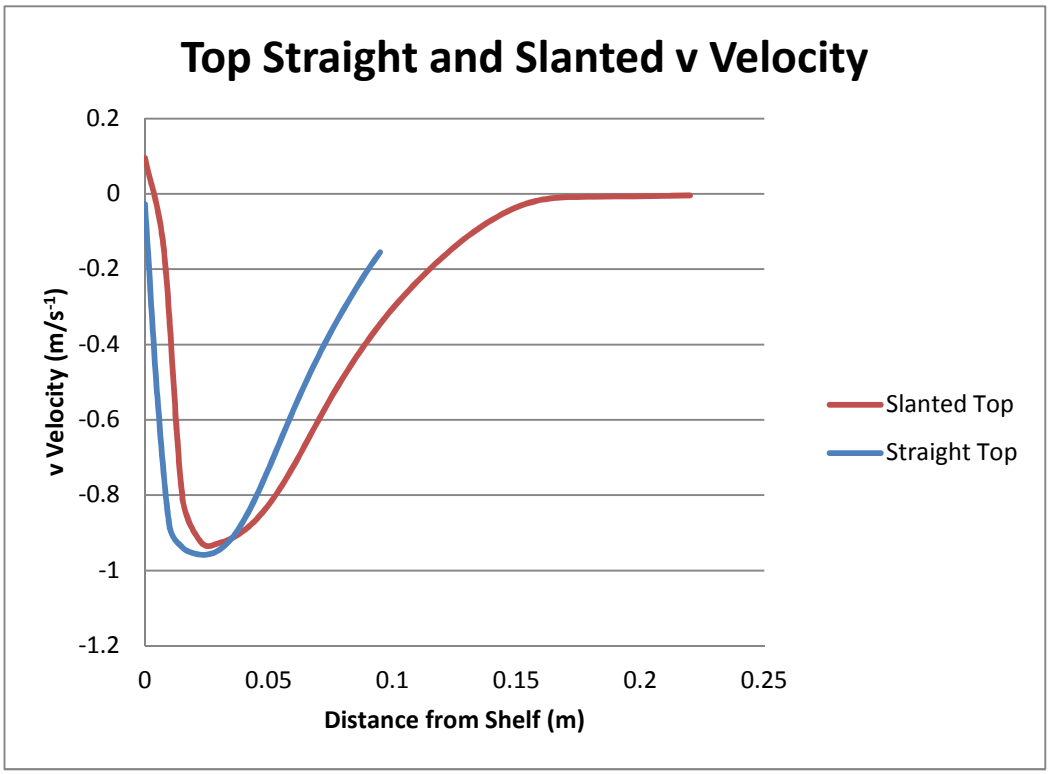

Fig. 81 - Top Straight and Slanted v Velocity Profile

The downward velocities of both slanted and straight scenarios are very similar in behaviour and magnitude. The straight shelf shows a slightly higher maximum downward velocity. The peak of the slanted shelf is also slightly off centre of the straight scenario.

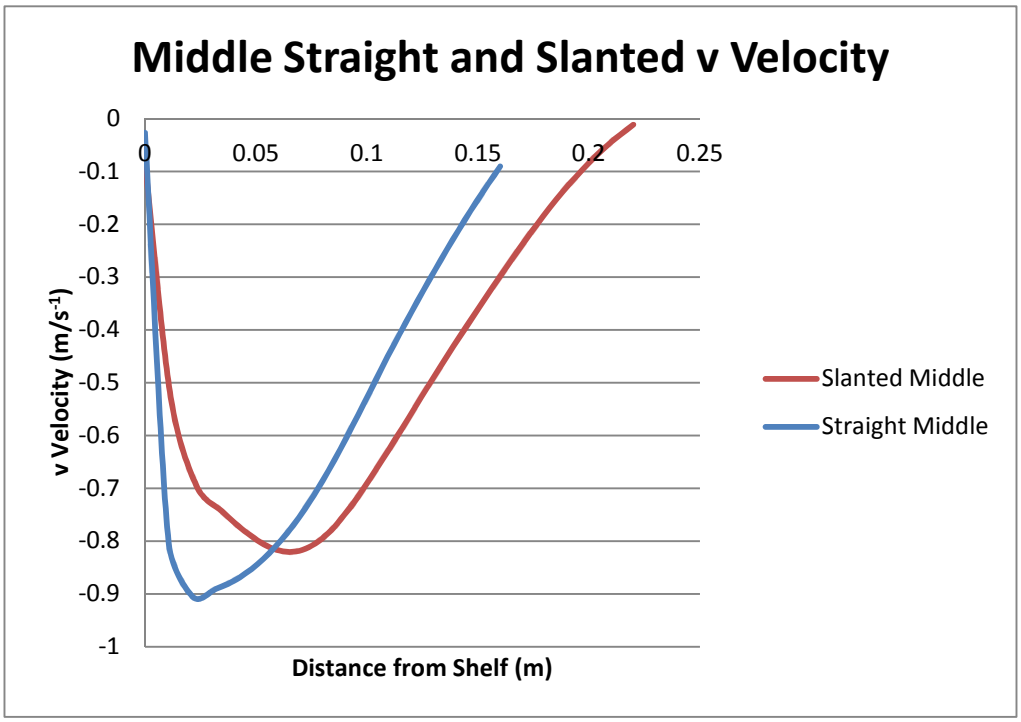

Fig. 82 - Middle Straight and Slanted Shelf Velocity Profile

As the air curtain moves to the middle shelf, the differences in the downward velocity become clearer. As expected the peak velocity for the slanted shelf is farther away from the shelf edge than the straight shelf scenario. The maximum velocity is also not as high as the straight shelf velocity.

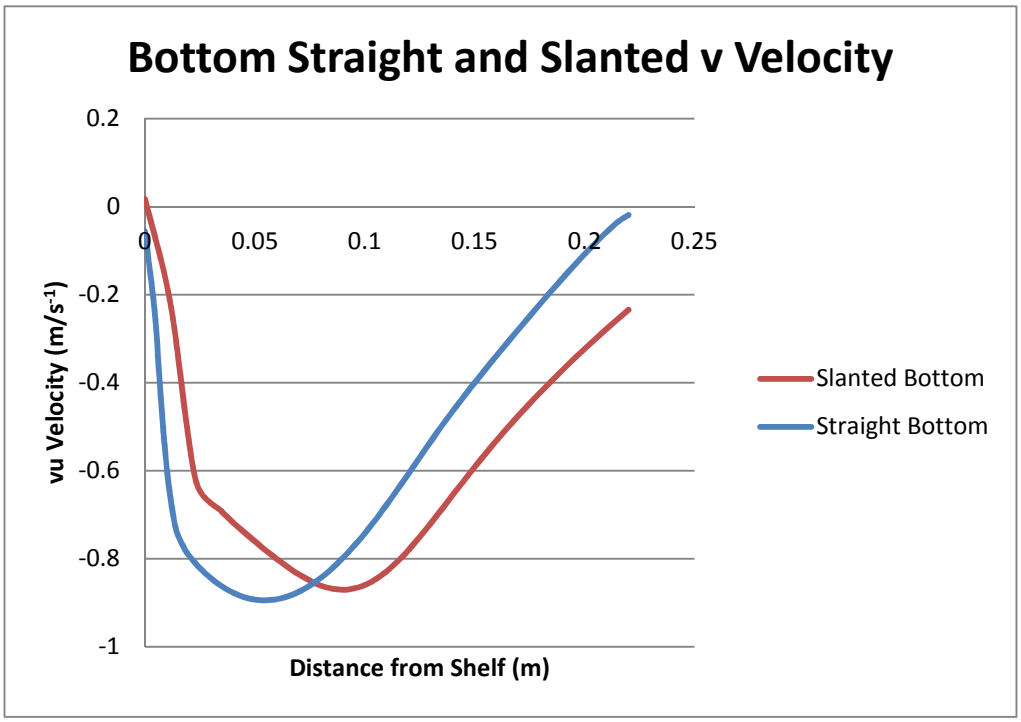

Fig. 83 Bottom Straight and Slanted Shelves v Velocity Profile

Magnitude wise the v velocity for both configurations is virtually identical at the bottom shelf. The peak location is different as the slanted shelf is more outside the cabinet than the straight shelves.

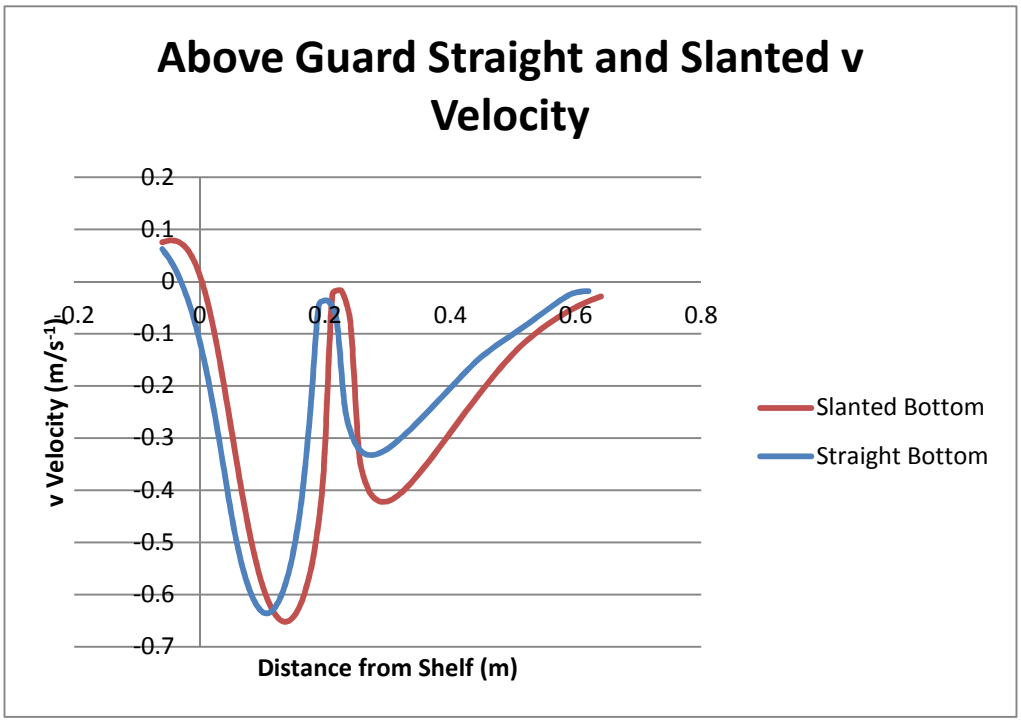

Fig. 84 - Above Return Grill Guard v Velocity Profile

The location above the return grill guard is very similar to Fig. 80 in that both profiles are almost identical except for a slight shift in position and magnitude. It should be noted that the straight shelf has a higher downward velocity overall save for this point where it has a noticeably lower downward velocity.

The u velocity graphs in Fig. 77, Fig. 78 and Fig. 79 show that the slanted shelf interferes most with the middle shelf interaction. The lack of a u velocity component in the middle shelf causes the lack of a moving vortex. The u velocity component also shows the large increase in the air curtains outward momentum due to the angle of the shelves. This causes a higher degree of turbulence and entrainment due to the increased mixing.

A higher v velocity of the air curtain when it passes the shelf is a positive characteristic to have in RDCs because it leads to increased forced convection and therefore results in less dominant buoyancy and, therefore, decreased entrainment. The peak v velocity for the slanted shelf is slightly farther than the peak for the straight shelves, as expected. Though less pronounced than in the experimental case, there was a increase in the v velocity by upwards of 10% when comparing straight and slanted shelves.

6.6 Summary

Upon further examination of the results, several observations can be made from the experimental data. The air curtain width is shown to expand greatly as the air curtain falls from the cabinet. This could be due to the large turbulence intensity caused by the introduction of the first shelf; this introduces mixing and entrainment and, eventually, increases the air curtain width as the air curtain falls to the lower regions of the cabinet. The NDACW provides a useful tool in understanding entrainment. Turbulence intensity helps us to see when entrainment happens and the NDACW shows us the results of the introduction of entrainment downstream. The effect of entrainment is not immediate and takes time to manifest in physical characteristics such as increasing the buoyancy of the air curtain and, therefore, increasing the air curtain width.

Furthermore, it can be stated that there are numerous differences between a slanted shelf case and a straight shelf case when referring to the fluid dynamics of the system. It is clear to see the extension of the air curtain with respect to shelf position using the NDACW diagrams. In Fig. 60 there is a clear extension of the air curtain because of the

slanted nature of the shelves out of the cabinet, which leads to more mixing of the curtain and the ambient air. In Fig. 59 the overall air curtain width can be observed and the NDACW (*l*) can be seen to be slightly larger than with the straight shelf.

The profiles of velocity components u and v support the experimental observation of the outward movement of the air curtain. There is great u velocity increase in the slanted scenario for the top and bottom shelf comparing with the middle slated shelf (Refer to Fig. 77 and Fig. 79). At the same time the straight shelf showed an almost constant outward u velocity throughout the height of the cabinet.

The v velocity numerical component showed the peak downward velocity of the slanted shelf configuration to be shifted outward compared to the straight shelf configuration through entire height of the cabin. This confirms that the main air curtain stream has been displaced more outward by the slanted shelves comparing with the straight shelves configuration

CHAPTER 7 - CONCLUSIONS

7.1 Experimental Analysis

From the experimental analysis conducted using the slanted and straight shelves configurations in RDCs, it was observed that the introduction of shelves into the air curtain system results in significant changes in the shape of the air curtain profile. Also it was observed that the differences in the value of the maximum velocity and its location, overall velocity magnitude, NDACW and turbulence intensity, for two different configurations with straight and slated shelves are significant. So it can be concluded that the differences in the air curtain when placing a slanted shelf and straight shelf into the system cannot be ignored.

We identified several factors that influence the air curtain velocity and shape of the velocity profile as the air curtain drops from the discharge grill. These values are changing with the height, which is directly related to the amount of entrainment, and angle of the shelves. It can also be observed that, from experiments, that there is an upward of 50% difference in maximum velocity when comparing straight and slanted shelves velocity profiles. This has direct relations to the kinetic energy component of the Ri and the momentum of the Re. It was clear to see from the experiments that the simple Ri and Re is not enough to determine the efficiency of a cabinet in it entirety.

The non-dimensional air curtain width (l) at each level chosen in this study showed to be a good indication of the amount of entrainment. As the entrainment level increases due to the air curtain interacting with the ambient air, the more the air curtain slows in velocity and expands. The turbulence intensity supports this conclusion as the effects of

turbulent mixing are not immediate. Turbulence intensity data also shows higher mixing with the slanted shelf scenario.

The position of the shelves is also important because of the interference they cause to the air curtain. From the flow visualization results it was observed that the air curtain has a tendency to move toward the back panel when there are no shelves present. This behavior is stopped by the shelves forcing the air curtain forward to the ambient air outside the cabinet. After the air curtain passes the shelves, it is seen to go towards the back of the cabinet again. It can be said that the straight shelves provide more support without adding too much turbulence intensity as opposed to slanted shelves.

It can be concluded that the l value and turbulence intensity are useful tools in analyzing the entrainment of the air curtain. The intruding of shelves also allowed for the air curtain to seal the cabinet despite the negative buoyant behavior thus, improving on a shelf less cabinet. However, straight shelves should be implemented when possible as it has been shown to result in less turbulence intensity and entrainment overall. Further optimization can proceed on the basis of the data gathered here, with the aim of improving the overall efficiency.

7.2 Numerical Analysis

From a numerical point of view the running of steady state simulations for RDCs cannot be recommended as it has been clearly indicated that the results are not as accurate. Due to the quasi-stable nature of the air curtain in the transient simulations and its accurate comparison to the experimental data, it was observed that a transient simulation of an air curtain system was far more accurate.

As far as modeling the RDCs in 2D or 3D models, a transient 2D simulation proved far superior to a steady state 3D counterpart. Due to computational limitations, a transient 3D simulation was not possible but should be explored as soon as the computational power of cluster computers can run a fine mesh 3D model.

Both turbulence intensity and kinetic energy showed to have increased value for the case of the slated shelves at the region close to the return grill further away from the cabinet. This increase in turbulence due to the shelf angle should not be ignored as these regions of high turbulence a can lead to more entrainment of the ambient air. There was also found to be a 10% increase in the v velocity component when comparing the straight and the slanted shelves.

7.3 Overall Conclusion

The use of experimental and numerical techniques to analyze the flow behavior and air curtain in open RDCs in this thesis has proven productive and yielded reliable results. As computational power increases it is advisable to proceed to full 3D models of RDCs under transient conditions. It is also recommended, based on the results obtained in this thesis, to use straight shelf cabinets when at all possible in open RDCs to decrease amount of entrainment with ambient air and therefore to improve efficiency of the air curtain.

REFERENCES

1. Cortella, G., *CFD-aided retail cabinets design.* Computers and Electronics in Agriculture 34 (2002) 43–66, 2002.
2. Chen, X.-L.Y., *Simulation of a cavity insulated by a vertical single band cold air curtain.* Energy conservation and Management, 2005. **46**: p. 1745-1756.
3. Faramarzi, R., *Efficient display case refrigeration.* ASHRAE Journal, 1999. **41**: p. 46-51.
4. *Supermarkets and superstores: market report 2003.* Key Note Publications Ltd, 2003.
5. Field, B.S., *An Air Curtain Along a Wall With High Inlet Turbulence.* Journal of Fluids Engineering, 2004. **126**: p. 391-398.
6. Zhikun Cao, J.H., Bo Gu, *Modeling of variable speed refrigerated display cabinets based on adaptive support vector machine.* Mechanical Systems and Signal Processing, 2010. **24**: p. 78-89.
7. Brandon S. Field, E.L., *Entrainment of refrigerated air curtains down a wall.* Experimental Thermal and Fluid Science, 2006. **30**: p. 175–184.
8. Mayar Amin, D.D., Homayun K. Navaz, *Tracer Gas Technique: A new approach fr the steady state inflitration rate measurment of open refrigerated display cases.* Journal of Food Engineering, 2009. **92**: p. 172-181.
9. Ke-zhi Yu, G.-l.D., Tian-ji Chen, *A correlation model of thermal entrainment factor for air curtain in a vertical open display cabinet.* Applied Thermal Engineering, 2009. **29**: p. 2904-2913.
10. Chen, X.-L.Y., *Experimental study of the performance of single-band air curtains for a multi-deck refrigerated display cabinet.* Journal of Food Engineering 69 (2005) 261–267, 2005.
11. Cao, Z., et al., *Application of an effective strategy for optimizing the design of Air curtains for open vertical refrigerated display cases.* International Journal of Thermal Sciences, 2010. **49**: p. 976-983.
12. Yu, K.-z., G.-l. Ding, and T.-j. Chen, *Modified two-fluid model for air curtains in open vertical display cabinets.* International journal of refrigeration, 2007: p. 1-11.
13. Yu, K.-z., G.-l. Ding, and T.-j. Chen, *Simulation of air curtains for vertical display cases with a two-fluid model.* Applied Thermal Engineering 2007. **27** p. 2583-2591.
14. Adams, P., *the intereffect of supermarket refrigeration and air conditioning.* ASHRAE, 1985. **CH-85-09**: p. 423-433.
15. Field, B.S. and E. Loth, *Entrainment of refrigerated air curtains down a wall.* Experimental Thermal and Fluid Science, 2006. **30**: p. 175–184.

16. Karine Loubiere, M.P., *Educing coherent eddy structures in air curtain systems.* Chemical Engineering Processing, 2007.
17. Navaz, H.K., et al., *Jet entrainment rate in air curtain of open refrigerated display cases.* International Journal of Refrigeration, 2005. **28**: p. 267-275.
18. Amin, M., D. Dabiri, and H.K. Navaz, *Effects of secondary variables on infiltration rate of open refrigerated vertical display cases with single-band air curtain.* Applied Thermal Engineering, 2012. **35**: p. 120-126.
19. Amin, M., D. Dabiri, and H.K. Navaz, *Comprehensive study on the effects of fluid dynamics of air curtain and geometry on infiltration rate of open refrigerated cavities.* Applied Thermal Engineering, 2011. **31**: p. 3055-3065.
20. H. Mhiri, S.E.G., *Numerical Study of the Thermal and Aerodynamic Insulation of a Cavity with a vertical Downstream Air Jet.* Int. Comm. Heat Meass Transfer, 1998. **25**(7): p. 919-928.
21. Chen, Y.-G., *Parametric evaluation of refrigerated air curtains for thermal insulation.* International Journal of Fluid Sciences, 2009. **48**: p. 1988-1996.
22. Chen, Y.-G., *Parametric evaluation of refrigerated air curtains for thermal insulation.* International Journal of Thermal Sciences, 2009. **48**: p. 1988-1996.
23. Hammond, E., J. Quarini, and A. Foster, *Development of a stability model for a vertical single band recirculated air curtain sealing a refrigerated cavity.* International Journal of Refrigeration, 2011. **34**: p. 1455-1461.
24. Evans, J.A., S. Scarcelli, and M.V.L. Swain, *Temperature and energy performance of refrigerated retail display and commercial catering cabinets under test conditions.* International Journal of Refrigeration, 2007. **30**: p. 398-408.
25. Gray, I., et al., *Improvement of air distribution in refrigerated vertical open front remote supermarket display cases.* International Journal of Refrigeration, 2007: p. 1-9.
26. Navaz, H.K., et al., *The Application of Advanced Methods in Analyzing the Performance of the Air Curtain in a Refrigerated Display Case.* ASME, 2002. **124**: p. 756-764.
27. Kocherscheidtk, M. Schmidts, and V.I.V. Ram, *LDV Measurements of the Response of the Swirling Turbulent Flow in a Pipe to a Rapid Temporal Change in Swirl.* Flow, Turbulence and Combustion, 2002. **69**: p. 79-94.
28. Furuichi, T.H., Masaya Kumada, *An experimental investigation of a large-scale structure of a two-dimensional backward-facing step by using advanced multi-point LDV.* Experiments in Fluids, 2004. **36**: p. 274-281.
29. Matsuzaki, et al., *A Study on Swirling Flows in a Rectangular Channel.* Journal of Thermal Sciences, 2001. **10**(3): p. 205-210.
30. Egon P. Hassel, G.F., *An LDV system for measuerment of spatial velocity correlations in turbulent gas-flows.* Engineering Research Bd. , 1994. **60**(10).
31. Byung-Joon Rho, J.-H.O., *LDV Measurments of Turbulent Flow Behavior of Droplets in a two Phase Coaxial Jet.* KSME Journal, 1995. **9**: p. 360-368.

32. Neto, L.P.C., M.C.G. Silva, and J.J. Costa, *On the use of infrared thermography in studies with air curtain devices.* Energy and Buildings, 2006. **38**: p. 1194-1199.
33. Ndoye, M., et al., *Experimental Study of the Cold Aisle Phenomenon in Supermarket Display Cabinet*, in *ICR*. 2011: Praague, Czech Republic.
34. Smale, N.J., J. Moureh, and G. Cortella, *A review of numerical models of airflow in refrigerated food applications.* International Journal of Refrigeration, 2006. **29**: p. 911-930.
35. Stribling, D., *INVESTIGATION INTO THE DESIGN AND OPTIMISATION OF MULTIDECK REFRIGERATED DISPLAY CASES*, in *Mechanical Engineering*. 1997, Brunel University. p. 187.
36. Mirade, P.-S., A. Kondjoyan, and J.-D. Daudin, *Three Dimensional CFD Calculations for Designing Large Food Chillers.* Computers and Electronics in Agriculture, 2002. **34**: p. 67-88.
37. Xia, B. and D.-W. Sun, *Applications of computational fluid dynamics (CFD) in the food industry: a review.* Computers and Electronics in Agriculture, 2002. **34**(5-24).
38. Ho, S.H., L. Rosario, and M.M. Rahman, *Numerical simulation of temperature and velocity in a refrigerated warehouse* International Journal of Refrigeration, 2010. **33**: p. 1015-1025.
39. Kondjyan, A., *A review on surface heat and mass transfer coefficients during air chilling and storage of food products.* International Journal of Refrigeration, 2006. **29**: p. 863-875.
40. Ge, Y.T. and S.A. Tassou, *Simulation of the performance of single jet air curtains for*
vertical refrigerated display cabinets. Applied Thermal Engineering, 2001. **21**: p. 201-219.
41. Foster, M.M., J.A. Evans, *The use of CFD to improve the performance of a chilled multi-deck retail display cabinet.* International Journal of Refrigeration 28 (2005) 698–705, 2004.
42. Cao, Z., et al., *A novel strategy for predicting the performance of open vertical refrigerated display cabinets based on the MTF model and ASVM algorithm.* International Journal of Refrigeration, 2010. **33**: p. 1413-1424.
43. D'Agaro, G. Cortella, and G. Croce, *Two- and three-dimensional CFD applied to vertical display cabinets simulation.* International Journal of Refrigeration, 2006(29): p. 178–190.
44. Foster, A.M., et al., *Three-dimensional effects of an air curtain used to restrict cold room infiltration.* Applied Mathematical Modeling, 2007. **31**: p. 1109-1123.